Effect of seepage on sediment transport

Liu, Xiaoxie

2010

Liu, X. (2010). Effect of seepage on sediment transport. Doctoral thesis, Nanyang Technological University, Singapore.

https://hdl.handle.net/10356/35245

https://doi.org/10.32657/10356/35245

EFFECT OF SEEPAGE ON SEDIMENT TRANSPORT

LIU XIAOXIE

SCHOOL OF CIVIL AND ENVIRONMENTAL ENGINEERING

COLLEGE OF ENGINEERING

NANYANG TECHNOLOGICAL UNIVERSITY

2010

Effect of Seepage on Sediment Transport

Liu Xiaoxie

School of Civil and Environmental Engineering

College Of Engineering

Nanyang Technological University

A thesis submitted to the Nanyang Technological University

in partial fulfillment of the requirement for

the degree of Doctor of Philosophy

2010

ACKNOWLEDGEMENTS

The author would like to express her sincere thanks to all who have extended their help and guidance during the entire duration of this project.

Special appreciation is made to her supervisor, Professor Chiew Yee Meng, for his valuable advice and extensive guidance throughout the entire period of the project. The author would like to thank Prof. Chiew's patience, dedication, understanding and willingness to impart his knowledge, thus enabling the author to gain much throughout the project.

Special thanks are also expressed to Associate Professor Cheng Nian Sheng for his constant assistance and encouragement at the beginning of the project.

Finally, the author would like to thank all staff from the Nanyang Technological University School of Civil and Environmental Engineering, for their efficiency in providing assistance and support in one way or another.

TABLE OF CONTENTS

ABSTRACT

This study presents the experimental results and theoretical analyses of seepage effects on sediment transport. A total of 529 experiments grouped under four different series of tests were conducted in a laboratory flume with a permeable sediment boundary to investigate the effect of seepage, the length of the suction zone and time on bedload transport rate. Two different types of cohesionless sand particles with diameters = 0.9 mm and 0.48 mm were used in the study.

Three dimensionless groups, viz. Einstein's parameter Φ, Shields' parameter without seepage τ_{*o} and modified densimetric Froude number Ω are chosen to examine how seepage affects bedload transport rate. Eleven undisturbed flow conditions were tested, five under clear water and six in live-bed condition. No bedforms with significant height were observed during the experiments. The results show that an increase in suction rate causes an increase in shear velocity excess, which is defined as the difference between the bed and critical shear velocities, leading to an increase in bedload transport rate. The experimental data also show that for the same undisturbed flow conditions, the dimensionless bedload transport rate increases linearly (in semi-logarithmic scale) with increasing suction rates. The equations for predicting bedload transport rate under suction are derived empirically; the predicted results using these empirical equations compared well with measured data, with an accuracy of ±20%. Published results from other researchers are used to compare with results obtained and inference drawn from the present study. The similarities and differences of these studies are highlighted.

On the other hand, the experimental results show that the sediment transport rate decreases with an increase in injection velocity, but the magnitude of the reduction

is comparatively smaller than that of the increment with suction. The equation for predicting bedload transport rate with injection is also empirically determined by fitting the ratio of Einstein's parameter Φ with injection to that without as a function of the ratio of modified densimetric Froude number with injection to that without.

The effect of the length of the seepage zone on sediment transport rate is investigated experimentally in this study. Only suction effects are studied in this part of the research. The results show that for the same undisturbed flow conditions and suction rate, the bed load transport rate, which is represented by Einstein's dimensionless parameter Φ, decreases with a reduction in suction zone length. A slope modifier is introduced to account for the length effect. The empirical equation for predicting the slope modifier is obtained in terms of the Shields' parameter without seepage and the relative suction zone length, which is defined as the ratio of the suction zone length to that at 2-m length.

Finally, the experimental results also show that the bedload transport rate in the presence of suction increases rapidly with time until it reaches a peak, beyond which, the transport rate decreases. The duration for the bedload transport rate to reach the peak is shorter for flows with higher sediment transport rates. With an increase in time, the bedload transport rate reduces, and eventually reaches a balance between the incoming and outgoing sediment transport, called the equilibrium condition, i.e., the sediment transport with no seepage condition.

LIST OF TABLES

LIST OF FIGURES

LIST OF SYMBOLS

A	=	coefficient of prediction equation for sediment transport rate
b	=	width of flume
B	=	coefficient of prediction equation for sediment transport rate
c	=	sediment concentration in ppm by weight
C	=	experimental constant
C_D	=	drag coefficient
C_L	=	lift coefficient
d	=	diameter of particles forming sedimentary bed
d_*	=	$\left[(S_s - 1)g d_{50}^3 / \nu^2\right]^{1/3}$
D	=	diameter of solitary particle
d_{16}	=	grain diameter when 16% of sand passing sieves
d_{50}	=	median grain diameter of sediment particles
d_{84}	=	grain diameter when 84% of sand passing sieves
f	=	specified function
f_*	=	a form of a friction factor
f_1	=	specified function
f_2	=	specified function
f_3	=	specified function
f_4	=	specified function
F_D	=	drag force
F_f	=	frictional force
F_L	=	lift force
F_s	=	seepage force
g	=	gravitational acceleration
h	=	water depth with seepage

H = developed dune height with seepage

h_c = water depth at the mid-section of seepage zone

h_o = water depth without seepage

H_o = original dune height without seepage

i = hydraulic gradient with seepage

i_c = hydraulic gradient at quick condition

I_o = energy slopes in open-channel flows without seepage

I_s = energy slopes in open-channel flows with seepage

K = coefficient of permeability

k_s = equivalent sand roughness (= $2d_{50}$)

L = length of the seepage zone

L_o = 2 m

l_{ε^*} = dimensionless characteristic dimension of voids

m = exponent = 1~2

N = seepage intensity parameter

n = porosity

n_o = number of transport particles per unit width per unit time

n_s = an order one parameter

Q = instantaneous flow discharge

q_{bo} = sediment transport rate per unit width without seepage

q_{bs} = sediment transport rate per unit width with seepage

Q_o = streamwise flow rate

Q_s = seepage flow rate

r_e = volumetric sediment erosion rate per unit area

R_f = roughness function

R_s = hydraulic radius of the bed with seepage

S_s = specific gravity of sand particle

t = time

t_{peak} = time for Einstein's parameter to reach the peak

t_{start} = time for the first measured date point

u = instantaneous velocity in the x axis

U = mean flow velocity with seepage

u_{*co} = critical shear velocity without seepage

u_{*cs} = critical shear velocity with seepage

u_{*o} = shear velocity without seepage

u_{*s} = shear velocity with seepage

u_b = approach velocity of flow over the bed at the particle

u_{bc} = approach velocity of flow over the bed at the particle at threshold

U_c = mean velocity with seepage at the mid-section of seepage zone

U_o = mean flow velocity without seepage

U_{ro} = velocity at reference depth without seepage

U_{rs} = velocity at reference depth with seepage

u_s = slip velocity at the bed surface

U_{ox} = velocity at the bed at section x from the beginning of suction zone

V_s = seepage velocity

V_{sc} = critical seepage velocity under quick condition

W = submerged weight force

w = width of control volume

x = coordinates tangential to the bottom boundary

X = horizontal lever arm

y = coordinates normal to the bottom boundary

y_* = $k_s \exp(-\kappa B)$

y_o = origin displacement of velocity profile for flow with bed suction

y_s = scour depth

y_{sm} = maximum scour depth

Z = vertical lever arm

α = empirical coefficient

β = momentum correction factor

γ = factor

δ = boundary layer thickness

ζ = constants dependent on the shape of particles

η = calibration factor

θ = angle of repose of the sediment particles

κ = von Karman's constant (≅ 0.4 in clear water)

λ = step length ratio =100

μ_s = coefficient of friction between the grain and the surrounding grains

ν = kinematic viscosity

ξ = constants dependent on the shape of particles

ρ = density of fluid

ρ_b = bulk density

ρ_s = density of particle

σ_g = geometric standard deviation

τ'_{*o} = Shields' parameter associated with skin friction

τ_{*co} = critical Shields' parameter without seepage

τ_{*o} = Shields' parameter without seepage = $u_{*o}^2 / (S_s - 1) d_{50} g$

τ_{*s} = Shields' parameter with seepage

τ_{bo} = bed shear stresses without seepage

τ_{bs} = bed shear stresses with seepage

τ_{co} = critical shear stress without seepage

τ_{cs} = critical shear stress with seepage

Φ = Einstein's parameter = $q_{bs} / \sqrt{d_{50}^3 g (S_s - 1)}$

Φ_{comp} = Einstein's parameter computed using Eqs. 5.4 to 5.6

Φ_o = Einstein's parameter without seepage = $q_{bo} / \sqrt{d_{50}^3 g (S_s - 1)}$

Φ_{peak} = Einstein's parameter for the peak

Φ_{start} = Einstein's parameter for the first measured date point

ω = slope modifier

Ω = modified densimetric Froude number = $\dfrac{U_o^2}{[(S_s-1)(1-n)-V_s/K]d_{50}g}$

Ω_c = modified densimetric Froude number at threshold condition

Ω_o = modified densimetric Froude number without seepage

= $\dfrac{U_o^2}{[(S_s-1)(1-n)]d_{50}g}$

Chapter 1

Introduction

Permeable boundaries are often encountered in engineering practice and natural environments. Typical examples are porous boundaries consisting of sediment particles in natural rivers and densely vegetated boundaries in irrigation canals. The permeable boundary enables mass and momentum transfer across the interface between the fluid and porous medium. Interactions between turbulent flow and the permeable boundary may result in changes to the characteristics of the flow as compared to those with an impermeable boundary.

Seepage, either inflow (injection) or outflow (suction), through the boundaries of an alluvial channel, has a significant influence on the sediment transport behavior on an alluvial channel. Due to changes to the boundary layer, erosion or deposition of sediment particles may occur with the presence of seepage flow. Thus, infrastructures subject to scour and siltation, such as bridges, roads, railways and other hydraulic structures, should be designed with an understanding of this effect in mind.

Sediment transport rate, especially bedload transport rate is an important variable in river engineering. The prediction of sediment discharge is very important for the assessment of bed erosion and deposition in a fluvial system, as well as the estimate of scour around hydraulic structures such as bridge piers or abutments. Formulas for predicting bedload transport rate with an impermeable bed (Engelund and Hansen, 1967; Bagnold, 1966; Ackers and White, 1973; Yalin, 1977; Cheng, 2002; and Yang and Lim, 2003) have been widely used in practice. However, the number of studies on bedload transport rate with a permeable boundary is considerably less than those associated with a non-porous boundary. Moreover, results from these limited studies do not lead to a unanimous conclusion.

The effect of suction on sediment incipient motion has not been investigated in the literature. Moreover, direct measurement of sediment transport rate as yet has not been conducted. Therefore, the objective of this research is to study seepage effects on sediment transport by directly measuring the bedload transport rate subjected to seepage. The characteristic of open-channel flows with seepage was investigated by conducting physical experiments. On the basis of these experimental results, empirical formulae to predict sediment transport rate in the case of seepage are derived.

Chapter 2, which is a review of published literature, presents previous experimental, theoretical and field studies of seepage effect on open channel flow and sediment entrainment from three aspects, viz., the bed shear stress, the critical shear stress and the sediment transport rate.

Chapter 3 describes the apparatus used in the experiments, methodologies for the measurement of the hydraulic parameters, and the procedure for the collection of the data in the study.

Chapter 4 presents the force analysis of a sediment bed consisting of non-cohesive particles subjected to seepage, with the intention of deriving relevant variables which affect sediment transport rate in the presence of seepage. Additionally, dimensional analysis is performed so that three dimensionless group, viz. Einstein's parameter, Shields' parameter without seepage and modified densimetric Froude number are chosen to examine how seepage affects bedload transport rate.

Chapter 5 analyzes the experimental results and investigates the effect of seepage, both injection and suction, on sediment transport rate using the dimensionless groups derived in Chapter 4. The equations for predicting sediment transport rate with seepage in a 2-m length seepage zone are empirically derived. Comparisons between results from previous investigations and the present study are also presented in this chapter.

Chapter 6 discusses the effects of suction zone length on sediment transport rate in the presence of suction. A force analysis is performed to determine the variables which may affect the bedload transport rate with different length of seepage zone in the presence of suction. The measured bedload transport rates with different length of suction zone are presented and discussed, with the intention of deriving the relevant formulae for predicting bedload transport rate with different seepage zone length in the case of suction.

Chapter 7 presents the measured experimental results of the sediment transport rate against time. The effects of time on sediment transport rate are discussed based on these data.

Chapter 8 contains the summary, conclusions and recommendations of this study.

Chapter 2

Literature Review

2.1 INTRODUCTION

Seepage through boundaries of alluvial channels, rivers and streams is a common occurrence due to the porosity of granular material. Water is continuously seeping into or out of the channel bed and banks because of the different levels between the free water surface in the channel and the adjoining groundwater table. Two typical types of seepage can be identified as shown in Fig. 2.1. One is parallel seepage, of which the direction is tangential to the boundary and thus parallel to the free-surface flow. Another type of seepage occurs normal to the boundary, which is referred to as normal seepage.

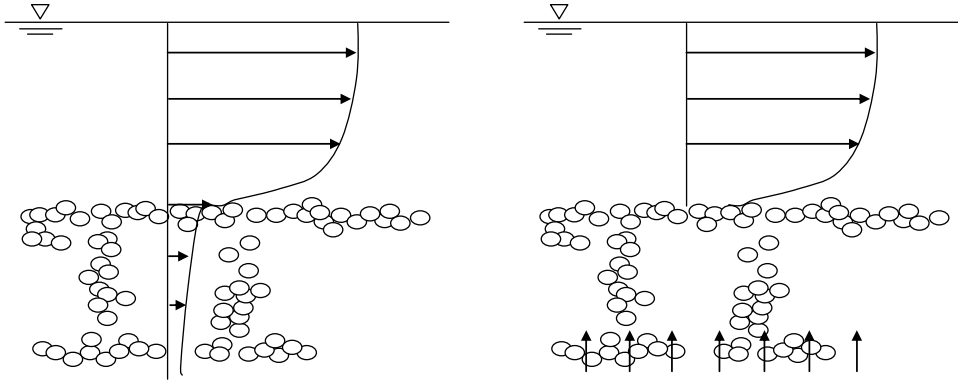

(a) Parallel Seepage (b) Normal Seepage

Figure 2.1 Schematic Diagram of Seepage Definition

To be consistent with the objective of this study, attention in this chapter is placed on previous studies on normal seepage through a permeable boundary. Depending on the direction of mass transfer, normal seepage can either be injection (seepage flow through a channel bed in an upward direction) or suction (seepage flow through a channel bed in a downward direction). Seepage, either injection or suction, through the boundaries of an alluvial channel has a significant influence on the sediment transport behavior on an alluvial channel. The number of studies in this area is significantly less than those associated with a non-porous boundary. Moreover, results from these studies do not lead to a unanimous conclusion. Briefly, some investigators (Oldenziel and Brink, 1974; Richardson et al, 1985; and Francalanci et al, 2008) stated that suction decreases the rate of sand transport whereas injection increases it. However, other researchers, such as Maclean (1991), Ramakrishna Rao and Sitaram (1999), Nielsen et al (2001), Ali et al (2003) and Lu and Chiew (2007) presented an exact opposite conclusion, stating that suction has a tendency to reduce the stability of bed particles, while injection decreases particle mobility on a transporting bed. Although Willetts and Drossos (1975) agreed that over a long zone of uniform suction, the grain transport rate would decrease slowly with distance downstream, yet they reported that under some circumstances suction increases the transport rate over a considerable length of

suction zone. Furthermore, Harrison and Clayton (1970) concluded that the upward seepage had little effect on the stream sediment transport rate even when the bed was quick; in contrast, O'Donnell et al (2002) stated that there is rapid erosion of sediment bed when the submerged weight of sediment particles become zero in the presence of upward seepage, known as quick condition. Lu et al. (2008) presented an extensive review of these studies. A summary of conclusions or inferences drawn from previous investigations is shown in Table 2.1.

Table 2.1 Summary of Previous Studies

Source	Flume Dimensions			Seepage Effects					
	Length (m)	Width (m)	Seepage Zone (m)	Bed Shear Stress		Critical Shear Stress		Sediment Transport Rate	
				Injection	Suction	Injection	Suction	Injection	Suction
Oldenziel and Brink (1974)	15	0.5	4	Decrease	-	-	-	Increase	Decrease
Willetts and Drossos (1975)	3.6	0.076	0.125	-	-	-	-	-	Increase
Richardson et al (1985)	9.45	0.3	3	-	-	-	-	Increase	-
Maclean (1991)	5	0.075	0.13	-	Increase	-	-	-	Increase
Ramakrishna Rao et al (1994)	14.16	0.615	1.275	Increase/ Decrease	Increase/ Decrease	-	-	-	-
Cheng and Chiew (1998a & 1998b)	30	0.7	2	Decrease	-	-	-	-	-

Cheng and Chiew (1999)	7.6	0.21	0.5	-	-	Decrease	-	-	-
Ramakrishna Rao and Sitaram (1999)	3.6	0.1575	2.4	-	-	Increase	Decrease	Decrease	Increase
Chen and Chiew (2004)	30	0.7	2	-	Increase	-	-	-	-
Dey and Zanke (2004)	Analytical Model			-	-	Decrease	-	-	-
Lu and Chiew (2007)	30	0.7	2	-	-	-	-	Decrease	Increase
Francalanci et al (2008)	15	0.61	1.1	-	-	-	-	Increase	Decrease

2.2 SEEPAGE EFFECTS ON BED SHEAR STRESS

Due to the inflow or outflow of water, the environment along the interface between the flow and channel bed in the seepage zone is different from that under no seepage condition. Therefore, the sediment transport behavior is affected by a modified boundary layer. Seepage causes a non-zero vertical velocity on the bottom boundary (Cheng and Chiew, 1998b) and increases turbulence along the interface (Nezu, 1977; Richardson et al, 1985; and Lu et al., 2008). With blowing or injection, the horizontal velocity decreases near the sand bed, while this velocity increases with suction (Oldenziel and Brink, 1974). The change of velocity causes a change in bed shear stress.

Oldenziel and Brink (1974) assumed that the change of bed shear stress due to seepage was contributed by three factors: (1) the variation of energy slope; (2) the momentum difference between the leading (upstream) section and the end (downstream) section of the seepage zone; and (3) the additional momentum losses caused by mixing between the discharge of the channel flow and seepage. They applied the momentum equation to determine the shear stress in the case of injection, and obtained the expression of the excess shear stress as follow

$$\tau_{bs} - \tau_{bo} = \rho g d_{50}\left(I_s - I_o\right) - 2\rho U_o V_s - \frac{2}{3}\rho\eta V_s\left(\frac{L\tau_{bo}V_s}{\rho\nu}\right)^{1/2} \qquad (2.1)$$

where τ_{bs} and τ_{bo} = bed shear stresses with and without seepage, respectively; ρ = mass density of fluid; g = gravitational acceleration; d_{50} = median size of sediment particles; I_s and I_o = energy slopes in open-channel flows, with and without seepage, respectively; U_o = mean flow velocity without seepage; V_s = seepage velocity; η = calibration factor; L = length of the seepage zone; and ν = kinematic viscosity.

They conducted experiments in a rectangular channel with a length of 15 m, a width of 0.5 m, and a test section with length = 4 m. The median grain sizes of the sand used were 0.57 mm, 0.38 mm, 0.22 mm and 0.13 mm. The bed shear stress calculated using Eq. 2.1 was compared with the equation given by Turcotte (1960):

$$\tau_{bs}/\tau_{bo} = 1 - 13.9(V_s/u_{*s}) \qquad (2.2)$$

where u_{*s} = shear velocity with seepage. The experimental data of Oldenziel and Brink (1974) showed that the bed shear stress decreases with the increase of injection rate. Furthermore, they also reported that the grain size of the transported particles is greater than that of the bed particles. This effect is enhanced with suction and is less pronounced for injection.

Maclean (1991) conducted experiments in a tilting perspex flume that was 75 mm wide and 5 m long over a short suction zone (130 mm) with seepage rates raging from 0.36 cm/s to 1.74 cm/s. The bed shear stress in the presence of suction with the sand particle of d_{50} = 1 mm was determined, using the same method as described in Maclean and Willetts (1986), by observation of the threshold condition of motion for indicator grains placed in the suction zone. Figure 2.2 shows his results in terms of a plot of the maximum relative bed shear stress against relative suction velocity. His results were quite close to those computed using the equation suggested by Willetts and Drossos (1975), which is shown below, with full side wall correction.

$$\tau_{bs} = \tau_{bo} + \rho U_{ox} V_s \qquad (2.3)$$

where U_{ox} = velocity at the bed at section x from the beginning of suction zone.

Maclean also compared his results with Fernandez Luque's (1974) equation which is shown as follows

$$\frac{\tau_{bs}}{\tau_{bo}} = \left(\frac{U_{rs}}{U_{ro}}\right)^2 \tag{2.4}$$

where U_{rs} and U_{ro} = velocity at a reference depth with and without seepage, respectively.

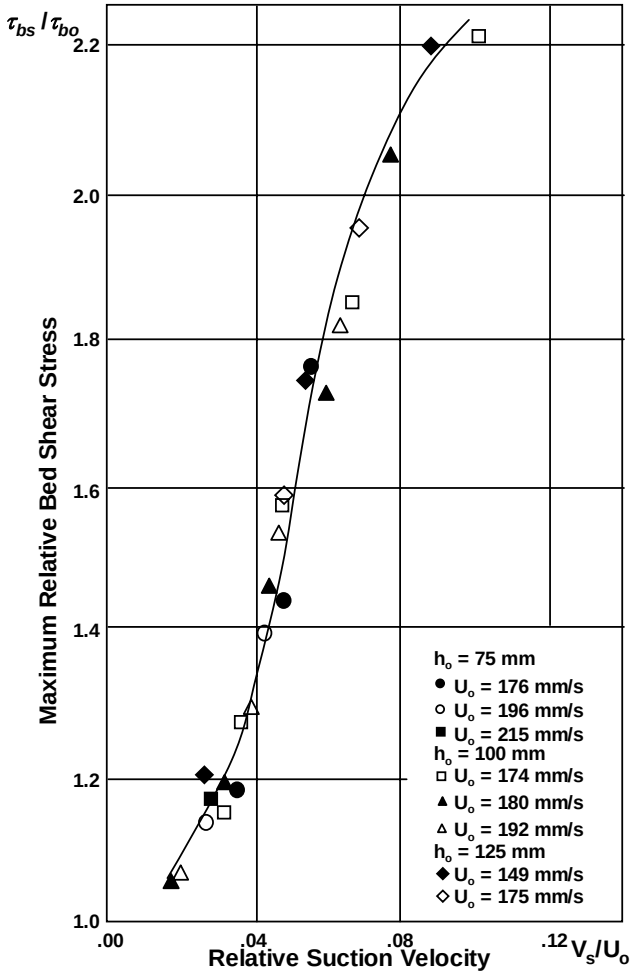

Figure 2.2 Maximum Relative Bed Shear Stress against Relative Suction Velocity (Maclean, 1991)

The value of τ_{bs}/τ_{bo} varies with the arbitrarily chosen reference depth. However, the agreement of these two results suggests that the approach of Fernandez Luque (1974) is at least a sound basis for estimating the bed shear stress (Maclean, 1991). Based on this analysis, Maclean (1991) concluded that the application of enforced

infiltration to the bed of an alluvial channel produces an increase in bed shear stress, and the magnitude of the increased bed shear stress is approximately 2.2 times the undisturbed bed shear stress when the suction velocity is 10% of the mean channel velocity.

Ramakrishna Rao et al (1994) conducted a series of experiments with three sizes of sand (0.34 mm, 0.53 mm and 0.80 mm) to observe the effect of seepage on open-channel flow. The flume used was 61.5 cm wide and 14.16 m long with a 1.275-m length seepage zone. Two types of flow, with and without sediment transport over the sand bed, were considered. A specially designed water jacket was used to supply either upward seepage or downward seepage through the sand bed. They found that the change in the bed shear stress caused by seepage depends on the critical shear stress for sediment entrainment without seepage, the sediment concentration and the seepage velocity. Based on the momentum principle (Chow, 1959) and the experimental results, two empirical relationships were formulated for the estimation of the ratio of the bed shear stress with seepage to that without seepage, τ_{bs}/τ_{bo}.

For a horizontal sand bed with seepage but without sediment transport, the ratio is

$$\frac{\tau_{bs}}{\tau_{bo}} = \left(\frac{\tau_{bo}}{\tau_{co}}\right)^{\pm CN} \pm N \quad \text{valid for} \quad \tau_{bo}/\tau_{co} < 1 \qquad (2.5)$$

where τ_{co} = critical shear stress without seepage; and C = experimental constant. Based on their experimental results, C was empirically determined as 2.7. In Eq. 2.5, the positive and negative signs are used to denote suction and injection, respectively. The parameter N may be termed as “seepage intensity parameter”, which is defined as:

$$\pm N = \frac{2\rho U V_s}{\tau_{bo}} \cdot \frac{R_s}{h} \tag{2.6}$$

where U = mean flow velocity with seepage; h = water depth with seepage; and R_s = hydraulic radius of the bed with seepage. In Eq. 2.6, the absolute value of V_s was used. The direction of seepage flow is denoted by the sign of N.

On the other hand, in the case of flows with sediment transport, a different relationship was proposed to estimate the ratio of the bed shear stresses as follow

$$\frac{\tau_{bs}}{\tau_{bo}} = \left(\frac{600}{c}\right)^{1.75N} + N \tag{2.7}$$

where c = sediment concentration in ppm by weight. Only the data with suction were used in the formulation of Eq. 2.7. Figure 2.3 graphically illustrates Eqs. 2.5 and 2.7.

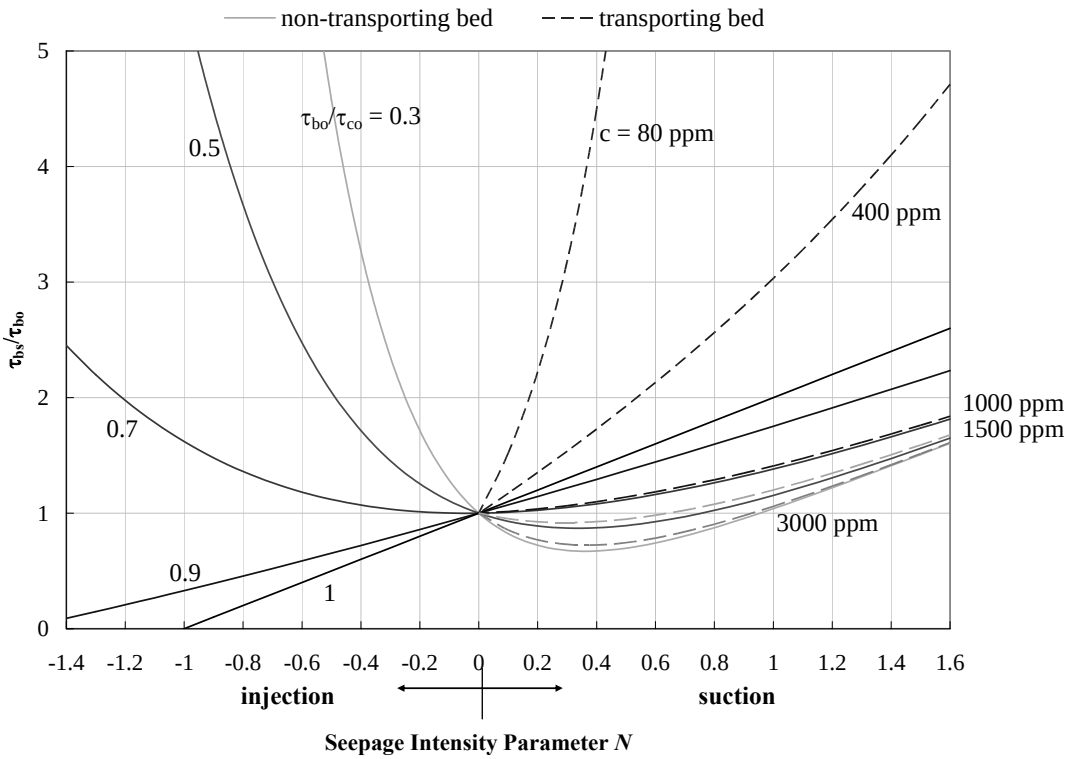

Figure 2.3 Ratios of Bed Shear Stress with Seepage to that without against Seepage Intensity Parameter *N*

Based on this result, Ramakrishna Rao et al (1994) concluded that injection and suction can increase or decrease the bed shear stress when compared to the no seepage condition; the influence is dependent on the shear stress ratio, τ_{bo}/τ_{co}, for initial non-transporting bed, and the sediment concentration c for the initial transporting bed. At the incipient motion of the bed particles, suction increases the bed shear stress, whereas injection decreases it.

Cheng and Chiew (1998b) conducted laboratory experiments in a glass-sided horizontal flume which was 30 m long, 0.7 m wide with a 2-m length seepage zone to measure turbulent open-channel flow subjected to an upward seepage (injection) using a two-dimensional Acoustic Doppler Velocimeter and a minipropeller. Their experimental results show that injection affects the time-mean streamwise velocity, the rms values of the velocity fluctuations, the Reynolds shear stress and the bed shear stress in open-channel flow. With an upward seepage, the increase of the time-average streamwise velocity is more apparent near the free-surface than that near the permeable bed. On the other hand, the rms values of the velocity fluctuations and the Reynolds shear stress exhibit opposite variations, i.e., they increase more rapidly near the bed than that near the surface layer of the flow.

Moreover, they derived a momentum integral equation from the controlling equations for the case of inflow seepage by using an analytical approach. This equation allows the bed shear stress to be computed using the water surface slope, seepage velocity and other flow parameters. The derived equation for bed shear stress computation is expressed as:

$$\tau_{bs} = -\rho g h \frac{dh}{dx}\left(1 - \frac{\beta U^2}{gh}\right) - 2\beta\rho U V_s \qquad (2.8)$$

The parameter β is known as momentum correction factor which is defined as

follows:

$$\beta = \frac{\int_0^h u^2 dy}{hU^2} \tag{2.9}$$

where u = instantaneous velocity in the x axis; and x and y = coordinates tangential and normal to the bottom boundary, respectively. Both the results calculated using the momentum integral equation and those obtained by extrapolating the measured Reynolds shear stress distributions to the boundary show that injection of water leads to a reduction of the bed shear stress.

Cheng and Chiew (1998a) derived a modified logarithmic law (Eq. 2.10) from turbulence kinetic energy equation to account for the effect of upward seepage on the velocity distribution in open-channel flow. The derived expression reverts to the logarithmic law in the absence of seepage.

$$\frac{u}{u_{*s}} = \frac{1}{\kappa}\ln\frac{h}{y_*} + \frac{V_s}{4u_{*s}^2}\left(\frac{1}{\kappa}\ln\frac{h}{y_*}\right)^2 \tag{2.10}$$

where $y_* = k_s \exp\left(-\kappa \cdot R_f\right)$; κ = von Karman's constant ($\cong$ 0.4 in clear water); and k_s = equivalent sand roughness (= $2d_{50}$).

The R_f, which is the roughness function, included in the modified logarithmic law in Eq. 2.10 depends not only on the boundary Reynolds number but also on the dimensionless seepage velocity. They proposed an empirical expression of the roughness function (Eq. 2.11), to enable the application of the modified logarithmic law to various turbulent flows, from a hydraulically smooth regime to a hydraulically rough regime.

$$R_f = \frac{8.5}{1 + V_s/u_{*s}} \tag{2.11}$$

By integrating the modified logarithmic law, the shear velocity is shown to relate to the depth-averaged velocity, water depth, boundary roughness, and seepage velocity as follow:

$$U = \frac{u_{*s}}{\kappa}\left(\ln\frac{h}{y_*} - 1\right) + \frac{V_s}{4\kappa^2}\left[\ln^2\frac{h}{y_*} - 2\left(\ln\frac{h}{y_*} - 1\right)\right] \qquad (2.12)$$

The relationship so obtained can serve as a convenient method to determine the bed shear stress of an open-channel flow with seepage.

Cheng and Chiew (1998a) used Eq. 2.12 to evaluate the bed shear stress over the entire seepage zone. The streamwise variation of the bed shear stress over the seepage zone for upward seepage is shown in Fig. 2.4. The computed results show that the bed shear stress is reduced sharply at the beginning of the seepage zone, followed by a gradual increase toward the downstream end of the seepage zone.

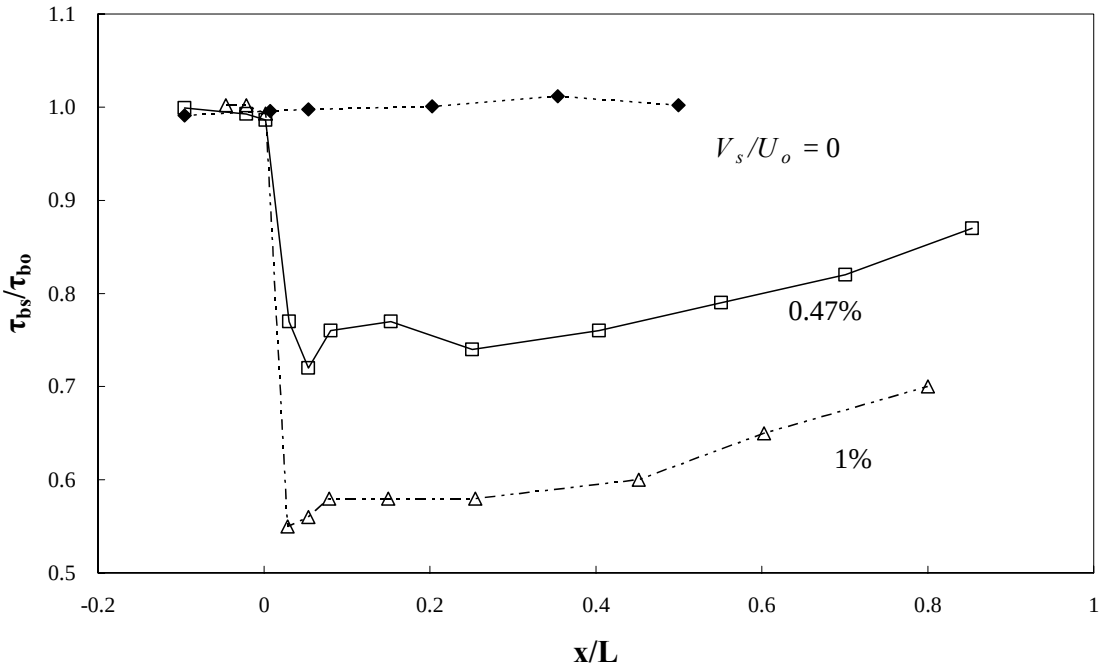

Figure 2.4 Longitudinal Distribution of Bed Shear Stress over Upward Seepage Zone (Cheng and Chiew, 1998a)

Chen and Chiew (2004) investigated the velocity distribution of turbulent open-channel flow with bed suction theoretically and experimentally, and proposed a modified logarithmic law for flows with suction. Besides being a function of flow velocity, water depth and seepage velocity, the bed shear stress under suction was also affected by the original displacement of the velocity profile and slip velocity at the bed surface as follows:

$$\frac{u-u_s}{u_s}=\frac{1}{\kappa}\ln\frac{y+y_o}{y_o}+\frac{V_s}{4u_{*s}}\left(\frac{1}{\kappa}\ln\frac{y+y_o}{y_o}\right)^2 \qquad (2.13)$$

where u_s = slip velocity at the bed surface; and y_o = origin displacement of velocity profile for flow with bed suction. Figure 2.5 shows the schematic definitions of u_s and y_o.

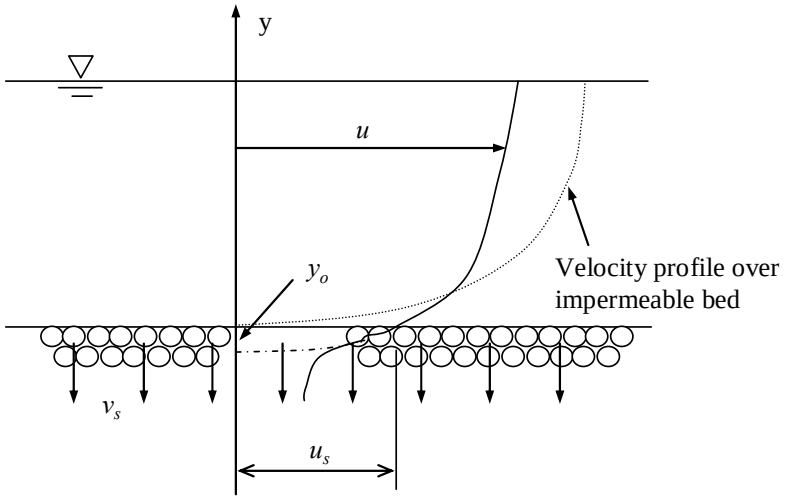

Figure 2.5 Schematic Diagram of Velocity Profile over Permeable Bed with Suction

They conducted experiments in the same 30-m length glass-sided horizontal flume used by Cheng and Chiew (1998a and 1998b). Their data show an increase in y_o, u_s and u_{*s} with increasing relative suction (V_s/U_o). Furthermore, the experimental data also show the occurrence of two flow regions in the suction zone: a transitional region in which the velocity re-adjusts rapidly; and an "equilibrium" zone. Figure

2.6 shows the streamwise variation of dimensionless shear velocity. In the transitional region, the flow is affected by a sudden introduction of bed suction at x = 0, causing the flow to re-adjust, increase in this case, rapidly. Beyond this region, the flow asymptotes towards an "equilibrium" region, because bed suction at this location is "uniform" and the suction velocity remains unchanged (Chen and Chiew, 2004).

By fitting Eq. 2.13 to their experimental data at the mid-section of the suction zone, Chen and Chiew (2004) obtained an empirical equation for bed shear stress with downward seepage or suction in the "equilibrium" region:

$$\frac{u_{*s}}{u_{*o}} = 0.073\left|\frac{V_s}{U_c}\right|^3 - 0.44\left|\frac{V_s}{U_c}\right|^2 + 0.9\left|\frac{V_s}{U_c}\right| + 1 \qquad (2.14)$$

where u_{*o} = shear velocity without seepage; and U_c = mean velocity with seepage at the mid-section of the seepage zone.

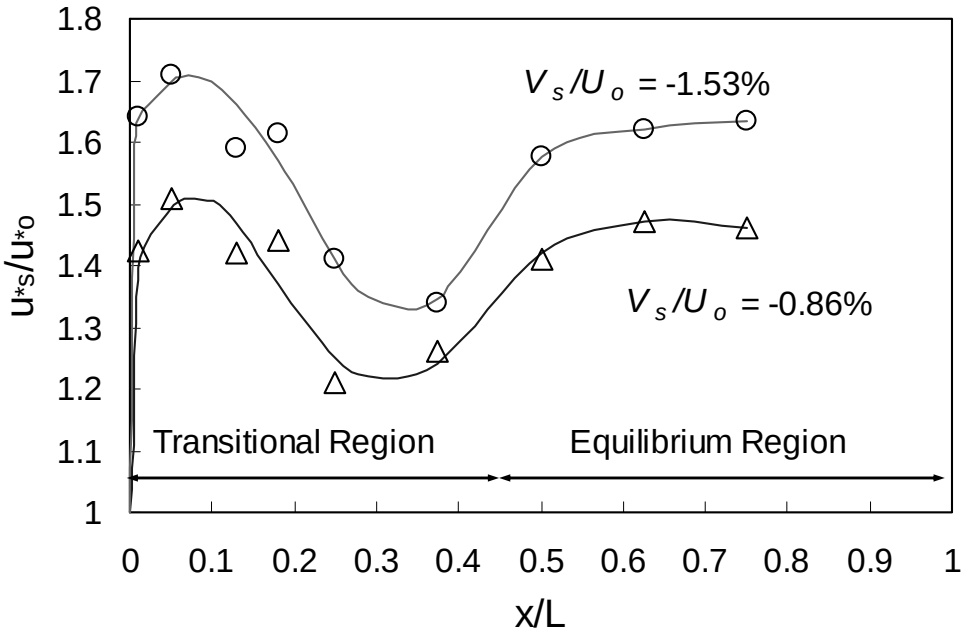

Figure 2.6 Streamwise Variation of Dimensionless Shear Velocity

Comments

Based on the published results on seepage effects on bed shear stress, the general consensus is that injection decreases the bed shear stress whereas suction increases it. As shown in Figs. 2.4 and 2.6, Cheng and Chiew (1998a) and Chen and Chiew (2004) found that at the beginning of the seepage zone, there is a rapid decrease and increase in bed shear stress with injection and suction, respectively. The amount of reduction and increment reduces toward the downstream end of the seepage zone for the case of injection and suction. The reason of these phenomena is the presence of backwater zone, which is located just upstream of the seepage zone as suggested by Francalanci et al. (2008). Due to the backwater effect, the water depth in this zone increases for injection and decreases for suction, compared with that without seepage condition. Therefore, the bed shear stress in the backwater zone decreases and increases for the case of injection and suction, respectively, resulting in a rapid decrease or increase at the upstream end of seepage zone. The water depth gradually increases and decreases toward the downstream end of seepage zone, leading to an increase and decrease in bed shear stress with injection and suction, respectively, compared with those at the upstream end of seepage zone.

The exception is that of Ramakrishna Rao et al (1994), who showed that both injection and suction can increase or decrease bed shear stresses. The reason may be due to the use of a different variable, i.e., the seepage intensity parameter N. According to the definition of N, once the initial flow conditions are predetermined, the change of N is not directly related to the seepage velocity V_s. This means that the increase or decrease in N is not necessarily due to a change of the magnitude of V_s. Therefore, the relationship between τ_{bs}/τ_{bo} and V_s may not be the same as that shown in Fig. 2.3. Nevertheless, they showed that at the incipient motion of the bed particles, suction increases the bed shear stress, whereas injection decreases it,

which is consistent with other published results.

2.3 SEEPAGE EFFECTS ON INCIPIENT SEDIMENT MOTION

When seepage velocity is introduced to a sand bed, there is an additional seepage force exerting on the sediment particles. Therefore, the incipient sediment motion, also called threshold condition, which is the condition at which sediment particles just begin to move, is expected to change. The bed shear stress, at which the incipient sediment motion occurs, is defined as critical shear stress for sediment particles. To-date, three studies can be found in the literature in which seepage effects on incipient sediment transport of cohesionless particles are investigated. These findings are presented in this section of the thesis.

Ramakrishna Rao and Sitaram (1999) modified the C-value of Eq. 2.5 that were derived previously by Ramakrishna Rao et al (1994) to 2.2 instead of 2.7 for fitting a wider range of experimental data (0.32 – 3 mm size uniform sand). Furthermore, they introduced equations for critical shear stress under a "pseudo-incipient motion", which they defined as the incipient motion of particle on a plane and stationary bed due to the application of suction or injection. The bed shear stress under the pseudo-incipient motion, calculated using Eq. 2.5 with C = 2.2, was then designated as τ_{cs}, critical shear stress with seepage. The computed values of τ_{cs}/τ_{co} are plotted against τ_{bo}/τ_{co} in Fig. 2.7. Figure 2.7 (a) and (b) show the experimental data collected under the pseudo-incipient motion with suction and injection, respectively. Based on the data shown in Fig. 2.7, Ramakrishna Rao and Sitaram (1999) presented an empirical correlation between τ_{cs}, τ_{bo} and τ_{co} as follows:

$$\ln\left(\frac{\tau_{bo}}{\tau_{co}}\right) = -0.2525\left(\frac{\tau_{cs}}{\tau_{co}}\right)^{-2.917} \quad \text{for} \quad \tau_{bo}/\tau_{co} < 1 \tag{2.15}$$

$$\ln\left(\frac{\tau_{bo}}{\tau_{co}}\right) = 0.2525\left(\frac{\tau_{cs}}{\tau_{co}}\right)^{1.68} \quad \text{for} \quad \tau_{bo}/\tau_{co} > 1 \tag{2.16}$$

Equation 2.15 is used for the case of initial non-transporting bed with suction, whereas Eq. 2.16 is used for the initial transporting bed with injection.

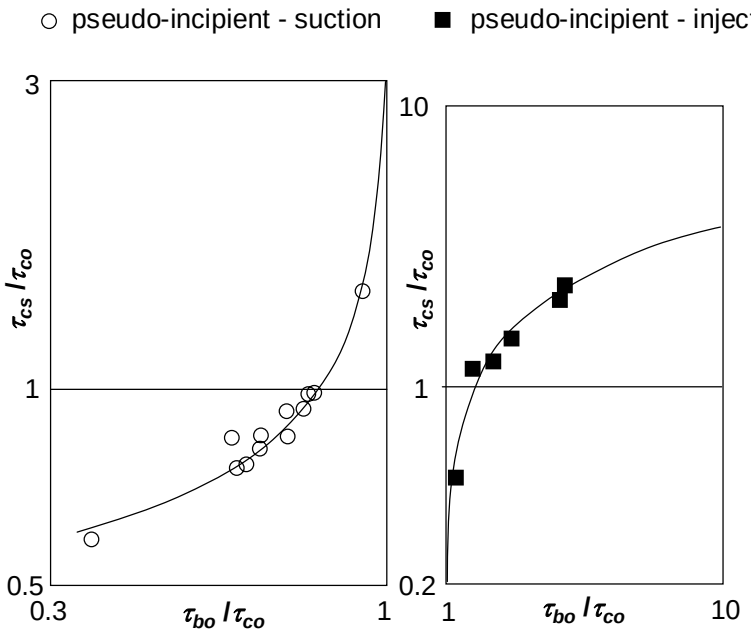

(a) (b)

Figure 2.7 Pseudo-incipient Motion with Seepage (Ramakrishna Rao and Sitaram, 1999)

Cheng and Chiew (1999) examined the effect of upward seepage on the critical condition of incipient sediment motion. The critical condition was established by analyzing the forces acting on a sediment particle lying on a permeable bed subject to normal seepage. They found that the critical shear velocity is reduced in the presence of upward seepage. The ratio of the critical shear velocity with seepage to that without seepage is expressed as a function of the ratio of the hydraulic

gradient of seepage to its value at the quick condition as follow:

$$\left(\frac{u_{*cs}}{u_{*co}}\right)^2 = 1 - \frac{i}{i_c} \tag{2.17}$$

where u_{*cs} and u_{*co} = critical shear velocity with and without seepage, respectively; i = hydraulic gradient with seepage; and i_c = hydraulic gradient at quick condition.

To relate the hydraulic gradient to the seepage velocity, Darcy's law (Bear, 1988) was generalized using an exponential function, as shown in Eq. 2.18, so that it can be applied to the porous medium consisting of coarse grains. The general relation between the hydraulic gradient and the seepage velocity is substantiated using experimental results for uniform cohesionless sediments.

$$i = \alpha V_s^{\ m} \tag{2.18}$$

where α = empirical coefficient; and m = exponent = 1-2. Substituting Eq. 2.18 into Eq. 2.17 yields

$$\left(\frac{u_{*cs}}{u_{*co}}\right)^2 = 1 - \left(\frac{V_s}{V_{sc}}\right)^m \tag{2.19}$$

where V_{sc} = critical seepage velocity under quick condition. The ratio of the critical shear velocity with seepage to that without seepage, u_{*cs}/u_{*co}, can thus be expressed as a function of the ratio of the seepage velocity to its critical value at the quick condition, V_s/V_{sc}. By fitting experimental data to Eq. 2.19, m was found to be:

$$m = \frac{1 + 2\delta \cdot l_{\varepsilon *}^2}{1 + \delta \cdot l_{\varepsilon *}^2} \tag{2.20}$$

where $l_{\varepsilon *}$ = dimensionless characteristic dimension of void $= \left(\frac{g}{\nu^2}\right)^{1/3} \frac{n \cdot d_{50}}{6(1-n)}$; δ = boundary layer thickness; and n = porosity.

The experimental data were analyzed to confirm that upward seepage through a

permeable bed affects the critical condition of sediment entrainment. Figure 2.8 shows their results of the critical shear velocity plotted against the injection rate for the three cohesionless sediments used (d_{50} = 0.63 mm, 1.02 mm, and 1.95 mm). For a particular size of sediment, the critical shear velocity is found to decrease significantly with increasing injection velocity.

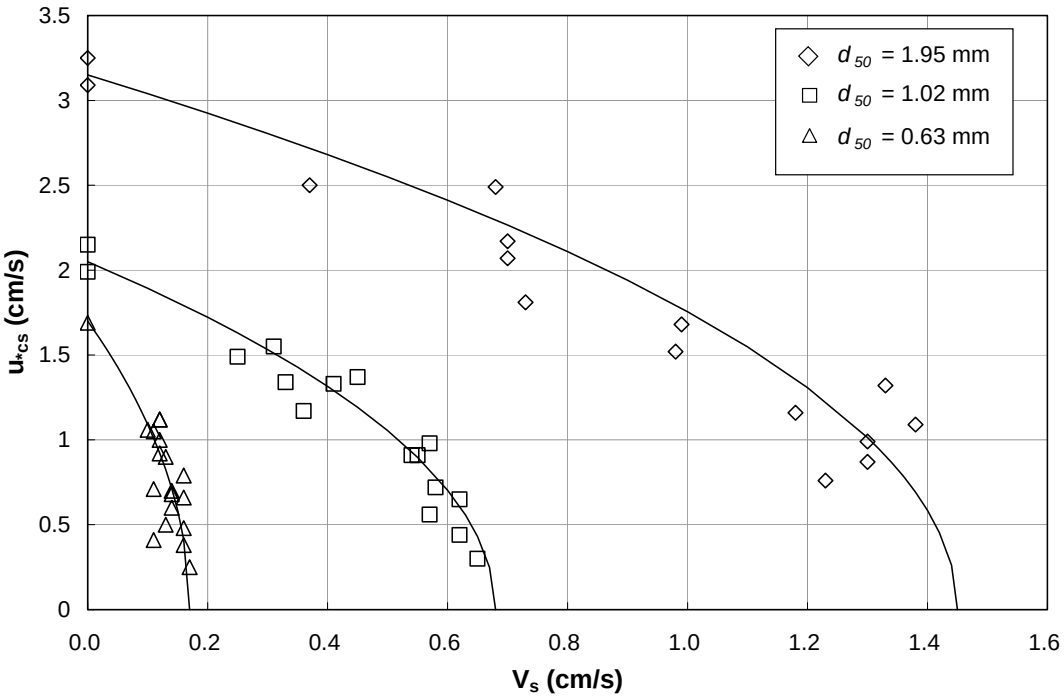

Figure 2.8 Reduction of Critical Shear Velocity Caused by Upward Seepage (Cheng and Chiew, 1999)

Dey and Zanke (2004) presented an analytical model to determine the critical bed shear stress for non-cohesive sediment motion subject to upward seepage on a horizontal sedimentary bed. They analyzed the hydrodynamics of the flow, seepage and micro-mechanical forces acting on a solitary sediment particle resting over a sedimentary bed under the slip-spinning conditions. In their model, they simulated the most stable three-dimensional configuration of a spherical solitary sediment particle of diameter *D* resting over three closely packed spherical particles

of identical diameter d forming the sedimentary bed in a unidirectional stream flow. The definition sketch of their model is shown in Fig. 2.9, in which γ = factor; δ = boundary layer thickness; X = horizontal lever arm; Z = vertical lever arm; F_L = lift force; F_D = drag force; and F_S = seepage force.

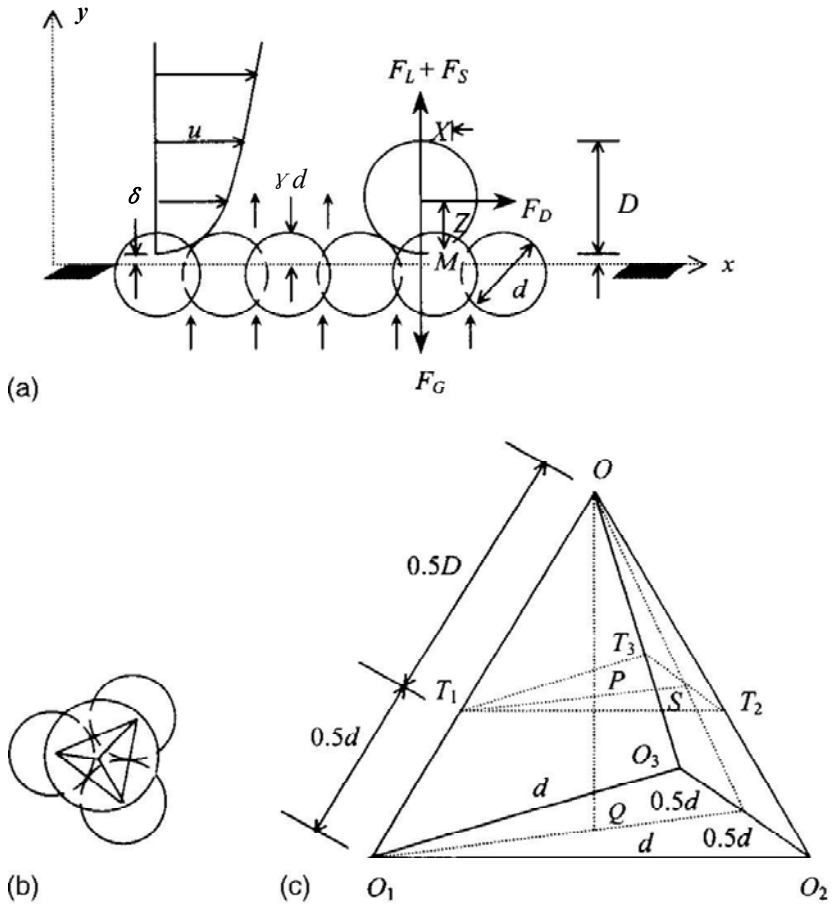

Figure 2.9 Definition Sketch of the Model in Dey and Zanke (2004): (a) diagrammatic presentation of forces acting on spherical solitary particle under stream flow with upward seepage; (b) top view of solitary particle resting over three closely packed bed particles; and (c) tetrahedron formed joining centers of four particles

Experimental data of sediment threshold with upward seepage reported by Cheng and Chiew (1999) were used to compare the results obtained from their analytical model, as shown in Fig. 2.10. The model showed a satisfactory agreement with

the experimental data; confirming that critical shear stress of sand particle decreases with the increase of injection.

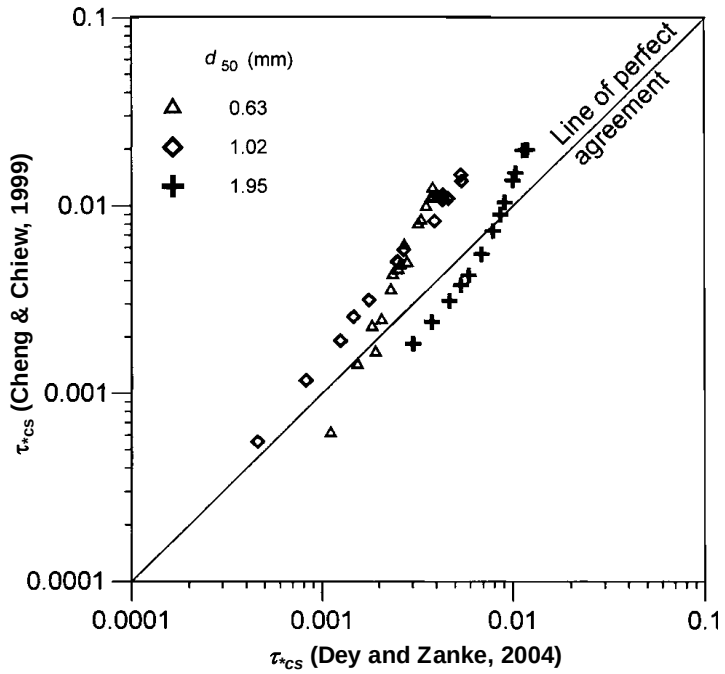

Figure 2.10 Comparison of Values of τ_{*cs} Computed Using the Model Derived by Dey and Zanke (2004) and Experimental Data of Cheng and Chiew (1999)

Comments

Both Cheng and Chiew (1999) and Dey and Zanke (2004) concluded that the critical shear velocity decreases with an increase of injection. The effects of suction on sediment incipient motion as yet have not been investigated in the literature. Even though the empirical equations has been proposed by Ramakrishna Rao and Sitaram (1999) to account for the effect of injection and suction on the incipient sediment condition for sediment transport, they cannot be generally applied. This is because they do not allow a change in seepage velocities, and hence are only valid for a specific condition.

2.4 SEEPAGE EFFECTS ON SEDIMENT TRANSPORT

Since seepage affects both bed shear stresses and incipient sediment motion, it likely will also have significantly influence on sediment transport rate. If the sediment transport rate within the seepage zone is different from that at the upstream section, erosion or deposition occurs. These phenomena are important for the studies of natural rivers subjected to infiltration or upward seepage (Owoputi and Stolte, 2001) and bed and bank stabilities (Shen, 1971; and Fox et al, 2005).

Oldenziel and Brink (1974) reported that the number of particles transported per unit width per unit time, n_o, was increased by inflow seepage and decreased by suction. The relative value of the sediment transport rate $n_o(V_s)/[n_o(V_s = 0)]$ is plotted as a function of the hydraulic gradient in the sand bed as shown in Fig. 2.11 for a constant flow discharge through the channel. For the case of injection, the relation of the sand with d_{50} = 0.13 mm and 0.38 mm was different from that of the sand with d_{50} = 0.23 mm and 0.57 mm. In contrast, for the case of suction, there was no difference for the sand with d_{50} = 0.38 mm and 0.57 mm. The reason of these phenomena was not explained by Oldenziel and Brink (1974).

Furthermore, they also found that in the absence of seepage the median size of the transported particles was greater than that of the bed sediment. With increasing rates of transport, the medium grain size decreased and approached the grain size of the sand bed. This change in the median size of sediment became more obvious for a downward seepage but less pronounced for an upward seepage.

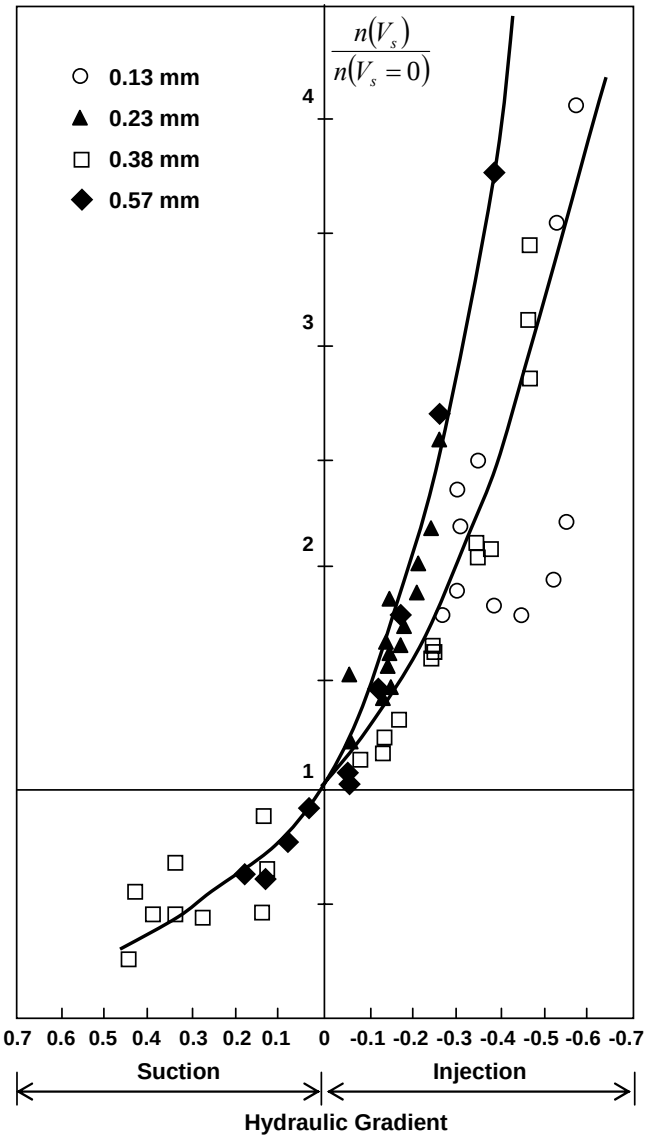

Figure 2.11 Sand Transport with Injection and Suction (Oldenziel and Brink, 1974)

Willetts and Drossos (1975) studied downward seepage or suction effects with a short seepage zone (125 mm long) in the flume which is 76 mm wide and 3.6 m long. They observed that with medium sand (d_{50} = 0.73 mm, 1.03 mm and 1.30 mm) suction always produced a localized scour hole in the seepage zone and a dune at its downstream end, and the scour hole quickly reached its stable size and shape. To compute the sediment transport rate over the seepage zone, Willetts and Drossos assumed that the erosion rate caused by seepage was proportional to the modified Shields parameter, which is defined as

$$\tau_{*s} = \frac{\zeta \tau_{bs} d_{50}^2}{\xi \rho g (S_s - 1) d_{50} + F_s} \tag{2.21}$$

where τ_{*s} = Shields' parameter with seepage; ζ and ξ = constants dependent on the shape of particles; S_s = specific gravity of sand particle; and the seepage force acting on a particle, F_s, was expressed as

$$F_s = \frac{4\pi}{3K} \rho g V_s d_{50}^3 \tag{2.22}$$

where K = coefficient of permeability. With the aid of Einstein's assumption on the erosion rate, Willetts and Drossos (1975) obtained an expression for the erosion rate in the presence of seepage as follows

$$r_e = \frac{q_{bo}}{\lambda d_{50}} \frac{\tau_{bs}}{\tau_{bo}\left[1 + \frac{V_s}{(S_s - 1)K}\right]} \tag{2.23}$$

where r_e = volumetric sediment erosion rate per unit width; q_{bo} = sediment transport rate under zero seepage; and λ = step length ratio = 100.

Willetts and Drossos (1975) stated that the method proposed was only suitable for a short seepage zone. However, based on their observations, they deduced that the grain transport rate would be expected to decay slowly with distance downstream in a long zone of uniform suction.

Richardson et al (1985) conducted experiments in an sediment-recirculating open-channel flume that was 0.3 m wide, 9.45 m long and a 3.0-m length suction zone. They noted that upward seepage can cause significant changes to the geometry of bedforms. The effect of upward seepage on stream power, water surface slope, flow depth, velocity and sediment transport was investigated. Both the stream power and water surface slope increase as inflow seepage increases. Since the flow depth is directly proportional to the stream power, a reduction in specific energy resulted in a decrease in flow depth for subcritical flow and an increase for supercritical flow. The upward seepage resulted in an increase in the mean stream velocity for lower regime flows, but a slight increase in velocity for upper regime flows. Richardson et al (1985) also observed that the sediment discharge in low regime flows was found to increase with an upward seepage as compared with that under the no-seepage condition. However, for upper regime flows, sediment transport was inhibited by upward seepage. For example, a low upward seepage discharge (0 ~ 0.8 l/s) increased the sediment transport rate by up to 23% for a channel discharge less than 18.9 l/s. The same amount of seepage reduced the sediment transport rate by up to 32% for a channel discharge greater than 18.9 l/s.

Maclean (1991) applied the concept of step length suggested by Einstein (1950), and derived the expression for calculating the local erosion rate under suction as follows

$$r_e = (1-n)\frac{\partial y_s}{\partial t} + \frac{q_{bs}}{\lambda d_{50}} \qquad (2.24)$$

where n = porosity; y_s = scour depth; t = time; and q_{bs} = sediment transport rate per unit width with seepage. The so-obtained erosion rates under different suction rate (Maclean and Willetts, 1984 and 1986) are tabulated in Table 2.2.

Table 2.2 Erosion Rate under Different Suction Velocity (Maclean and Willetts, 1984 &1986)

Test Number	U_o *(m/s)*	$\lvert V_s/U_o \rvert$ *(%)*	h_o *(mm)*	τ_{bo} *(N/m^2)*	r_e *(mm/s)*
M1	0.294	0.094	100	0.494	0.00562
M2	0.339	0.052	75	0.683	0.00848
M3	0.339	0.063	75	0.683	0.01778
M4	0.392	0.065	75	0.912	0.02683
M5	0.392	0.055	75	0.912	0.03433
M6	0.392	0.071	75	0.912	0.04047

Furthermore, he observed a clear linear relationship between the final scour depth y_{sm} and the ratio $(\tau_{bs} - \tau_{cs})/\tau_{cs}$ (as shown in Fig. 2.12), where τ_{cs} for the 1-mm-diameter bed grains was determined from a threshold value of 0.033 for the modified Shields shear parameter of Willetts and Drossos (1975). Maclean (1991) finally concluded that the infiltration through the river bed causes local scour. As scour developed, the near bed velocity decrease until the bed shear stress falls to the threshold value and the rate of scour decreases until eventually a stable bedform is achieved for a given suction velocity.

In addition, he suggested that the net rate of erosion was directly equivalent to the rate at which particles are eroded from rest, and not merely the difference between the rate of erosion and the rate of deposition.

On the other hand, Maclean (1991) observed that as scour developed and the bed shear stress decreased, the effect of grain deposition again became significant, until eventually a balance between erosion and deposition was re-established and the bedforms stabilized.

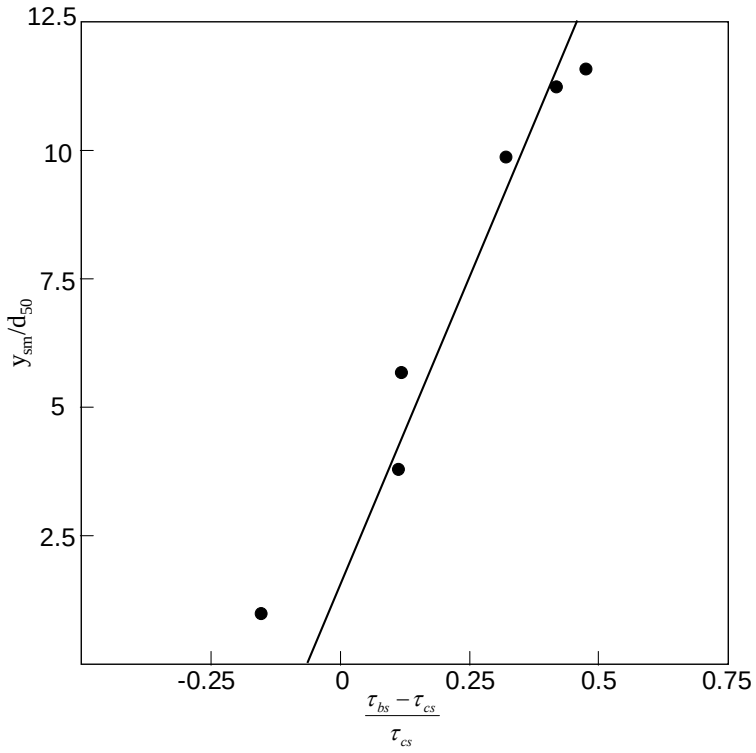

Figure 2.12 Relationship between Maximum Depth of Scour and Bed Shear Stress in Presence of Suction (Maclean, 1991)

Lu and Chiew (2007) conducted experiments in a horizontal glass-sided flume (30 m long and 0.7 m wide) with a 2-m long seepage zone, and studied seepage effects on the dimensions of a dune, viz. its height, length and lee-side slope. The critical slope with seepage of cohesionless material, which is also called the angle of repose, was found to be related to the ratio of the hydraulic gradient with seepage to its critical value under quick condition, i.e. i/i_c. Moreover, they assumed that in the case of seepage the stable lee-side slope of a dune inclines at the critical slope with the same seepage rate. Figure 2.13 shows their measured critical slope against the relative seepage hydraulic gradient, i/i_c, for the three sediment used in their tests (d_{50} = 0.9 mm, 1.41 mm and 1.64 mm), and the fully developed lee-side slope of dunes. As shown in Fig. 2.13, the critical slope and the lee-side slope of dunes decrease with increase of injection, and increase with increase of suction.

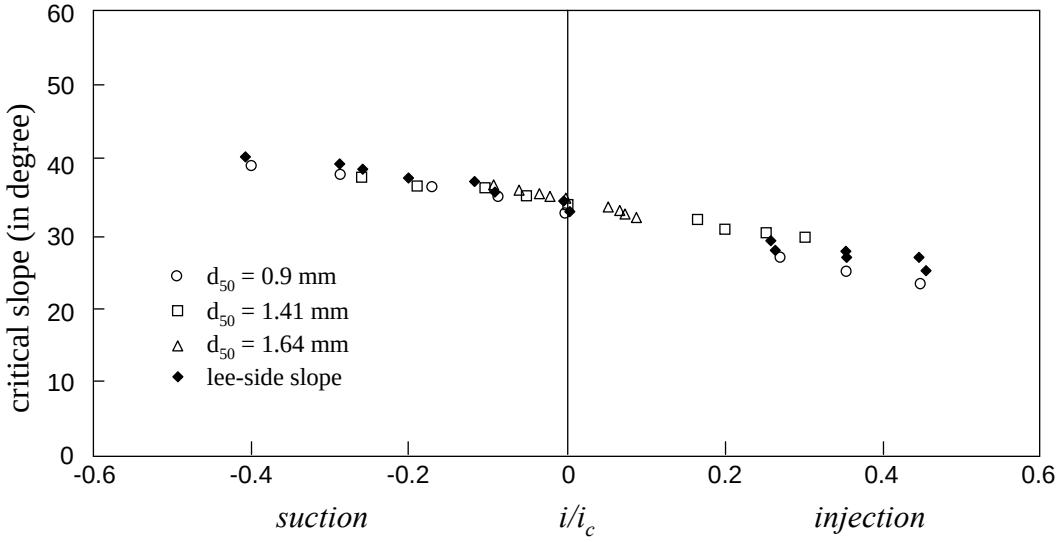

Figure 2.13 Seepage Effect on Critical Slope and Lee-Side Slope of Dune (Lu and Chiew, 2007)

Furthermore, they observed that the height and the length of the dune were reduced when injection is present; while suction increases them. The experimental results of the ratio of the developed dune height H to the original dune height without seepage H_o are plotted against i/i_c in Fig. 2.14 for two cases of undisturbed flow condition, in which h_o = flow depth without seepage.

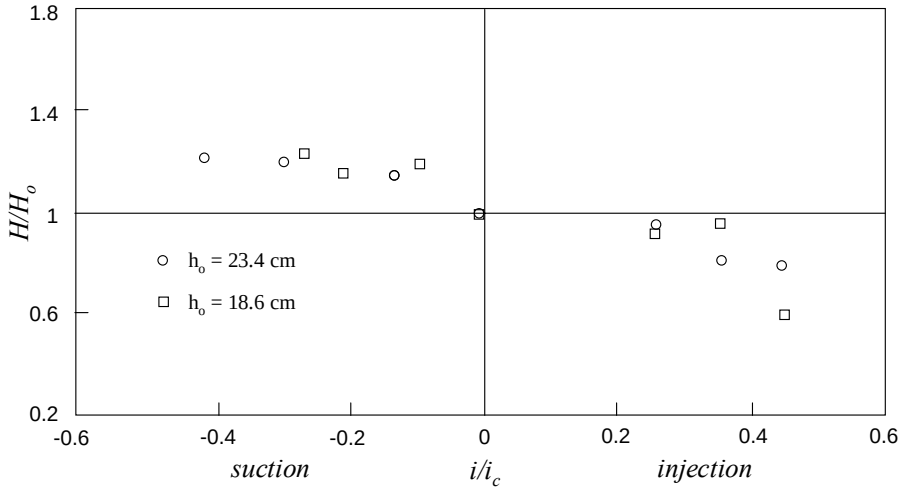

Figure 2.14 Seepage Effect on Dune Height (Lu and Chiew, 2007)

It can be concluded from their experimental findings that injection decreases the dune height, length and lee-side slope, whereas suction increases them. A plausible explanation of these phenomena is related to changes of the dune celerity. Their experimental data showed that a dune moves faster or slower when it propagates into the seepage zone subjected to suction and injection, respectively. Figure 2.15 shows the data associated with seepage effects on dune celerity, which refers to the speed of a point on the dune crest. However, it was observed that the succeeding dune, which lies outside the seepage zone, still moves at the undisturbed celerity.

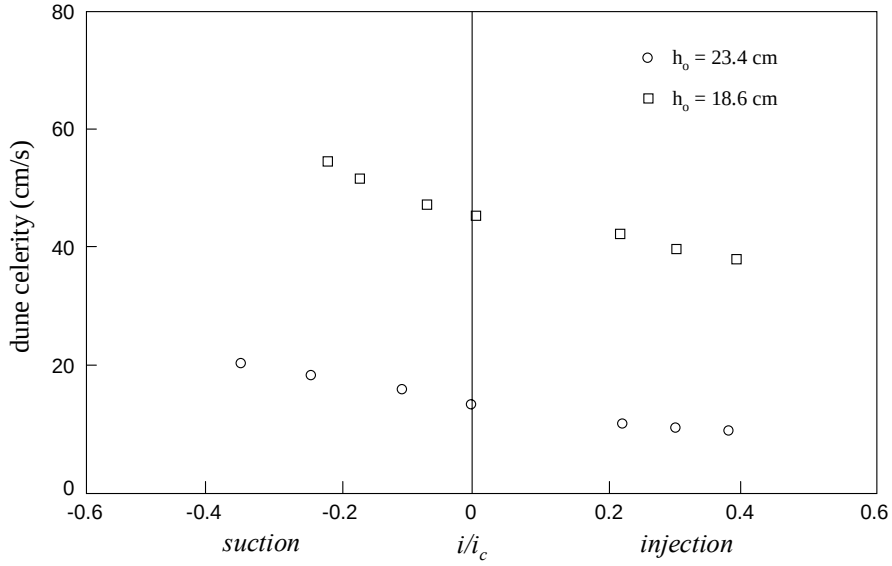

Figure 2.15 Seepage Effects on Dune Celerity (Lu and Chiew, 2007)

Francalanci et al (2008) presented both experimental and numerical studies on seepage effects on bedload transport rate. By considering the seepage induced nonhydrostatic pressure distribution (Francalanci, 2006), they proposed a generalized Shields number for the case of seepage, τ_{*s} as follow

$$\tau_{*s} = \frac{\tau_{bs}}{\left[\rho_s - \rho\left(1+\frac{V_s}{K}\right)\right] g d_{50}} \tag{2.25}$$

where ρ_s = density of particle; and K = permeability.

The experiments were conducted using sediment particles with d_{50} = 0.84 mm in a glass-sided sediment-recirculating, water-feed flume for both seepage and no-seepage conditions. The flume, which was 15 m long, 0.61 m wide and 0.4 m deep, has a seepage zone that is 1.1 m long. Based on their experimental results measured in the absence of seepage, they empirically obtained the bedload transport rate equation as follow

$$\Phi_o = \frac{q_{bo}}{\sqrt{d_{50}^3 g\left(S_s - 1\right)}} = 4.4158\left(\tau'_{*o} - \tau_{*co}\right)^{1.5} \tag{2.26}$$

where Φ_o = Einstein's parameter without seepage; τ'_{*o} = Shields number associated with skin friction; and the value of critical Shields' parameter without seepage, τ_{*co}, was estimated to be 0.0332, in accordance with the criteria of Shiels (1936). Equation 2.25 is similar to the corrected form of the bedload transport equation of Meyer-Peter and Muller (1948) given in Wong and Parker (2006).

Their experimental results measured in the presence of seepage showed that upward seepage (injection) induces scour and downward seepage (suction) causes deposition. It may be inferred from their results that injection and suction increases and decreases bedload transport rate, respectively.

Francalanci et al (2008) introduced the idea of a backwater zone which is just

upstream of the seepage zone. The profiles of flow depth h and bed shear stress τ_{bs} immediately after the commencement of upward seepage over a short zone are schematized in Fig. 2.16. Upward seepage creates a backwater effect upstream, such that h increases and bed shear stress τ_{bs} decreases according to that shown in the figure. Hence, the bed shear stress in the middle of the seepage zone is less than that when seepage is absent, but above the bed shear stress in the backwater zone immediately upstream of the seepage zone. This pattern causes deposition in the backwater zone upstream of the zone of upward seepage, but scour in the seepage zone itself. The pattern is reversed in the case of downward seepage.

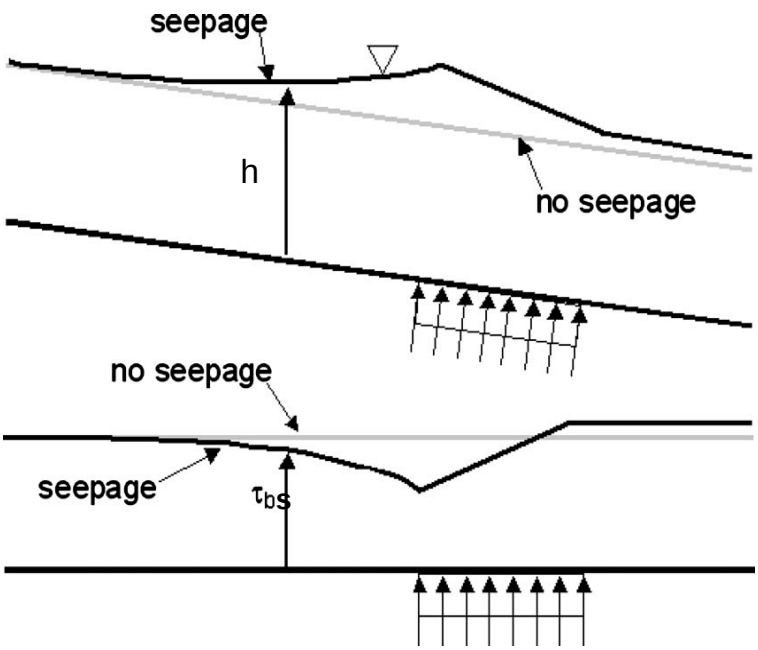

Figure 2.16 Schematic Diagrams Showing Patterns of Flow Depth and Bed Shear Stress Induced by Short Zone of Upward Seepage

Comments

According to previous investigations on seepage effects on sediment transport, there are two groups of researchers. The first group, viz. Oldenziel and Brink (1974), Richardson et al (1985), and Francalanci et al (2008), stated that injection increases the sediment transport rate, whereas suction decreases it. On the other hand, Willetts and Drossos (1975), Maclean (1991) and Lu and Chiew (2007) obtained the opposite findings. By carefully comparing the experimental setups and procedures of those investigations, the flume types used during the tests are different. Richardson et al (1985) and Francalanci et al (2008) used sediment-recirculating flume, whereas the others chose sediment-feed flume. This may be the reason leading to the discrepancy of the conclusions.

Willetts and Drossos (1975) mentioned that their observations were only valid for a short seepage zone, and agreed that the sediment behaviour might be different in a long zone of uniform suction. Therefore, besides the seepage velocity, the seepage zone length should also affect the sediment transport.

As mentioned in Maclean (1991), the erosion rate caused by downward seepage decreased with time, and the bedform was eventually stabilized. One may infer from observation that the sediment transport rate is changing with time while seepage is applied. Hence, the sediment transport behaviour is affected by time too.

2.5 SUMMARY

Results from the above limited studies of seepage effects on the sediment transport behavior, especially bedload transport rate, do not lead to a unanimous conclusion. Moreover, even though the sediment transport behavior has already been studied by several researchers, so far, only the erosion rate and the scour depth have been investigated (Willetts and Drossos, 1975; Maclean, 1991; and Francalanci et al, 2008). Direct measurement of sediment transport rate as yet has not been conducted. To this end, the direct measurement of the bedload transport rate is necessary to study the effect of seepage on sediment transport, with the intention of deriving a general formula for predicting bedload transport rate with seepage. Published results by Maclean (1991), Ramakrishma Rao and Sitaram (1991), and Francalanci et al (2008) are used to compare with results obtained and inference drawn from the present study. The similarities and differences of these studies are highlighted.

Chapter 3

Experimental Apparatus and Measurement Techniques

3.1 INTRODUCTION

This chapter describes the apparatus and techniques used in all the experiments conducted in this study. The experiments consisted of four series of tests. The first was designed to determine the time-average streamwise flow velocity without seepage. The experimental data in this series are used as the undisturbed flow conditions for the analyses in Chapters 5 to 7.

The second series was designed to investigate the influence of seepage on sediment transport rate in open-channel flow. Both upward and downward seepage are taken into consideration. Further discussions of the experimental results are presented in Chapter 5.

The effect of seepage zone length on sediment transport rate was investigated in the third series of experiments. This series was measured with three types of suction

zone length in the presence of downward seepage. The experimental results are further discussed in Chapter 6.

The last series of experiments were used to investigate the variation of sediment transport rate with time. The experimental data were presented and discussed in Chapter 7.

3.2 EXPERIMENTAL APPARATUS

The experimental apparatus included an open-channel flume with a sand trap. The equipment used for measurement is described in the following sections.

3.2.1 Open-Channel Flume

The glass-sided horizontal flume, which is 30 m long, 0.7 m wide and 0.6 m deep, was supported on a steel truss. Figure 3.1 shows the schematic diagram of the flume and its auxiliary facilities.

As shown in Figure 3.1, the flume was divided into three reaches: the upstream section, test section and downstream section. Water was supplied to the flume using a submersible pump installed in the laboratory reservoir. The flume pumping system was capable of recirculating up to a maximum of 200 L/s of water. The flow rate in the flume, monitored with an electromagnetic flow meter, was controlled using a speed inverter and valve. At the entrance to the flume, flow straighteners were installed to minimize large scale turbulence and circulations. The 12-m-long upstream reach together with the head tank (see Fig. 3.1), permitted stabilization of the flow.

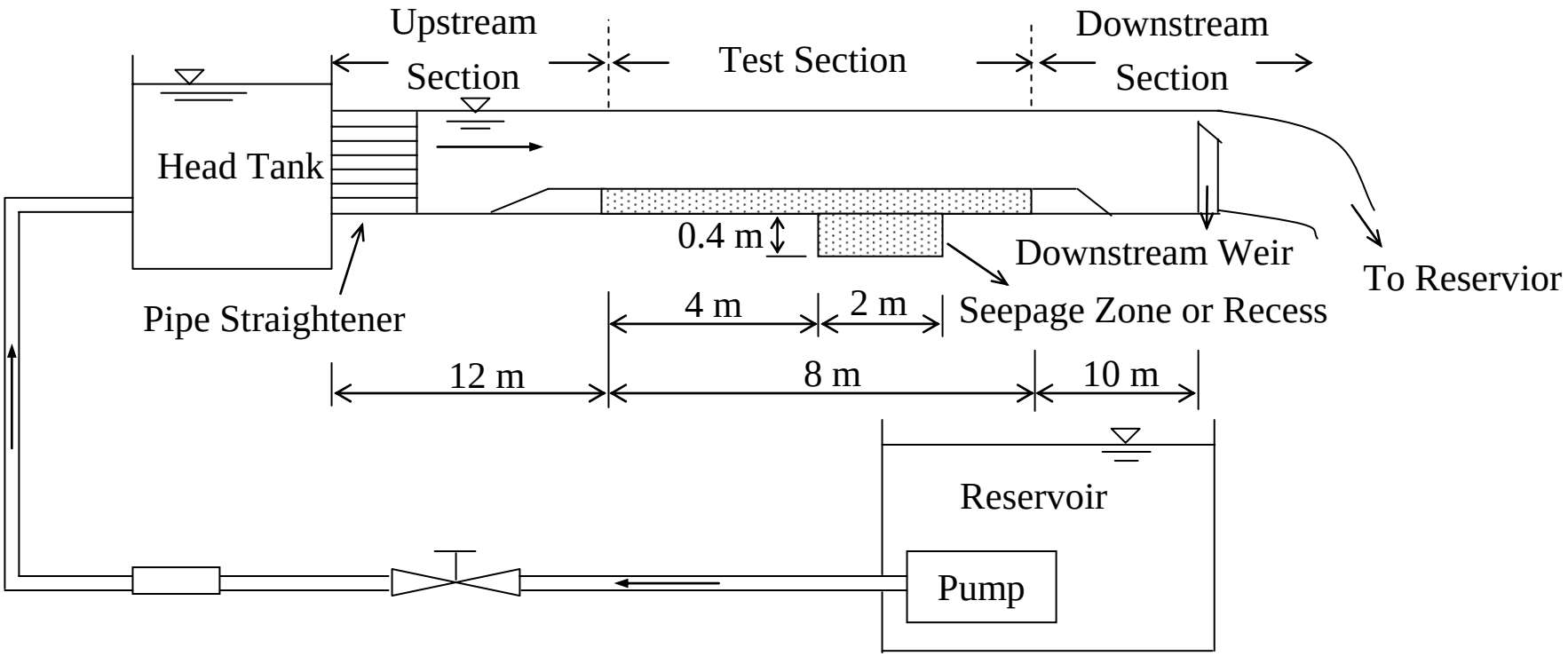

Figure 3.1 Schematic Diagram of Open-Channel Flume (Drawing not to Scale)

Located in the middle reach of the flume with length = 8 m was the test section that included a seepage zone in the form of a recess. The seepage zone, where either upward or downward seepage can be introduced, was 2 m long, 0.4 m deep, and spans the width of the flume. The seepage zone was designed to ensure uniform seepage velocity over the entire area. The setup of the seepage recess is schematically shown in Fig. 3.2. The permeable bed in the seepage zone was leveled to the elevation of the adjacent bed. Sand was placed on top of a filter cloth, which in turns, overlay a perforated metal plate. The use of the filter net prevented the sediment particles from falling to the bottom of the recess, which might clog the pipe holes. Water was allowed to seep through the perforated plate, filter net and sand layer to ensure uniform seepage flow within the granular materials.

In the case of suction, twelve identical pipes, each with a valve to control suction discharge, were fixed onto the bottom of the recess to drain water out uniformly. On the other hand, a separate submersible pump, whose capacity is up to a maximum of 20 L/s, installed in the laboratory reservoir was used to generate injection; its flow discharge, which was regulated using a speed inverter and valve, was monitored using a flow meter. The capacity of the pump is sufficient to provide the upward discharges which were tested in previous investigations (Oldenziel and Brink, 1974; Richardson et al., 1985; Cheng and Chiew, 1998a & 1998b; Ramakrishna Rao and Sitaram, 1999; and Fracalanci et al., 2008). Before water seeps through the granular materials, it was first pumped through the perforated pipes with identical diameter holes to ensure uniform seepage velocity in the entire seepage zone.

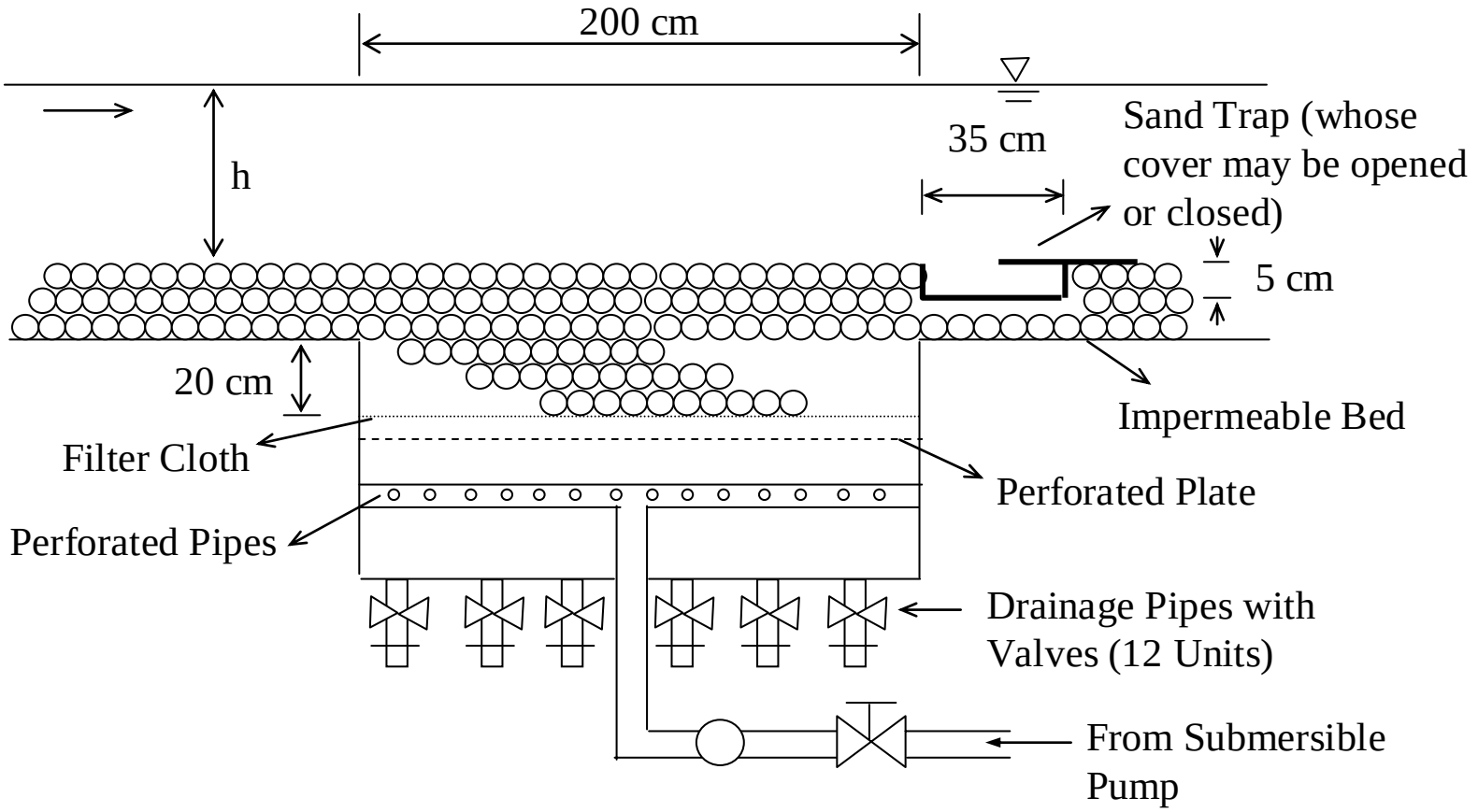

Figure 3.2 Schematic Diagram of Test Section (Drawing not to Scale)

The downstream reach occupied the last 10 m of the flume. It served as an outlet section to minimize backwater effects on the test section. A tailgate weir, which was placed at the end of the flume, allowed adjustment of the water depth.

3.2.2 Sand Trap

A transparent sand trap, which was 35 cm long, 70 cm wide and 5 cm deep, was placed directly downstream of the seepage zone. Figure 3.2 shows the schematic diagram of the position of sand trap. The photo of the sand trap is shown in Fig. 3.3. Steel sticks could be inserted into holes drilled onto the cover of sand trap. This set-up allowed one to open or close the sand trap.

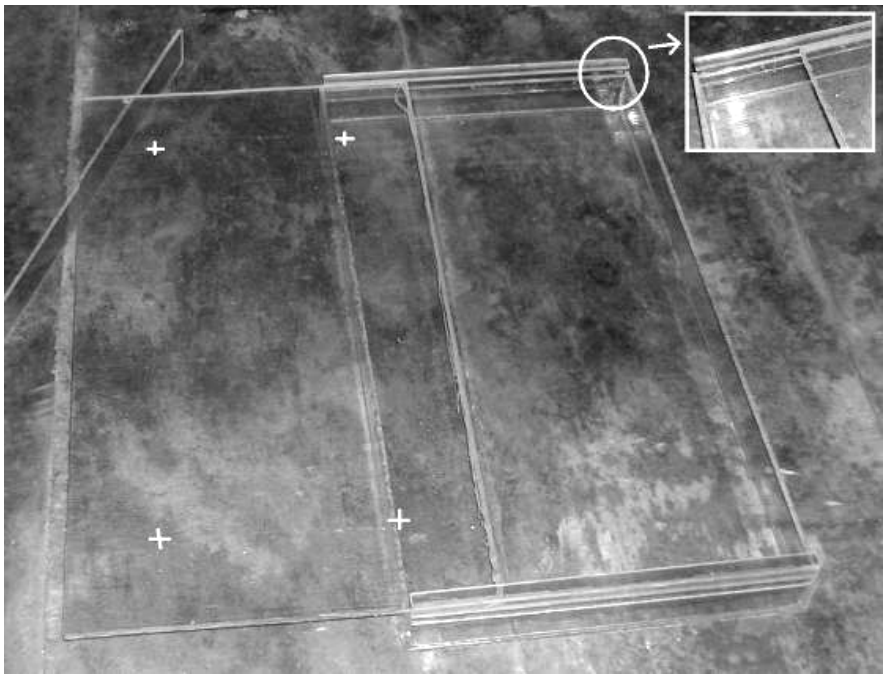

Figure 3.3 Photo of Sand Trap

3.3 BED MATERIALS CHARACTERISTICS

3.3.1 Size Distribution of Sediment Particles

In this study, the sieve analysis method was used to determine the size distribution of the sediment particles, in which a series of sieves was fitted one over another with the mesh size decreasing in the downward direction. A sediment sample was placed on the top sieve and the sieve column was shaken using a mechanical shaking machine.

A total of two sets of sediment were used in this study. Figure 3.4 shows the particle size distribution curves obtained by plotting the percentage by weight passing through each sieve in a sieve analysis, in which d_{16} = grain diameter when 16% of sand passing sieves; and d_{84} = grain diameter when 84% of sand passing sieves. A granular material composed entirely, or almost entirely, of particles of a particular size is called uniform. Using d_{16}, d_{50} and d_{84}, uniformity coefficient, or geometric standard deviation σ_g, is defined by:

$$\sigma_g = \frac{1}{2}\left(\frac{d_{84}}{d_{50}} + \frac{d_{50}}{d_{16}}\right) \tag{3.1}$$

Table 3.1 shows the results of the sieve analysis, and some other properties of the sediment particles used in the study.

Table 3.1 Properties of Sediments Used in the Study

Median Diameter d_{50} *(mm)*	*Uniformity Coefficient* σ_g	*Porosity* n	*Permeability* K *(cm/s)*	*Specific Gravity* S_s	ρ_b *(kg/m*^{3}*)*
0.48	1.30	0.499	0.167	2.662	1534.7
0.90	1.25	0.419	0.56	2.643	1334.5

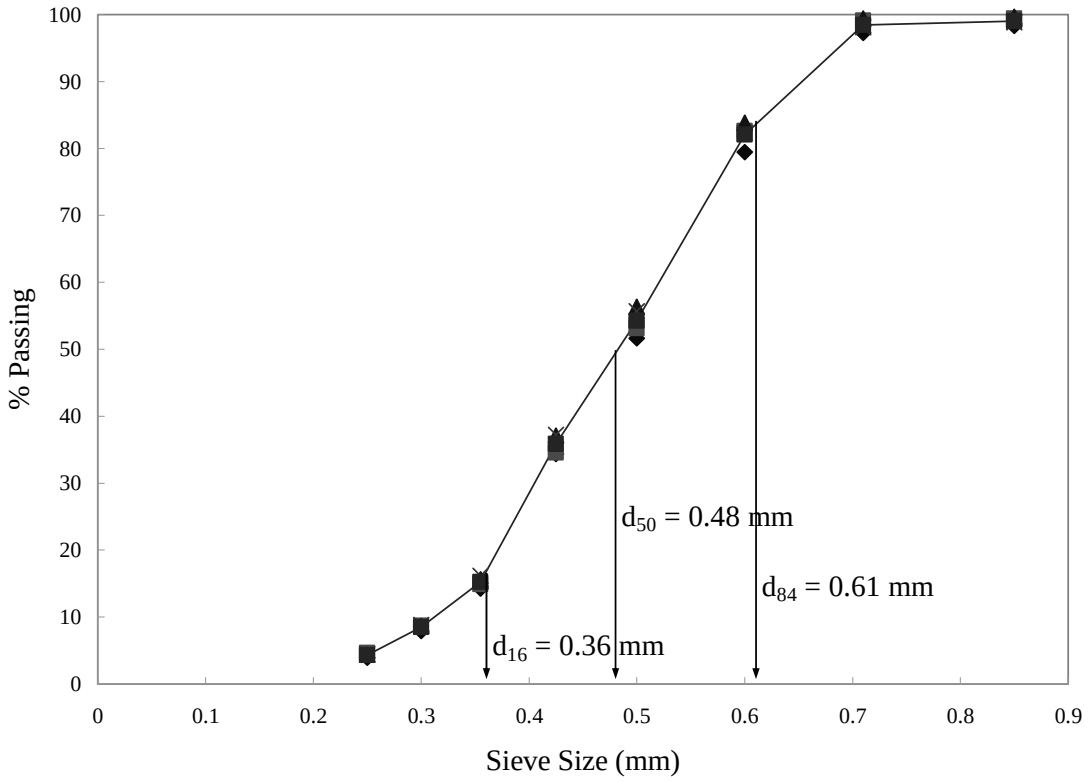

(a) Size Distribution for Sand with d_{50} = 0.48 mm

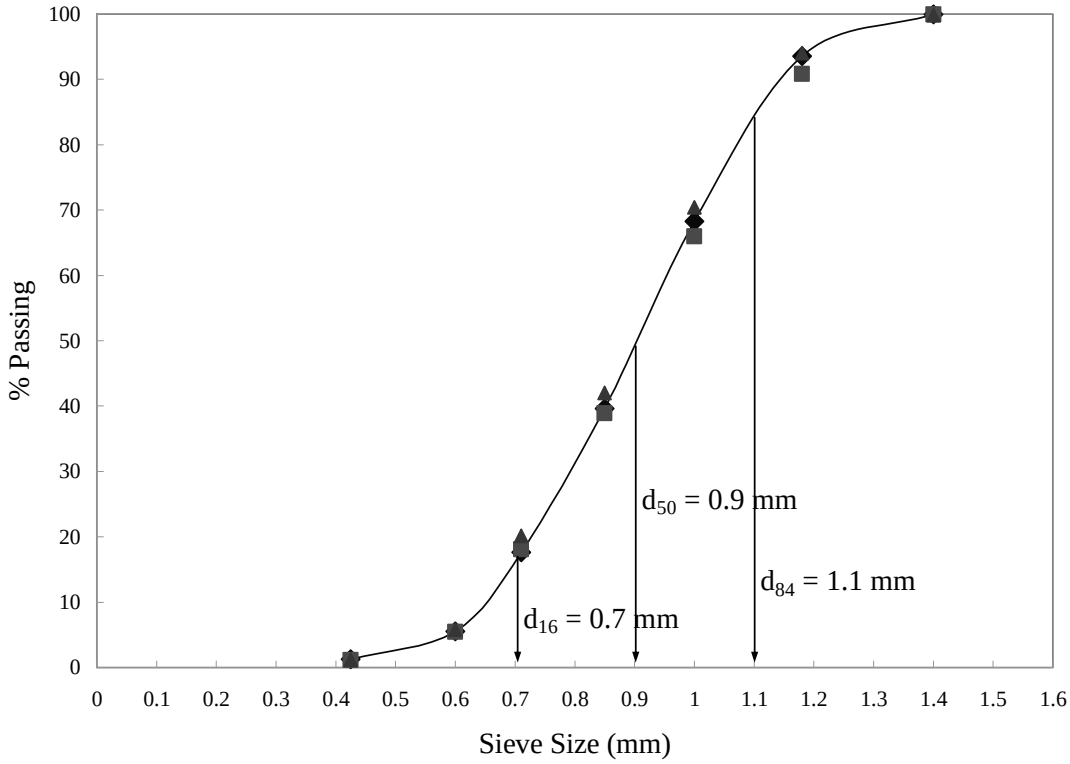

(b) Size Distribution for Sand with d_{50} = 0.9 mm

Figure 3.4 Grain Size Distribution of Sediment Samples

3.3.2 Specific Gravity, S_s

The specific gravity of the sediment particles is an important parameter, which is defined as the ratio of the sediment density to the density of water. In this study, the specific gravity of the sediment samples was determined from the measured sediment weight and volume according to the following equation:

$$S_s = \frac{\text{Weight of container and sand} - \text{Weight of container}}{\text{Weight of water} - \text{Weight of water with sand inside}} \qquad (3.2)$$

The experimental procedure is repeated six times to minimize uncertainties caused by measurement errors. The specific gravities of two sediments used in the study are shown in Table 3.1.

3.3.3 Bulk Density, ρ_b

Bulk density is a property of particulate materials, especially used in reference to soil. It is the mass of particles of the material divided by the volume they occupy. The volume of a sample includes particle volume as well as that of the void. As a result, bulk density is not an intrinsic property of a material; it can change depending on how the material is handled. The bulk densities of two sediment particles used in this study were measured using the weight of sand particles fully filled in a cylindrical container divided by the volume of the container. Since the experimental procedure has a significant effect on porosity due to compaction or consolidation, the same experiments for the each type of sediment particle were repeated three times. The average value of porosity for each sediment sample was used for subsequent data analysis. The computed results are tabulated in Table 3.1.

3.3.4 Porosity of Sediment, *n*

Porosity, which is a macroscopic porous medium property, is the percentage of voids in the total space occupied by a known number of sediment particles. In nature, porosity depends not only on the size, uniformity and shape of particles, but also on the pattern of deposition. Loose packing occurs when sediments settle from suspension in still water. When seepage is present, the porosity of the granular material becomes very important when compared with other properties of the sediment particles.

In this study, porosity was calculated using the following equation (Eq. 3.3) with measured specific gravity and bulk density. The computed porosity values of the two sediments are also tabulated in Table 3.1.

$$n = \frac{\rho_s - \rho_b}{\rho_s} = 1 - \frac{\rho_b}{\rho \cdot S_s} \tag{3.3}$$

3.3.5 Permeability, *K*

Permeability is a measure of the ability of a material to transmit fluids. It is important in determining the flow characteristics for a permeable river bed with the appearance of seepage. Based on Darcy's law (Bear, 1988), the permeability is expressed as follow

$$K = \frac{V_s}{i} \tag{3.4}$$

A typical constant head permeability test was conducted. The velocity of water passing through the sand was computed using the volume of the water per unit time divided by the cross-sectional area of the container. The hydraulic gradient was calculated using the difference of the water level in the piezometer between top and

bottom of the container divided by the distance in between. The permeability was then determined according to its definition. The same experiments for each size of sediment particles were repeated three times, and the average value of permeability is tabulated in Table 3.1.

3.4 MEASUREMENT TECHNIQUES

3.4.1 Measurement of Mean Streamwise Flow Velocity

In this study, since only the mean velocity was concerned for the analysis, an 8-mm minipropeller current meter was used for measurement. The minipropeller current meter was designed to measure velocity in the range of 4 to 300 cm/s. Its probe was connected to a digital reading meter, which displayed the frequency of the current meter. A pre-calibrated chart was used to convert the frequency into velocity.

3.4.2 Measurement of Water Depth

The water depth, which is defined as the vertical distance between the sand bed and the water surface, was measured using water level elevations measured at the flume centerline of the leading section, the middle length and the end section of the seepage zone. Water surface elevations are measured using a point gauge with a vernier scale. This gauge, capable of measuring water levels with an accuracy of ± 0.5 mm, was fixed on a movable device mounted on the flume. The water depth at the middle length of seepage zone was chosen as the representative value for the whole seepage region, and was used to estimate the spatially-averaged mean bed shear stress in later analyses.

3.4.3 Measurement of Seepage Velocity

The injection flow discharge in the seepage zone, controlled using a speed inverter and valve, was measured using turbine flow meters and a stopwatch. On the other hand, the suction flow discharge, controlled by twelve drainage pipes, was computed using the volume of water collected divided by the collection time which was measured using a stopwatch. The injection and suction velocities were then determined by calculating the injection and suction discharges per unit time divided by the seepage area, respectively.

3.4.4 Measurement of Streamwise Flow Discharge

Since the undisturbed flow condition was maintained for different seepage rates, the same streamwise flow discharge need to be controlled for a series of tests. The flow discharge through the head tank of the flume was monitored using an electromagnetic flow meter. In order to ensure the accuracy of the electromagnetic flow meter, an 8-mm diameter minipropeller, which was used for measuring the mean flow velocity, was used for calibration. Multiplied by the width of flume and the flow depth, the streamwise flow discharge based on the measurements of the minipropeller was obtained. Measurement of the streamwise flow discharge obtained by the electromagnetic flow meter and the minipropeller agreed well with each other, as illustrated in Fig. 3.5. Therefore, to ensure the same undisturbed flow condition, only the electromagnetic flow meter needs to be set to the same value.

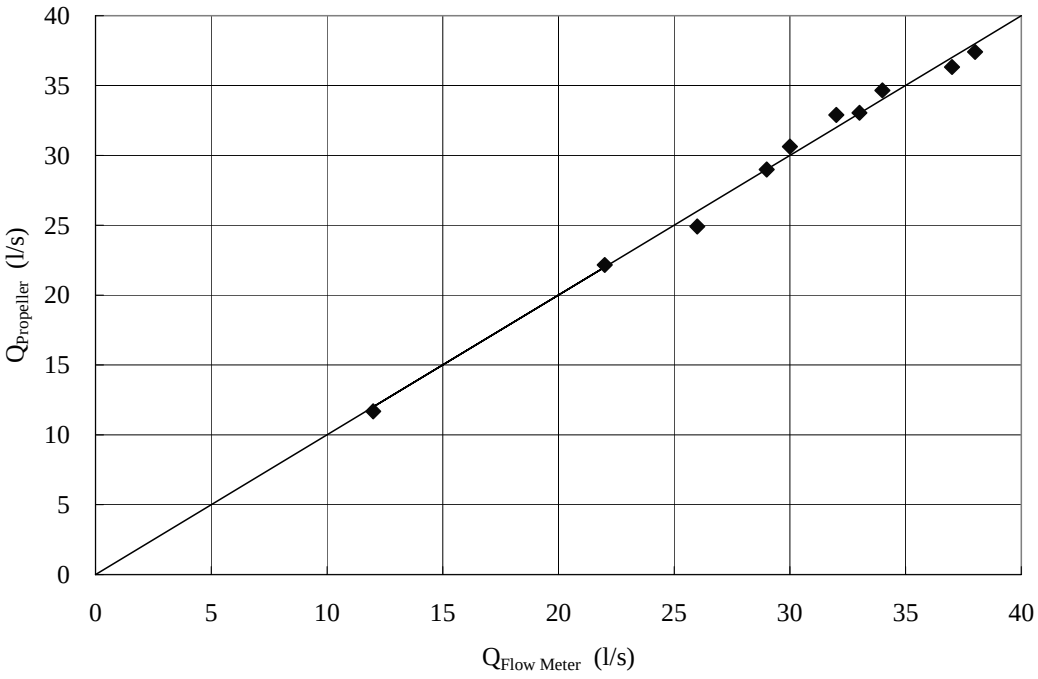

Figure 3.5 Comparison of Streamwise Flow Rate Measured by Electromagnetic Flow Meter and Minipropeller

3.5 EXPERIMENTAL PROCEDURES

Since this study focused on the direct measurement of sediment transport rate under various streamwise velocities and seepage flow rates, four experimental series were carried out to investigate the effects of seepage velocity, seepage zone length and experiment running time on sediment transport rate.

3.5.1 Experimental Series I

This series of experiments was conducted to determine the time-average streamwise flow velocity without seepage by using an 8-mm diameter propeller. Two sizes of uniform sand (d_{50} = 0.48 mm and 0.9 mm) were used as bed materials.

The sand surface in the seepage zone was first leveled to the same elevation of the adjacent sand bed. Water for the main flow was slowly pumped to the head tank of the flume at a controlled rate. The tailgate was then adjusted to avoid the shallow water depth in the channel, and then fixed for all series of tests in this study. The propeller, mounted on the point gauge which is described in Section 3.4.2, was adjusted vertically to measure the instantaneous flow velocity at 2-mm interval. The velocity distributions along the centerline of the flume at the upstream end, middle length and downstream end of seepage zone were measured. The measurements at each location were repeated at least three times. The average of the mean flow velocity among three locations was used for further analyses.

3.5.2 Experimental Series II

This series of experiment was designed to investigate the effect of seepage velocity on sediment transport rate. The experiments were conducted with the 2-m length seepage zone. The uniform sand with d_{50} = 0.9 mm was used as bed material for tests with upward seepage or injection. For the case of suction, both the sand particles with d_{50} = 0.48 mm and 0.9 mm were used.

The following procedure applied to all the tests in this series of tests. The sand surface in the seepage region was first leveled to the same elevation as the adjacent sand bed. Water for the main flow was slowly pumped to the head tank of the flume. The streamwise flow discharge was controlled and monitored to a preset value using the electromagnetic flow meter. The pump for injection, or the valves on the suction drainage pipes, were then turned on or opened and the seepage discharge was gradually increased to the pre-determined value. To ensure a uniform suction rate across the entire suction zone, twelve valves were opened simultaneously with almost the same opening-angle to generate downward seepage.

This technique was also applied to Experimental Series III and IV. To ensure a constant condition for each run, both the flow rates and the water depth were frequently checked and monitored during the test. No bedforms were observed during the experiments for both initial clear-water and live-bed conditions.

At 40 to 50 minutes after commencement of the test, the cover of the sand trap was opened to collect the transported sediment particles within a time duration ranging from 90 to 300 seconds, which is recorded using a stopwatch. The duration is dependent on the rate of bedload transport. A peristaltic pump, as shown in Fig. 3.6, with 600-rpm drive motor and 2.3 L/min discharge, was used to suck out the trapped particles. The wet sand particles collected were then put in a 120°C oven for 24 hours duration to reach oven-dry condition. The dry sediment was weighed and volumetric sediment transport rate per unit width was then calculated with the known bulk density. The experiment was repeated three times for each suction rate and their average was used for further analysis. A total of 114 tests with the presence of injection and 201 tests for the case of suction were conducted in this series.

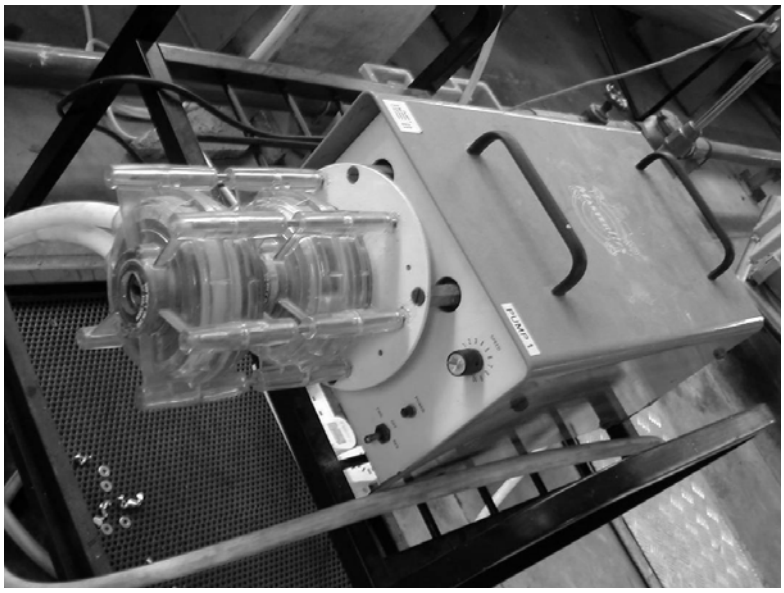

Figure 3.6 Photo of Peristaltic Pump

3.5.3. Experimental Series III

The objective of this experimental series was to explore the effect of suction zone length on sediment transport rate. The same two uniform sand (d_{50} = 0.48 mm and 0.9 mm) were used as bed materials.

Two plastic plates that are 1 m and 1.5 m in length, 0.7 m in width were placed at the bottom of the sand in the seepage zone to change the length of the suction zone to 1 m and 0.5 m, respectively. Figure 3.7 shows the schematic drawing of the shortened suction zones. With the same measurement procedure and technique described in Section 3.5.2, the sand particle with d_{50} = 0.9 mm were tested with 1-m length suction zone, and the sand with d_{50} = 0.48 mm were tested with both 0.5-m and 1-m length suction zone. Additional 132 tests were conducted in this series.

3.5.4. Experimental Series IV

This experimental series is conducted to study time effects on sediment transport rate subjected to suction. The experiments were conducted with the 2-m length seepage zone. The sand particle with d_{50} = 0.48 mm was used as the bed material in this series.

After the undisturbed flow condition was preset as described in Section 3.5.1, the suction discharge was then applied to the pre-determined value using the valves on the drainage pipes. The moving sand particles were collected using the same measurement technique described in Section 3.5.2 for every 5-minute. Since the transported sediment was collected over a certain period, linear approximation was made within this time duration. The mid-time of this duration was reported as the corresponding time to the sediment transport rate measured within this period.

The wet sand particles collected were prepared as the same as that in section 3.5.2. A total of 82 tests were conducted in this series.

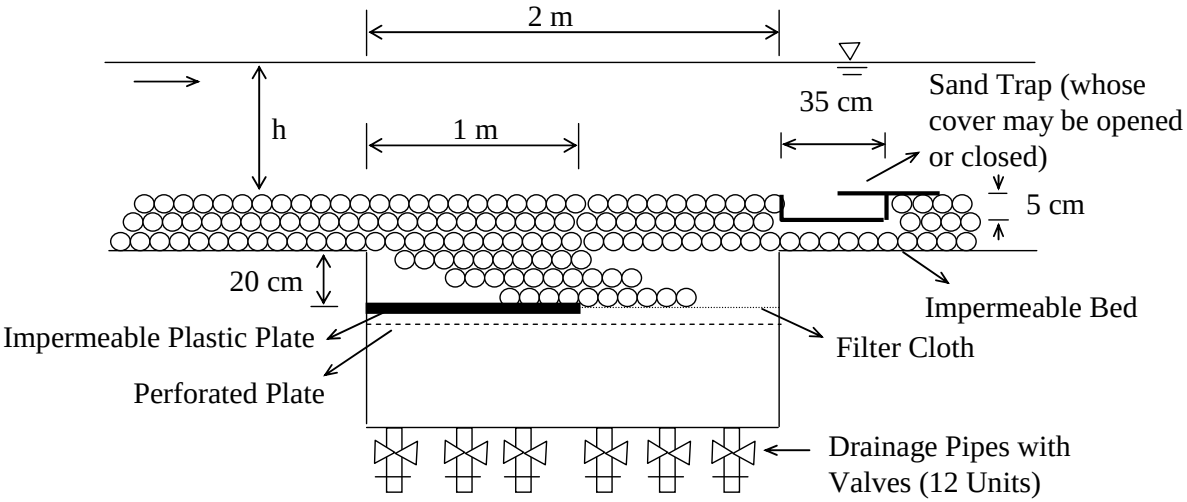

(a) Suction Zone = 1 m

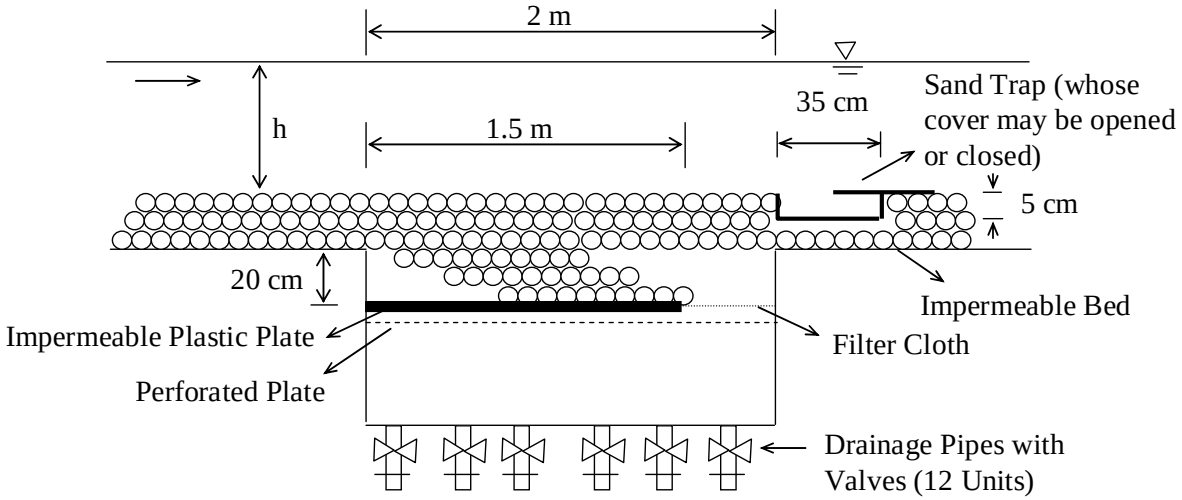

(b) Suction Zone = 0.5 m

Figure 3.7 Schematic Drawing of Shortened Suction Zone

Chapter 4

Physics of Sediment Transport under Seepage

4.1 INTRODUCTION

The presence of seepage through a porous boundary may cause modification to the forces exerting on the bed particles. This chapter focuses on how seepage affects the physics of sediment transport behavior. Dimensional analysis is presented to investigate the variables affecting the sediment transport rate with the appearance of seepage.

4.2 FORCE ANALYSIS

Consider a horizontal plane bed consisting of uniform, cohesionless sediment particles, where the bed sediment is subjected to both seepage and open-channel flow (see Fig. 4.1). A cohesionless sediment particle on the porous bed experiences the submerged weight force W, drag force F_D, lift force F_L, and seepage

force F_s.

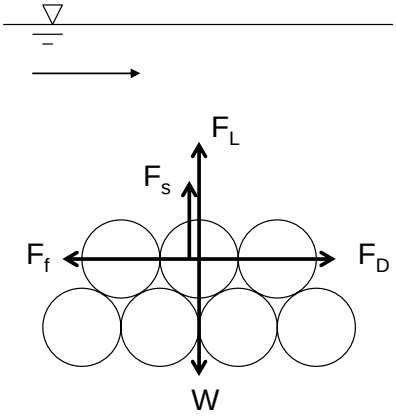

Figure 4.1 Forces Exerting on a Bed Particle

In the following discussion, the sediment particle is assumed to be as a sphere for simplicity and the shape effects are accounted for sufficiently well by using the median diameter.

The submerged weight of the sediment particle can be expressed as

$$W = (\rho_s - \rho) g \frac{\pi d_{50}^3}{6} \tag{4.1}$$

where ρ_s = density of particle.

The horizontal drag F_D consists of skin friction acting on the surface of the grain and form drag due to a pressure difference between the up-downstream sides of the grain because of flow separation. For the same spherical sediment particle, the drag force is expressed as

$$F_D = C_D \frac{\pi d_{50}^2}{8} \rho u_b^2 \tag{4.2}$$

where u_b = approach velocity of flow over the bed at the particle; and C_D = drag coefficient, which is known to depend on the local Reynolds number.

Generally a lift force F_L in excess of the natural buoyancy is also created by the flow. This lift is primarily due to deviations from the hydrostatic pressure distribution around the grain. Near the upper part of the grain the pressure will locally decrease below the hydrostatic pressure, while a higher pressure is formed at the lower part of the grain. As a result, a positive lift force on the grains is formed. The lift force has a similar expression as its drag counterpart as expressed in Eq. 4.2. It can likewise be expressed as

$$F_L = C_L \frac{\pi d_{50}^2}{8} \rho u_b^2 \tag{4.3}$$

where C_L = lift coefficient.

If one assumes that the direction of the seepage flow is normal to the bed, the seepage force will act in the same line of action as the lift force. When seepage is introduced it augments the magnitude of the life force, causing the latter to increase and decrease for injection (upward seepage) and suction (downward seepage), respectively. Furthermore, one may define injection as positive and suction as negative. Cheng and Chiew (1999) stated that the seepage force exerting on a particle is

$$F_S = \frac{i \rho g \pi d_{50}^3}{6(1-n)} \tag{4.4}$$

where i = hydraulic gradient for seepage; and n = porosity.

The hydraulic gradient represents the driving force that causes seepage and can be related to the seepage velocity. According to Darcy's law (Bear, 1988), the seepage flow through the porous medium is linear. The seepage velocity, V_s, is directly proportional to the hydraulic gradient, and the constant of proportionality is known as the coefficient of permeability, K:

$$V_s = Ki \tag{4.5}$$

The stabilizing forces can be modeled as frictional forces F_f acting on a particle which is expressed as

$$F_f = \mu_s (W - F_s - F_L) \tag{4.6}$$

where μ_s = coefficient of friction between the grain and the surrounding grains, which can be taken as

$$\mu_s = \tan\theta \tag{4.7}$$

where θ = angle of repose of the sediment particles.

Generally, the movement of the sediment particles, represented by the sediment transport rate, is governed by the excess net force between the driving force and the resistance forces acting on the sediment particles, which may be expressed as $F_D - F_f$. When $F_D - F_f < 0$, the particles will not move and the sediment transport rate = zero; when $F_D - F_f = 0$, the particles just begin to move, which is customarily known as the threshold condition; and when $F_D - F_f > 0$, the sediment particles are transporting.

Substituting Eqs. 4.1 to 4.7 into the excess net force, $F_D - F_f$, leads to

$$F_D - F_f = \frac{\pi\rho d_{50}^2}{2}\left\{u_b^2\left(\frac{C_D}{4} + \frac{C_L}{4}\tan\theta\right) - \frac{\tan\theta}{3(1-n)} g d_{50}\left[(S_s - 1)(1-n) - \frac{V_s}{K}\right]\right\} \tag{4.8}$$

where $S_s = \rho_s/\rho$ = specific gravity of sand particle. For the case of the threshold condition, $F_D - F_f = 0$, then Eq. 4.8 becomes

$$\frac{C_D}{4} + \frac{C_L}{4}\tan\theta = \frac{\frac{\tan\theta}{3(1-n)} g d_{50}\left[(S_s - 1)(1-n) - \frac{V_s}{K}\right]}{u_{bc}^2} \tag{4.9}$$

where u_{bc} = approach velocity of flow over the bed at the particle at the threshold condition. Substituting Eq. 4.9 into Eq. 4.8 leads to

$$F_D - F_f = \frac{\pi\rho d_{50}^3}{2}\frac{\tan\theta}{3(1-n)}g\left[(S-1)(1-n)-\frac{V_s}{K}\right]\cdot\left(\frac{u_b^2}{u_{bc}^2}-1\right) \tag{4.10}$$

Since the volumetric bedload transport rate per unit width with the presence of seepage, q_{bs} is proportional to the excess net force $F_D - F_f$, one may infer from Eq. 4.10 that

$$q_{bs} = f\left(d_{50}, \rho_s, \rho, g, n, K, V_s, u_b, u_{bc}\right) \tag{4.11}$$

The approach velocity may be considered as the instantaneous velocity along the streamwise velocity profile at a depth = sediment size. Therefore, it could be expressed in terms of the mean flow velocity without seepage, U_o, i.e.,

$$u_b = f\left(U_o\right) \tag{4.12}$$

The above relationship may be expressed in terms of the undisturbed shear velocity as follows (Chiew and Parker, 1994)

$$u_b = \frac{u_{*o}}{\sqrt{f_*}} \tag{4.13}$$

where u_{*o} = shear velocity without seepage, f_* = a form of a friction factor. At the threshold condition, Eq. 4.13 becomes

$$u_{bc} = \frac{u_{*co}}{\sqrt{f_*}} \tag{4.14}$$

where u_{*co} = critical shear velocity without seepage.

Considerations of Eqs. 4.10 and 4.12 to 4.14 allow one to rewrite the general function of q_{bs} (Eq. 4.11) as

$$q_{bs} = f\left(d_{50}, \rho_s, \rho, g, n, K, V_s, U_o, u_{*o}, u_{*co}\right) \tag{4.15}$$

The symbol f denotes a specified function. Since the critical shear velocity without seepage, u_{*co}, can be calculated based on the basic properties of the sand particle and fluid, the term u_{*co} is then a dependent variable and should be removed from Eq. 4.15. As a result, the general function of q_{bs} may be expressed as follows

$$q_{bs} = f\left(d_{50}, \rho_s, \rho, g, n, K, V_s, U_o, u_{*o}\right) \tag{4.16}$$

4.3 DIMENSIONAL ANALYSIS

Using the Buckingham pi theorem, one may obtain appropriate pi-terms for Eq. 4.16. The variables d_{50}, ρ, and g were chosen as repeating variables for the dimensional analysis, resulting in the derivation of the following seven pi terms:

$$\Pi_1 = \frac{q_{bs}}{\sqrt{d_{50}^3 g}} \tag{4.17}$$

$$\Pi_2 = \frac{\rho_s}{\rho} = S_s \tag{4.18}$$

$$\Pi_3 = n \tag{4.19}$$

$$\Pi_4 = \frac{K}{\sqrt{d_{50} g}} \tag{4.20}$$

$$\Pi_5 = \frac{V_s}{\sqrt{d_{50} g}} \tag{4.21}$$

$$\Pi_6 = \frac{U_o}{\sqrt{d_{50} g}} \tag{4.22}$$

$$\Pi_7 = \frac{u_{*o}}{\sqrt{d_{50} g}} \tag{4.23}$$

Based on energy considerations such as the stream-power concept, Engelund and Hansen (1967) derived the total load discharge formula in the absence of seepage as follow:

$$\Phi_o = \frac{q_{bo}}{\sqrt{(S_s - 1)gd_{50}^3}} = 0.05\tau_{*o}^{2.5}\frac{U_o^2}{u_{*o}^2} \tag{4.24}$$

where $\tau_{*o} = \frac{u_{*o}^2}{(S_s - 1)d_{50}g}$ = Shields' parameter without seepage. Re-arrangement of Eq. 4.24 leads to

$$\Phi_o = \frac{q_{bo}}{\sqrt{(S_s - 1)gd_{50}^3}} = 0.05\tau_{*o}^{1.5}\frac{U_o^2}{(S_s - 1)gd_{50}} \tag{4.25}$$

According to the Engelun-Hansen formula, the Einstein's parameter without seepage Φ_o is a function of τ_{*o} and the densimetric Froude number, $\frac{U_o^2}{(S_s - 1)gd_{50}}$.

The densimetric Froude number is also used by Aguirre-Pe et al (2003) for the prediction of sediment transport rate with an impermeable bed on a steep slope. Therefore, one may infer from this that Einstein's parameter with the presence of seepage Φ may also be a function of τ_{*o} and the densimetric Froude number with the modification of seepage effect.

By re-arranging Eqs. 4.17 to 4.23, the seven pi terms are reduced to three dimensionless groups as follow:

$$\Phi = \frac{q_{bs}}{\sqrt{d_{50}^3 g(S_s - 1)}} = f\left\{\frac{u_{*o}^2}{(S_s - 1)d_{50}g}, \frac{U_o^2}{[(S_s - 1)(1 - n) - V_s/K]d_{50}g}\right\} \tag{4.26}$$

The first dimensionless term, $\Phi = q_{bs}\Big/\sqrt{d_{50}^3 g(S_s - 1)}$, is the well-known Einstein's parameter which is widely used as the dimensionless volumetric sediment transport

rate in previous studies. The second group of variables, $u_{*o}^2/[(S_s-1)d_{50}g]$, is the Shields' Parameter in the absence of seepage, τ_{*o}, which describes the initial condition of the sediment bed before seepage is introduced. The final dimensionless term $\Omega = U_o^2/\{[(S_s-1)(1-n)-V_s/K]d_{50}g\}$, is a modified densimetric Froude number. The modifier $(S_s-1)(1-n)-V_s/K$ is used to account for seepage and porosity effects. When injection is present, V_s is positive; on the other hand, when suction is introduced, V_s is negative. In the absence of seepage and porosity effects, i.e., n = 0 and V_s = 0, Ω reduces to the densimetric Froude number, which is $=U_o/\sqrt{(S_s-1)d_{50}g}$. Note that for an increase in injection and suction velocity, the modified densimetric Froude number, Ω increases and decreases, respectively. For the case of no-seepage condition, the modified densimetric Froude number Ω become as follows

$$\Omega_o = \frac{U_o^2}{[(S_s-1)(1-n)]d_{50}g} \tag{4.27}$$

where Ω_o = modified densimetric Froude number without seepage.

To dimensionally scale results from laboratory model to the prototype, the basis of dynamic similarity through the Froude law should be followed, in order to maintain similar gravitational characteristics to those found in the model and prototype. Keeping the Froude numbers equal in the model and prototype yields:

$$(F_r)_p = (F_r)_m \quad \text{or} \quad \left(\frac{U}{\sqrt{gL}}\right)_p = \left(\frac{U}{\sqrt{gL}}\right)_m \tag{4.28}$$

where F_r, U, g and L are the Froude number, mean velocity, gravitational acceleration and the length of the prototype and model, respectively.

4.4 SUMMARY

In this chapter, the force analysis is performed on a spherical cohesionless sediment particle resting on a horizontal plane bed. The variables which affect the bedload transport rate are derived. The sediment transport rate in the presence of seepage is affected by the properties of sand particle, the undisturbed flow condition and the seepage velocity. The dimensional analysis is presented and three dimensionless groups, viz. Einstein's parameter, Shield's parameter without seepage and modified densimetric Froude number are chosen to examine how seepage affects bedload transport rate.

Chapter 5

Seepage Effects on Sediment Transport Rate

5.1 INTRODUCTION

This chapter focuses on the effect of seepage, both upward and downward, on sediment transport rate. The measured sediment transport rate data with the presence of seepage, as described in Chapter 3 Experimental Series II, are presented in this chapter. The analyses of the effect of downward seepage or suction on sediment transport rate are discussed using the dimensionless groups derived in Chapter 4. Following that, the injection effects are analyzed. The equations for predicting sediment transport rate with seepage are empirically derived. Comparisons between previous investigations and present study are also discussed in this chapter.

5.2 EXPERIMENTAL RESULTS OF TESTS SUBJECTED TO SUCTION

5.2.1 Undisturbed Flow Conditions

In the present study, two sizes of sediment particles were used. Their medium grain diameters are 0.9 and 0.48 mm. Table 5.1 shows the properties of the two sand particles used in the study, in which $d_* = \left[(S_s - 1)gd_{50}^3/\nu^2\right]^{1/3}$. The critical seepage velocity under quick condition, V_{sc}, was obtained according to Darcy's Law when the submerged weight of the particle is zero. The critical shear velocity without seepage in the table, u_{*co}, which is $=\sqrt{\tau_{*co}(S_s - 1)gd_{50}}$, was computed using the Shields function in Van Rijn (1984):

$$\tau_{*co} = 0.04 d_*^{-0.1} \qquad 10 < d_* \le 20 \qquad (5.1)$$

$$\tau_{*co} = 0.013 d_*^{0.29} \qquad 20 < d_* \le 150 \qquad (5.2)$$

Table 5.1 Properties of Sediments Used in the Study

d_{50} (mm)	K (cm/s)	n	S_s	ρ_b (kg/m^3)	d_*	V_{sc} (cm/s)	u_{*co} (cm/s)
0.90	0.560	0.419	2.643	1534.7	22.77	0.534	2.158
0.48	0.167	0.499	2.662	1334.5	12.14	0.139	1.561

The average velocity profile of those measured at the beginning, the mid-section and the end of the seepage zone for each undisturbed flow condition measured using the 8-mm diameter propeller in Experimental Series I is shown in Fig. 5.1 for both sand particles used in the study. The lines shown in the velocity distributions are fitted to the logarithmic law equation. The sand with d_{50} = 0.9 mm were measured under seven different undisturbed flow conditions, whereas the sand with d_{50} = 0.48 mm were measured under four.

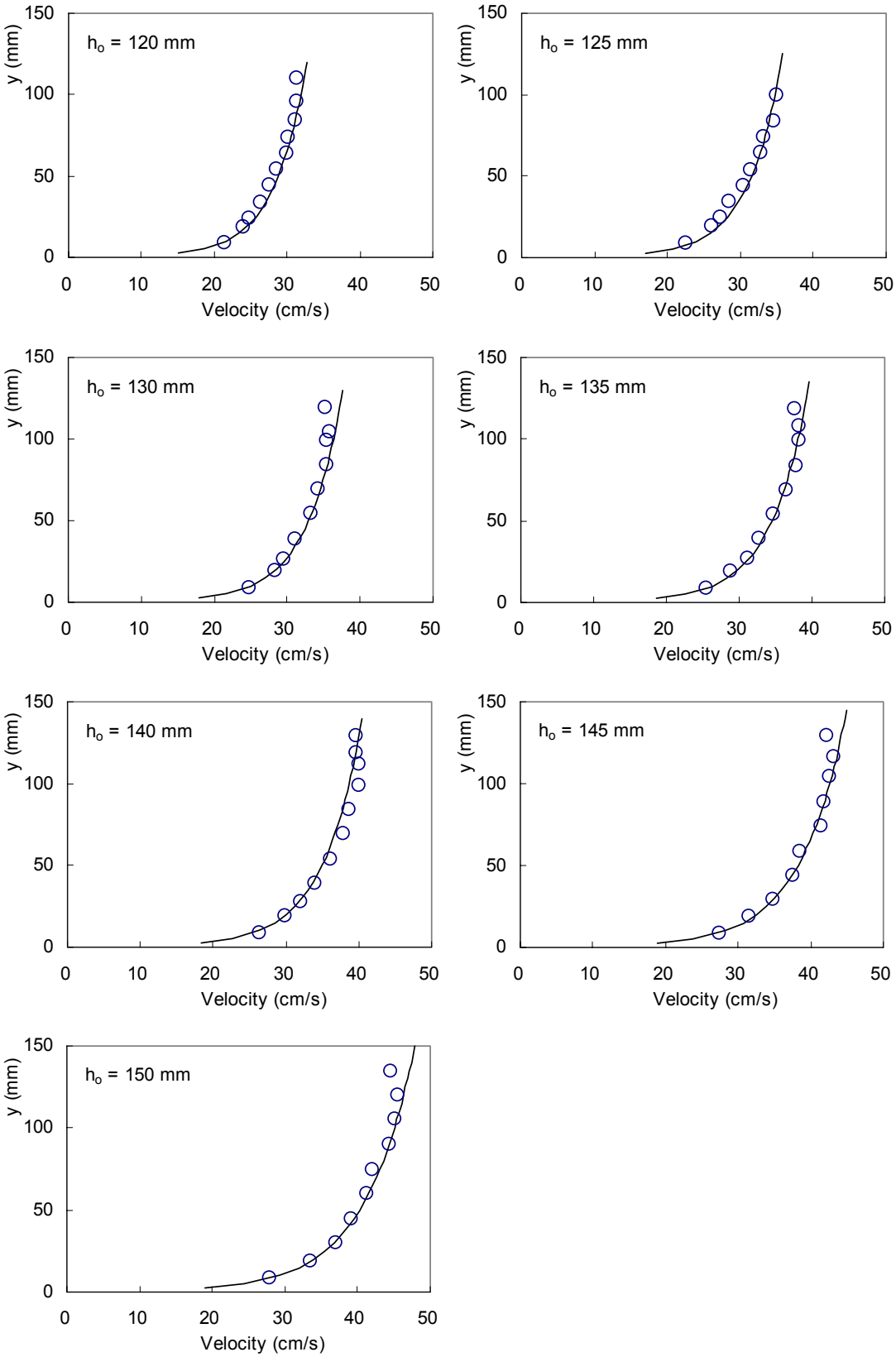

(a) Undisturbed Velocity Distributions for d_{50} = 0.9 mm

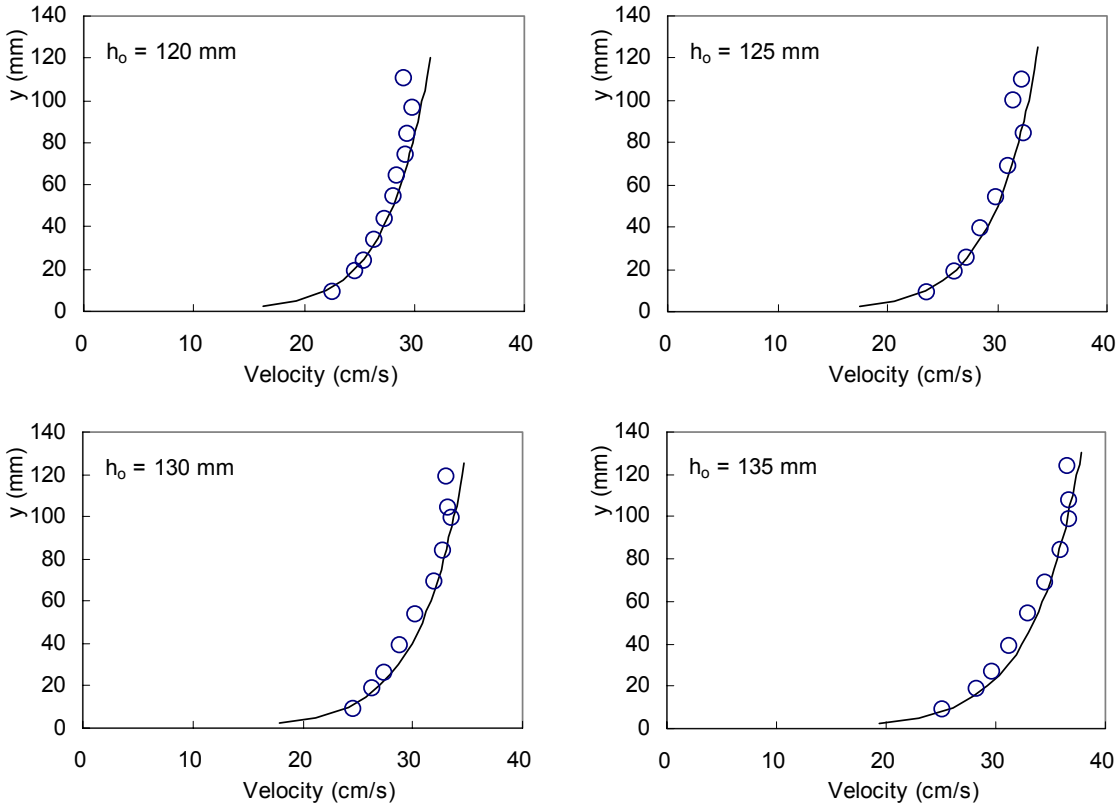

(b) Undisturbed Velocity Distributions for d_{50} = 0.48 mm

Figure 5.1 Velocity Distributions without Seepage

The streamwise mean flow velocity, U_o, was calculated using the area under the velocity distribution curve divided by the water depth. The undisturbed streamwise flow rate, Q_o, was computed by multiplying U_o with the width of the flume and the undisturbed water depth. By examining the slope of the velocity distribution curve in logarithmic scale, the shear velocity without seepage u_{*o} was obtained. The undisturbed flow conditions of each series are summarized in Table 5.2.

Table 5.2 Undisturbed Flow Condition of Each Series

d_{50} (mm)	Series	h_o (mm)	Q_o (m^3/s)	U_o (cm/s)	u_{*o} (cm/s)	u_{*o}/u_{*co}	τ_{*o}
0.90	1-1	120	23.7	28.26	1.774	0.82	0.0217
	1-2	125	27.2	31.13	1.876	0.87	0.0242
	1-3	130	29.8	32.75	1.962	0.91	0.0265
	1-4	135	32.6	34.48	2.066	0.96	0.0294
	1-5	140	34.4	35.11	2.145	0.99	0.0317
	1-6	145	39.2	38.64	2.516	1.17	0.0436
	1-7	150	43.0	40.95	2.759	1.28	0.0525
0.48	2-1	120	23.2	27.59	1.527	0.98	0.0298
	2-2	125	26.0	29.67	1.633	1.05	0.0341
	2-3	130	27.9	30.65	1.678	1.08	0.0360
	2-4	135	31.5	33.38	1.818	1.16	0.0422

For the sand with d_{50} = 0.9 mm, Series 1-1 to 1-4 are initial non-transporting bed in the absence of seepage, since the corresponding values of $u_{*o}/u_{*co} < 1$. In contrast, with $u_{*o}/u_{*co} > 1$, Series 1-5 to 1-7 and Series 2-2- to 2-4 are initial transporting bed. Series 1-4 and 2-1 could be considered as the threshold condition as the value of u_{*o}/u_{*co} is very close to zero.

5.2.2 Sediment Transport Rates with Suction

The bedload sediment transport rate q_{bs} was measured for each type of the sand particles by varying the undisturbed flow rate (a total of eleven different flows rates) and seepage velocity, where injection velocity is denoted as a positive number and suction is denoted as a negative number. The sediment transport rates with the presence of suction were measured for all the series tabulated in Table 5.2. The

ranges of suction rates applied are tabulated in Table 5.3. This table shows that the suction rates applied to Series 1-4 to 1-7 start from zero and gradually increase. On the other hand, the applied suction rates for the rest of the series start directly from a higher value. The reason is that when the suction velocity is lower than the minimum applied value, the sediment transport rate is too small for measurement.

Table 5.3 Range of Suction Rate for Each Series

d_{50} (mm)	Series	τ_{*o}	Range of Suction $\|V_s\|$ (cm/s)
0.90	1-1	0.0217	0.290 – 0.440
	1-2	0.0242	0.231 – 0.505
	1-3	0.0265	0.169 – 0.416
	1-4	0.0294	0 – 0.415
	1-5	0.0317	0 – 0.575
	1-6	0.0436	0 – 0.466
	1-7	0.0525	0 – 0.367
0.48	2-1	0.0298	0.124 – 0.292
	2-2	0.0341	0.080 – 0.280
	2-3	0.0360	0.075 – 0.293
	2-4	0.0422	0.152 – 0.371

The measured bedload transport rates are plotted against suction velocities in Fig. 5.2. The series labeled with "S2" refer to the data measured with the d_{50} = 0.48 mm sand. The details of the experimental data are tabulated in Appendix I. All the series of data in Fig. 5.2 show the same trend that the sediment transport rate increases with an increase in suction velocity for the same undisturbed flow condition.

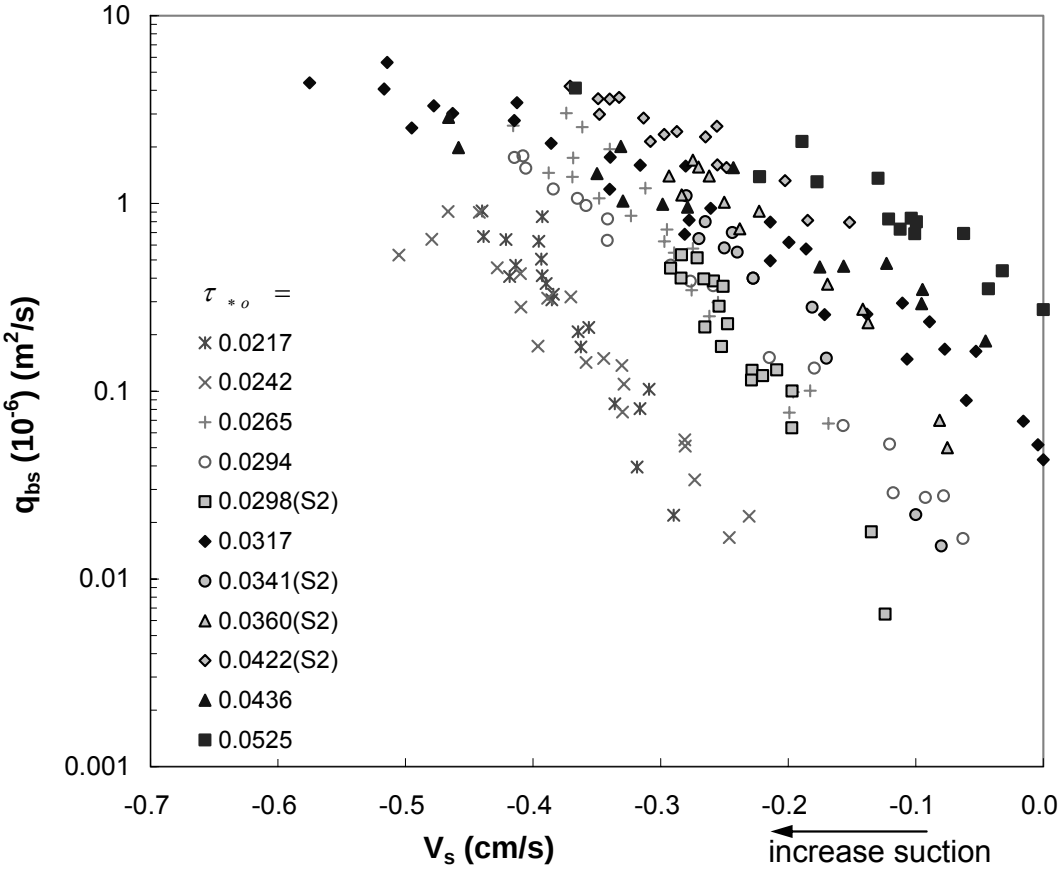

Figure 5.2 Relationship of q_{bs} and V_s for Different Undisturbed Flow Conditions with Suction

In order to have a better perception, the experimental results are plotted in terms of the dimensionless terms Φ and Ω as shown in Fig. 5.3 to collapse the data with different undisturbed flow conditions and sediment particles sizes.

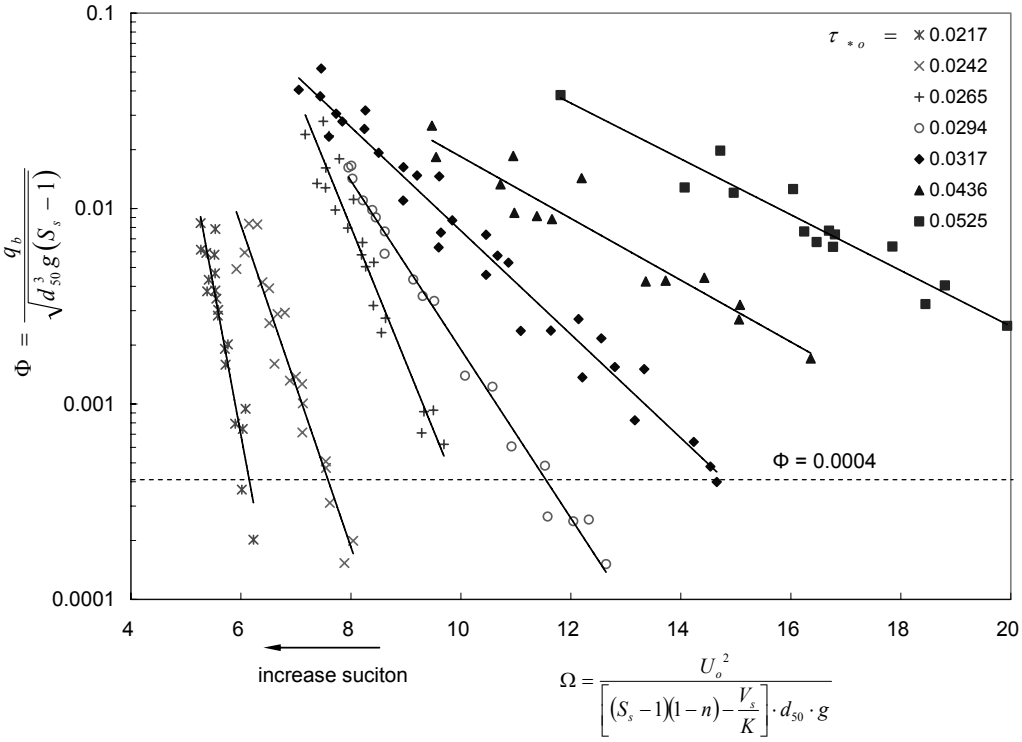

(a) Relationship of Ω and Φ under Different τ_{*o} –values with d_{50} = 0.9 mm

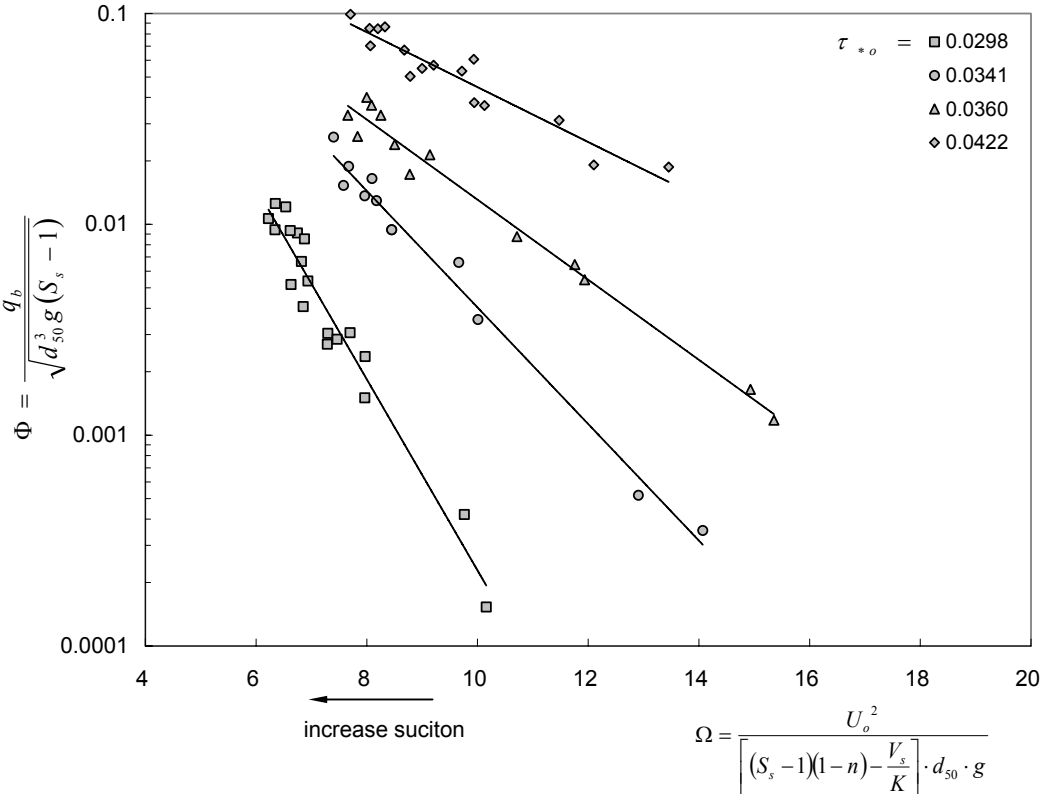

(b) Relationship of Ω and Φ under Different τ_{*o} –values with d_{50} = 0.48 mm

Figure 5.3 Relationships of *Ω* and *Φ* for Data Subjected to Suction

The figure shows that with the same τ_{*o}, Φ increases with a decrease in Ω, i.e., an increase in suction. When V_s = 0, the corresponding Φ-value is the Einstein parameter in the absence of suction. Fig. 5.3 shows that the slope of Series 1-1 (τ_{*o} = 0.0217, u_{*o}/u_{*co} = 0.82) is very steep. It may be inferred from this trend when τ_{*o} is small or the bed particles is stable, even a small increase in suction velocity or decrease in Ω will cause a large increase in the bedload transport rate. It also may be inferred from Fig. 5.3 that for the same undisturbed flow condition, the bedload transport rate, which also may be represented by Einstein's dimensionless parameter Φ, is increasing linearly in a semi-logarithmic scale with an increase in suction rate.

One may surmise that since a sediment feeding arrangement is not installed in the experimental set-up, there may be a possibility that general bed degradation or aggradation within the suction zone during the preparatory stage of the tests (duration ≈ 1 hour), hence compromising the experimental results. It must be stated that observations made during the tests did not show such an occurrence. In fact, using the highest measured bedload transport rate of $\Phi_o = 2.31\times10^{-3}$, associated with Series 1-7, which corresponds to the highest τ_{*o} of all the tests (see Table 5.2), the transported volume of sediment particles may be computed for the duration of 1 hour. Dividing this value by the surface area of the suction zone yields a mere 0.22 mm, which is very insignificant as far as bed degradation is concerned. The computed value supports the observation that general bed degradation or aggradation is negligible during the tests.

5.3 EFFECT OF SUCTION ON SEDIMENT TRANSPORT

As discussed previously, the sediment transport rate is affected by the excess net force acting on the sediment particles. From another view point, the sediment transport rate could also be expressed as a function of the difference between the acting shear velocity at the bed and the critical shear velocity (Aguirre-Pe et al, 2003), called the shear velocity excess, $u_{*s} - u_{*cs}$, where u_{*s} = shear velocity with suction and u_{*cs} = critical shear velocity with suction. The shear velocity, u_{*s}, signifies the driving force acting on the bed particles. The critical shear velocity, u_{*cs}, on the other hand, represents the resistant force when sand particles are just about to move. If the shear velocity excess, $u_{*s} - u_{*cs}$ increases, the difference between the driving force and resistance force becomes larger and the sediment particles will move faster. A simple corollary from the measured data which show that bedload transport rate increases with suction is that the shear velocity excess, $u_{*s} - u_{*cs}$, must have increased.

Chen and Chiew (2004) had shown that bed shear stresses increase with suction rates. Using the same experimental set-up as that used in this study, they presented an empirical equation to calculate u_{*s} for given V_s/U_c and u_{*o} as follows:

$$\frac{u_{*s}}{u_{*o}} = 0.073\left|\frac{V_s}{U_c}\right|^3 - 0.44\left|\frac{V_s}{U_c}\right|^2 + 0.9\left|\frac{V_s}{U_c}\right| + 1 \qquad (5.3)$$

On the other hand, Cheng and Chiew (1999) showed that the critical shear velocity is reduced in the presence of upward seepage or injection. It may be inferred from their results that a downward seepage or suction will cause an increase in critical shear velocity.

Based on results from these two studies, one may deduce that both shear velocity and critical shear velocity will increase with an increase in suction. In order for

the sediment particles to move faster with suction as shown in the experiments, the increase in shear velocity must be higher than that in critical shear velocity, resulting in an increase of shear velocity excess, $u_{*s} - u_{*cs}$. We now will discuss how suction affects these two variables. In order to show the consistency with previous investigations by other researchers, the shear velocities mentioned in the following section are not actually measured but calculated using published equations.

5.3.1 Effect of Suction on Critical Shear Velocity

The tests in Series 1 (d_{50} = 0.9 mm) were chosen to illustrate how suction affects the critical shear velocity and bed shear velocity, since it is the only series which contains data with an initial non-transporting bed. Series 1-5, where u_{*o}/u_{*co} = 0.99, could be considered as the threshold condition for sediment entrainment before suction is introduced. Additionally, there were initial non-transporting beds (Series 1-1 to 1-4), and initial transporting beds (Series 1-6 and 1-7). By defining Φ = 0.0004 as the threshold condition, the corresponding critical values of Ω for test series with $u_{*o}/u_{*co} < 1$ can be determined from Fig. 5.3(a). It must be stated that this value of Φ is chosen because it is the bedload transport rate for Test Series 1-5 (u_{*o}/u_{*co} = 0.99) in the absence of suction. Since this is so close to the critical shear velocity for sediment entrainment computed using Shields' function, the corresponding transport rate can safely be assumed to be that of the critical condition. Table 5.4 shows the values of modified densimetric Fround number at the threshold condition, Ω_c, obtained directly from Fig. 5.3(a). It must be stated that it is impossible to determine the Ω_c value for Series 1-6 and 1-7 because suction can only increase the bedload transport rate. For these two test series, the bed was already in motion, i.e., $u_{*o}/u_{*co} > 1$ at V_s = 0. Hence the bed cannot revert to the critical condition by introducing suction.

Table 5.4 Critical Shear Velocity with Suction

Series	u_{*o}/u_{*co}	$\Phi = 0.0004$			
		Ω_c	V_s (cm/s)	u_{*cs} (cm/s)	u_{*cs}/u_{*co}
1-1	0.82	6.16	-0.298	2.741	1.27
1-2	0.87	7.59	-0.275	2.824	1.31
1-3	0.91	9.88	-0.154	2.619	1.21
1-4	0.96	11.57	-0.117	2.608	1.21
1-5	0.99	14.84	0	2.158	1.00

Using the Ω_c obtained for Series 1-1 to 1-4, one can compute the corresponding V_s and hence the shear velocity using Eq. 5.3. The water depth at the mid-point of the suction zone, h_c, which is used for calculating U_c in the equation, was extrapolated from the h-V_s relationships for Series 1-1 to 1-4, which are shown in Fig. 5.4. The so-computed shear velocities, which are also tabulated in Table 5.4, represent the critical shear velocities with suction for these undisturbed flow conditions. The values in the last column in Table 5.4 show the computed values of u_{*cs}/u_{*co}; they clearly show that the critical shear velocity for sediment entrainment increases with the increase of suction rates. This is to be expected because suction creates a downward force on the sediment particles, making them more resistant to motion. This result is consistent with the earlier work by Cheng and Chiew (1999), who show that injection reduces the threshold condition for sediment entrainment. The experimental data of Cheng and Chiew (1999) conducted with injection (d_{50} = 1.02 mm) are plotted together with the present data (d_{50} = 0.9 mm) obtained with suction in Fig. 5.5. Despite the marginal difference in grain size, the data collapse to form a smooth curve, showing the effect of suction and injection on the critical shear velocity for sediment entrainment.

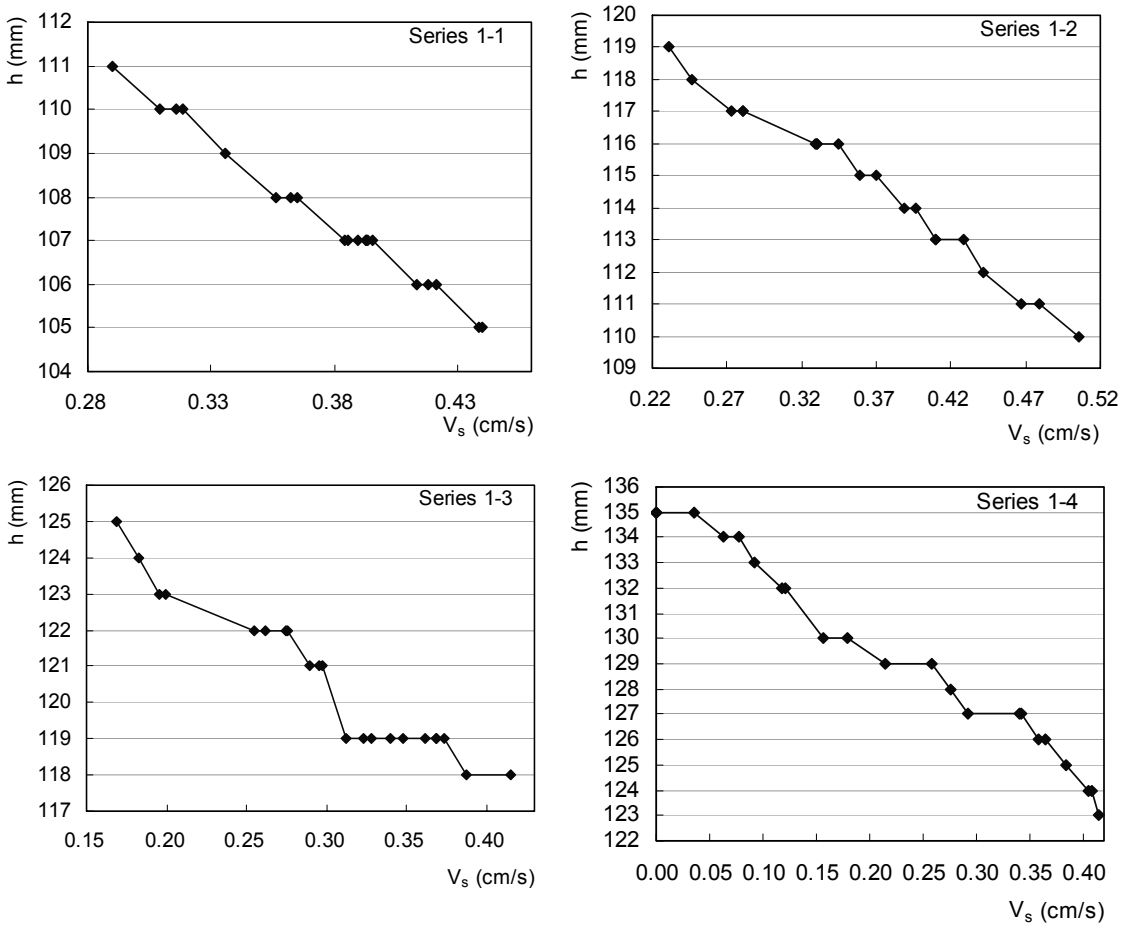

Figure 5.4 *h*-V_s Relationships for Series 1-1 to 1-4

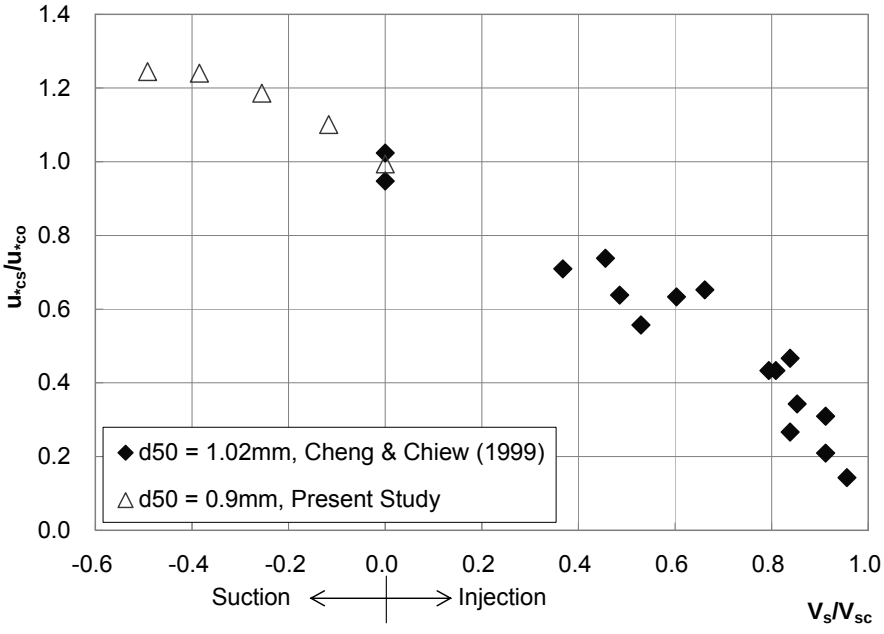

Figure 5.5 Critical Shear Velocities with Seepage

5.3.2 Effect of Suction on Shear Velocity

The preceding section outlines how suction increases the critical shear velocity for sediment entrainment. We now are ready to investigate the influence of suction on shear velocity, and hence its overall effect on shear velocity excess. Two suction velocities at V_s = -0.154 and -0.298 cm/s for Series 1-3 and 1-1, respectively, were chosen to illustrate this phenomenon. Their corresponding critical shear velocities have been previously computed as 2.619 and 2.741 cm/s, respectively (see Table 5.5). Similarly, the shear velocity, u_{*s} is computed using Eq. 5.3 proposed by Chen and Chiew (2004). The results are tabulated in Table 5.5, and they clearly show that the shear velocity increases with suction for all u_{*o}/u_{*co}. This result is to be expected and consistent with published data (Maclean, 1991; Ramkrishna Rao et al., 1991; Chen and Chiew, 2004) since suction brings high momentum fluid near the bed, and therefore, increases the shear velocity.

Table 5.5 Shear Velocity Excess with Different Suction Rates

Series	u_{*o}/u_{*co}	V_s = -0.154 cm/s u_{*cs} = 2.619 cm/s		V_s = -0.298 cm/s u_{*cs} = 2.741 cm/s	
		u_{*s} (cm/s)	u_{*s} - u_{*cs} (cm/s)	u_{*s} (cm/s)	u_{*s} - u_{*cs} (cm/s)
1-1	0.82	2.432	-0.19	2.741	0.00
1-2	0.87	2.533	-0.09	2.858	0.12
1-3	0.91	2.619	0.00	2.958	0.22
1-4	0.96	2.731	0.11	3.095	0.35
1-5	0.99	2.829	0.21	3.206	0.46

Taking u_{*o}/u_{*co} = 0.87 (Series 1-2) as an example, the shear velocity excess = -0.09 when V_s = -0.154 cm/s, i.e., that it is less than critical and therefore the bed remain immobile. When suction increases to -0.298 cm/s, however, the shear velocity has

increased to 2.858 cm/s. Even though the critical shear velocity has also increased (to 2.741 cm/s), the resulting shear velocity excess now becomes 0.12, showing that the bed has now become mobile.

Results from this simple computation confirm that suction increases both the shear and critical shear velocity but the overall results is an increase in the shear velocity excess, and hence an increase in bedload transport rate. The same inference can be drawn for all the other four u_{*o}/u_{*co} tested in Table 5.5; the results support the experimental observation that with the same undisturbed flow condition, the bedload transport rate increases with suction.

5.3.3 Determination of Empirical Φ-Ω Function

Figure 5.3 shows that Ω generally has a linear relationship with $log\Phi$ for a given τ_{*o}, which can be shown in equation as follows:

$$\log \Phi = A \cdot \Omega + B \qquad (5.4)$$

where A and B = coefficients. By empirically fitting the experimental data, the values of the coefficients A and B for different τ_{*o}, and the corresponding R^2-value of each series are obtained and tabulated in Table 5.6. As shown in Figure 5.3, the results do not fit to a perfect straight line. In this case, the measurements were subjected to experimental uncertainties. These uncertainties may be caused by the flow fluctuations due to the pump, the errors in measurement of suction velocity, the eyes and hand coordination to start and stop the watch, and the change of permeability of sediment particles due to downward seepage. However, to minimize the effects of uncertainties on the results, the method of least square curve fitting was performed in data analyses. The R^2-values tabulated in Table 5.6 shows that the experimental measurements can be considered as precise.

Table 5.6 Values of Coefficients *A* and *B* and corresponding R^2-values

	Series	τ_{*o}	*A*	*B*	R^2
d_{50} = 0.9 mm	1-1	0.0217	-1.5220	5.9727	0.8829
	1-2	0.0242	-0.8230	2.8523	0.9281
	1-3	0.0265	-0.6919	3.4401	0.9407
	1-4	0.0294	-0.4315	1.5936	0.9886
	1-5	0.0317	-0.2651	0.5374	0.9668
	1-6	0.0436	-0.1580	-0.1552	0.9147
	1-7	0.0525	-0.1522	0.3971	0.9271
d_{50} = 0.48 mm	2-1	0.0298	-0.4531	0.8895	0.9468
	2-2	0.0341	-0.2765	0.3706	0.9845
	2-3	0.0360	-0.1899	0.0164	0.9817
	2-4	0.0422	-0.1302	-0.0468	0.9051

As shown in Table 5.6, the coefficients *A* and *B* are functions of τ_{*o}; they are then plotted against τ_{*o} in Fig. 5.6. The black diamonds in the figure are data for Series 1, with d_{50} = 0.9 mm, and the open triangles refer to data for Series 2, with d_{50} = 0.48 mm. The data in Series 2 are chosen for verification, while those in Series 1, with d_{50} = 0.9 mm, are used for the determination of the empirical equation. The coefficients *A* and *B* were empirically fitted with τ_{*o}, giving the following equations:

$$A = 0.24 - \frac{0.057}{\tau_{*o}} + \frac{3.06\times10^{-3}}{\tau_{*o}^2} - \frac{5.71\times10^{-5}}{\tau_{*o}^3} \tag{5.5}$$

$$B = 11.83 - \frac{1.08}{\tau_{*o}} + \frac{2.86\times10^{-2}}{\tau_{*o}^2} - \frac{1.74\times10^{-4}}{\tau_{*o}^3} \tag{5.6}$$

The respective R^2-values are 0.980 and 0.941, and the two equations above are valid for $0.0217 \le \tau_{*o} \le 0.0525$. Using these three empirical determined equations (Eqs. 5.4 to 5.6), one can compute Φ-values for all the modified densimetric Froude number tested in the study. Figure 5.7 shows the comparison between the

measured and computed Φ-values, and they generally lie within an accuracy range of ±20%. This accuracy range is well within the acceptance level of most, if not all sediment transport studies. The good agreement between the computed and measured data shows that the empirically determined Eqs. 5.4 to 5.6 may be used to calculate bedload transport rate under the influence of suction. The semi-logarithmic function, which relates Φ with Ω, may be used once the coefficients A and B are known.

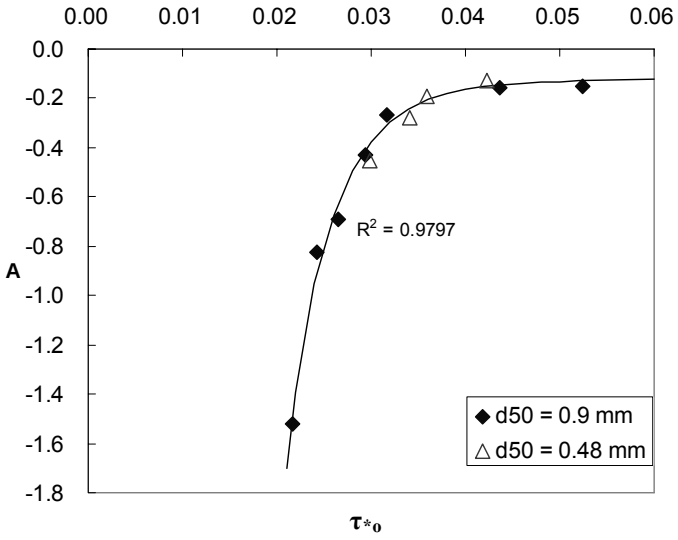

(a) Coefficient A against τ_{*o}

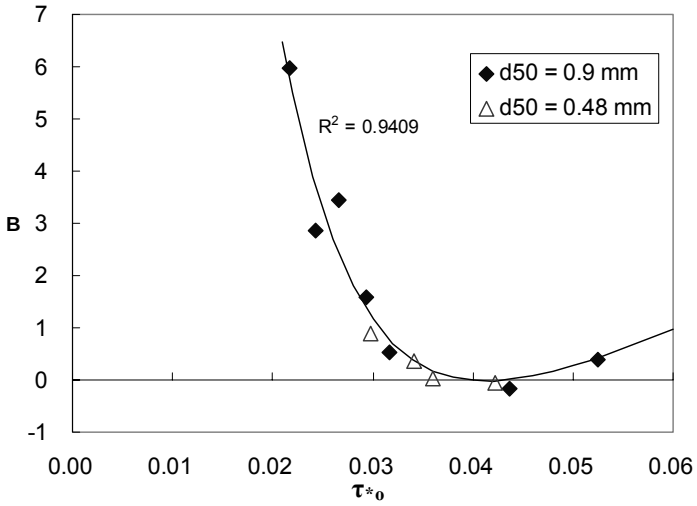

(b) Coefficient B against τ_{*o}

Figure 5.6 Relationships of Coefficient A and B against τ_{*o}

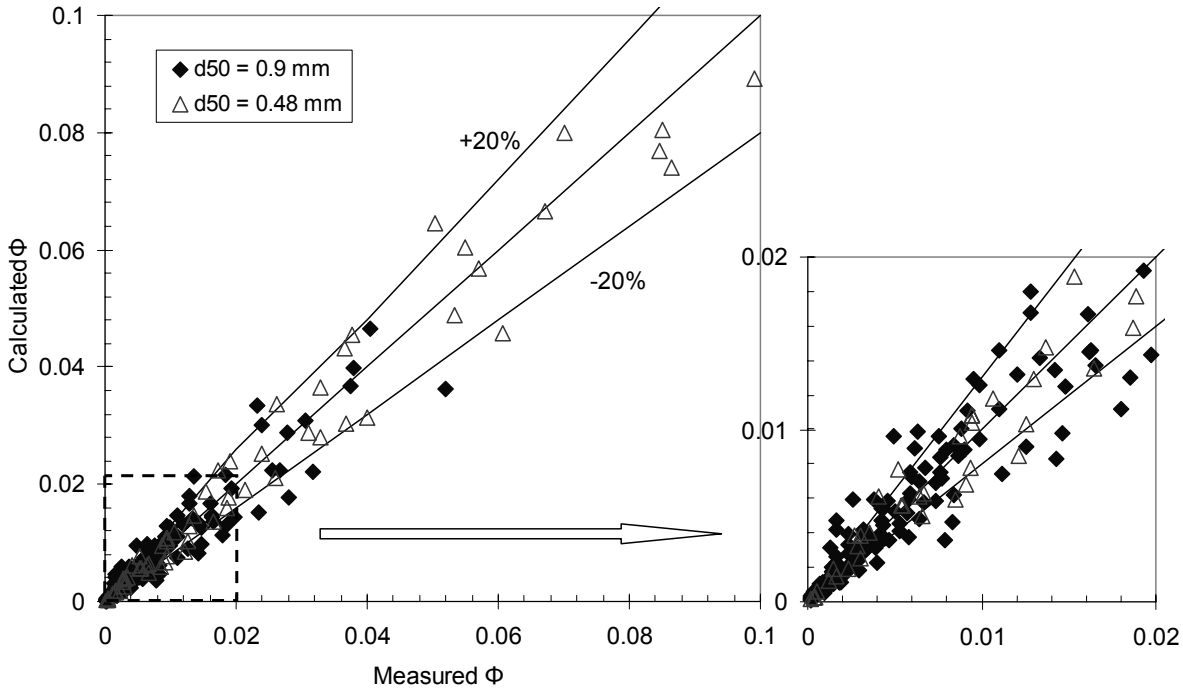

Figure 5.7 Calculated-Measured Comparison in *Φ*

5.3.4 Comparison with Previous Investigations

In this section, comparisons between previous studies and results of the present work are discussed. Due to the limitation of experimental information and results provided in published literature, only the works of Maclean (1991), Ramakrishna Rao and Sitaram (1999) and Francalanci et al. (2008) were chosen as the representative.

5.3.4.1 Maclean (1991)

Maclean (1991) conducted laboratory experiments with sediment d_{50} = 1 mm in a tilting perspex flume that is 75 mm wide and 5 m long to determine the increase in bed shear stress and local scour depth over a short suction zone (130 mm long). He reported that the application of suction to the bed of an alluvial channel

produces an increase in bed shear stress that results in local scouring. The experimental results (Maclean and Willetts, 1984 and 1986) obtained are shown in Table 5.7, in which r_e = volumetric sediment erosion rate per unit area; and τ_{bo} = bed shear stress without suction.

Table 5.7 Erosion Rate under Different Suction Velocity (Maclean and Willetts, 1984 and 1986)

Test Number	U_o *(m/s)*	$\lvert V_s/U_o \rvert$ *(%)*	h_o *(mm)*	τ_{bo} *(N/m^2)*	r_e *(mm/s)*
M1	0.294	0.094	100	0.494	0.00562
M2	0.339	0.052	75	0.683	0.00848
M3	0.339	0.063	75	0.683	0.01778
M4	0.392	0.065	75	0.912	0.02683
M5	0.392	0.055	75	0.912	0.03433
M6	0.392	0.071	75	0.912	0.04047

With the information given in Table 5.7, one may compute the bedload transport rate using the method proposed in this study. The specific gravity, S_s and the permeability, K, which could not be confirmed from Maclean's paper, are assumed to be the same as those of the d_{50} = 0.9 mm sand particle used in this study. The dimensionless shear stress, τ_{*o} is computed using the following equation

$$\tau_{*o} = \frac{\tau_{bo}}{(S_s - 1)\rho g d_{50}} \tag{5.7}$$

Moreover, the coefficients of A and B are calculated using Eqs. 5.5 and 5.6, respectively. Table 5.8 shows Maclean's measured data and those computed using the proposed method. The error between the predicted Φ-values using Eqs. 5.4 to 5.6 and those calculated base on Maclean's results ranges from 19.5% to 97.4%, which is within acceptability for sediment transport rate computations.

Table 5.8 Comparison between Prediction Using Eqs. 5.4 to 5.6 and Maclean's Results

Test Number	U_o *(m/s)*	V_s *(cm/s)*	Ω	τ_{*o}	*A*	*B*	Φ *(Predicted)*	Φ *(Maclean)*	*%Error*
M1	0.294	-0.028	8.79	0.0307	-0.3432	0.9811	0.0092	0.0058	59.7
M2	0.339	-0.018	11.90	0.0425	-0.1511	-0.0151	0.0154	0.0087	76.8
M3	0.339	-0.021	11.82	0.0425	-0.1511	-0.0151	0.0158	0.0132	19.5
M4	0.392	-0.025	15.69	0.0567	-0.1267	0.7230	0.0543	0.0275	97.4
M5	0.392	-0.022	15.80	0.0567	-0.1267	0.7230	0.0526	0.0352	49.3
M6	0.392	-0.028	15.62	0.0567	-0.1267	0.7230	0.0553	0.0415	33.4

Generally speaking, Maclean's data agree with the results of this study in that their conclusion points to an increase in bed shear stress and local scouring with the introduction of suction. Moreover, their measured data, to a large extent, also support the predictive method proposed in this study.

5.3.4.2 Ramakrishna Rao and Sitaram (1999)

Both injection and suction effects on sediment transport were studied by Ramakrishna Rao and Sitaram (1999) in a titling rectangular channel that is 15.75 cm wide and 3.6 m long over a 2.4 m-length suction zone. They stated that suction reduces the stability of bed particles, while injection decreases particles mobility on a transporting bed. Table 5.9 tabulates their experimental data for the test series with d_{50} = 1.0 mm, S_s = 2.64, and u_{*co} = 2.304 cm/s, in which Q_o = streamwise flow rate; Q_s = seepage flow rate; and h_c = water depth at the mid-section of seepage zone. The sediment particles in all these 3 test runs, namely Tests RR1-1, RR2-1 and RR3-1 were not transporting (NT), i.e., $u_{*o} < u_{*co}$, before suction was introduced. Suction was then progressively increased until the incipient motion condition (I) was reached, labeled as Tests RR1-2, RR2-2 and RR3-2 in Table 5.9.

Table 5.9 Experimental Data of Ramakrishna Rao and Sitaram (1999)

Test Number	Q_o *(l/s)*	Q_s *(l/s)*	h_c *(mm)*	*Bed Condition*
RR1-1	1.355	0	28.1	NT
RR1-2	1.355	-0.219	24.8	I
RR2-1	1.355	0	29.3	NT
RR2-2	1.355	-0.168	26.6	I
RR3-1	1.092	0	25.0	NT
RR3-2	1.092	-0.196	22.5	I

With the values given in Table 5.9, the shear velocity without seepage, u_{*o}, could be computed using the mean velocity equation for a rough bed, or what is customarily called the Keulegan equation (Keulegan, 1938) with $2d_{50}$ as the roughness height. The bed shear velocity, u_{*s} for each test is calculated using Eq. 5.1 while the critical shear velocity, u_{*cs}, is computed using the same method in the present study. The so-computed critical shear velocities based on the data of Ramakrishna Rao and Sitaram (1999) are superimposed in Fig. 5.8 as open square; and they generally support the conclusion drawn from the present study that an increase in suction rate causes an increase of the critical shear velocity. Using the computed u_{*cs}-values, the shear velocity excess, $u_{*s} - u_{*cs}$, is calculated and tabulated in Table 5.10, which shows that when suction rate increases, the bed shear stress and critical shear stress increase simultaneously. Moreover, the shear velocity excess, u_{*s} - u_{*cs}, increases from less than zero to nearly zero that is the threshold condition. These data indicate that suction causes the bed to change from a non-transporting to the threshold condition. One may deduce from this result that the bed particles would start moving if suction rate were allowed to increase further, although this was not conducted in the experiment. It may be inferred from this analysis that the result of Ramakrishna Rao and Sitaram (1999) also support the inference drawn from this study.

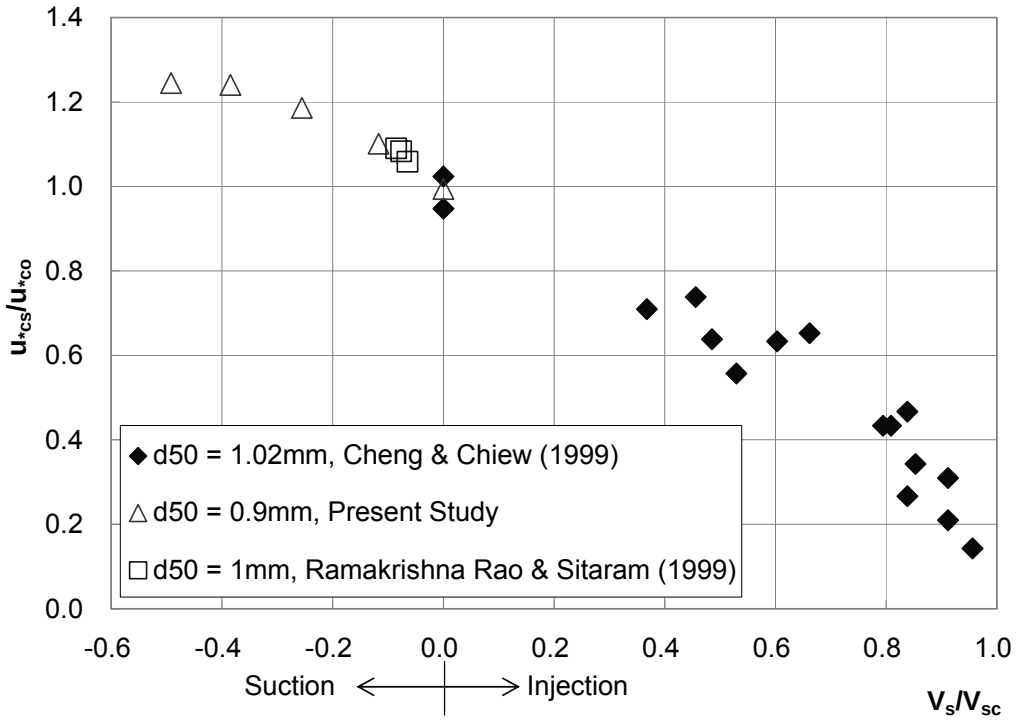

Figure 5.8 Critical Shear Velocity with Seepage with u_{*cs} from Ramakrishna Rao and Sitaram (1999)

Table 5.10 Shear Velocity Excess for Ramakrishna Rao and Sitaram's Data

Test Number	U_o *(cm/s)*	V_s *(cm/s)*	u_{*o} *(cm/s)*	u_{*s} *(cm/s)*	u_{*cs} *(cm/s)*	$u_{*s} - u_{*cs}$	*Bed Condition*
RR1-1	30.62	0	2.222	2.222	2.304	< 0	NT
RR1-2	30.62	-0.058	2.222	2.508	2.512	≈ 0	I
RR2-1	29.36	0	2.175	2.175	2.304	< 0	NT
RR2-2	29.36	-0.044	2.175	2.464	2.439	≈ 0	I
RR3-1	27.73	0	2.166	2.166	2.304	< 0	NT
RR3-2	27.73	-0.052	2.166	2.485	2.496	≈ 0	I

5.3.4.3 Francalanci et al. (2008)

Contrary to the conclusions drawn by Maclean (1991), Ramakrishna Rao and Sitaram (1999) and the present study, Francalanci et al. (2008) arrived at a completely different position based on their experimental study. Their experiments were conducted using sediment particles with d_{50} = 0.84 mm in a glass-sided sediment-recirculating, water-feed flume. The flume, which was 15 m long, 0.61 m wide and 0.4 m deep, has a seepage zone that is 1.1 m long. Their experimental results showed that upward seepage (injection) induces scour and downward seepage (suction) causes deposition. It may be inferred from their results that injection and suction increases and decreases bedload transport rate, respectively. Clearly, this is contrary not only to the results of this study but also those of Maclean (1991) and Ramakrishanan Rao and Sitaram (1999). We will attempt to offer an explanation for this disparity.

Francalanci et al. (2008) explained their experimental results with reference to the formation of a backwater surface profile that forms upstream of the suction zone when suction is introduced. They argued that the water depth upstream of the suction zone is lowered due to backwater effects and the actual water depth lowering is, presumably, caused by suction itself. Hence, the bed shear stress in the backwater zone is higher than that with the undisturbed flow condition. They further claimed that the bed shear stress within the suction zone is smaller than that in the backwater zone, resulting in scouring in the backwater zone, and deposition in the suction zone.

If their analysis were true, one may reasonably conclude that their observed deposition associated with suction is not directly due to a change in the shear velocity excess, but simply a response to the different sediment transport rate.

Specifically, the deposition is due to the fact that the amount of sediment entering the suction zone per unit time is higher than that leaving. Therefore, their results cannot be construed to mean that suction reduces the bedload transport rate. Since the experimental studies conducted by the other researchers did not allowed sediment input to the suction zone, deposition clearly cannot take place and a "real" response of the sediment mobility to suction is revealed.

Another important difference between the study conducted by Francalanci et al. (2008) and that of the present study and those by Maclean (1991) and Ramakrishanan Rao and Sitaram (1999) is that the former was carried out in a sediment-recirculating flume while the rests were conducted in a sediment-feed flume. Parker and Wilcock (1993) compared the difference between sediment feed and sediment recirculating flume when sediment mixtures are used. Using their argument, the difference between the use of a sediment-feed and recirculating flume to study bedload transport with seepage is examined and discussed.

Regardless of the type of flume, the following constraints hold:

$$Q_o = U_o b h_o \tag{5.8}$$

$$U_o h_o = U_c h_c + V_s L/2 \tag{5.9}$$

where b = width of flume; and L = length of suction zone. Both b and L are constants for a given flume. Equation 5.9 is the continuity equation at the middle section of the suction zone. In addition to the foregoing mass conservation relations, general constitutive relations for sediment transport and bed resistance must hold at equilibrium. These can take a variety of forms, but for simplicity, the following general forms are used:

$$\Phi_o = \frac{q_{bo}}{\sqrt{(S_s-1)g d_{50}^3}} = f_1\left(\tau_{*o}, \frac{U_o^2}{(S_s-1)g d_{50}}\right) \tag{5.10}$$

$$\frac{U_o}{u_{*o}} = f_2\left(\frac{h_o}{k_s}\right) \tag{5.11}$$

where $k_s = n_s d_{50}$; and n_s = an order-one parameter. As discussed in Parker and Wilcock (1993), the value of n_s could be reasonably assumed as a constant value. The symbols f_1 and f_2 denote specified functions.

According to the equation proposed by Chen and Chiew (2004), the bed shear velocity could be calculated using u_{*o}, V_s and U_c. Moreover, it is also found in the present study that Einstein's parameter Φ with seepage is a function of τ_{*o} and the modified densimetric Froude number Ω. Therefore, two more relations could be added:

$$\frac{u_{*s}}{u_{*o}} = f_3\left(\frac{V_s}{U_c}\right) \tag{5.12}$$

$$\Phi = f_4\left(\tau_{*o}, \Omega\right) \tag{5.13}$$

The symbols f_3 and f_4 denote specified functions.

Eqs 5.8 to 5.13 specify six equations and fourteen variables – Q_o, U_o, h_o, U_c, h_c, V_s, u_{*o}, u_{*s}, q_{bo}, q_{bs}, S_s, d_{50}, K and n. In a sediment-feed flume, which is used in the present study, Q_o and V_s are pre-determined using the electromagnetic flow meter and direct measurement of the flow through the seepage pipes, respectively, and therefore are known values. The water depth without seepage, h_o is controlled by adjusting the weir height; d_{50}, S_s, n and K are specified by the type of material fed; and q_{bo} are determined by the feed-rate at the upstream end of the flume. These specify eight more constraints in addition to Eqs. 5.8 to 5.13, allowing for a solution for U_o, U_c, h_c, u_{*o}, u_{*s}, and q_{bs} in terms of Q_o, h_o, V_s, q_{bo}, S_s, d_{50}, K and n. In this case, each solution carried forward in time has the same q_{bo}-value, since q_{bo} is constant with time.

In a re-circulating flume, the constraints given by Q_o, h_o, V_s, S_s, d_{50}, K and n are similar to those in the sediment-feed flume. However, the incoming sediment transport rate at the upstream end of seepage zone, q_{bo}, is equal to that at the end of the flume at the previous time step. That means that q_{bo} is changing with time, and could not be specified in advance. As a result, the problem of predicting the final equilibrium state from the constraints of flume operation becomes indeterminate. To determine the final equilibrium state, the time function of q_{bo} must be specified, i.e., $q_{bo}(t)$. Therefore, in the re-circulating case, each solution carried forward in time has a different q_{bo}-value. The final solution likely will be different from that in a sediment-feed flume which has a constant q_{bo}. This difference may be the reason between the experimental results obtained by Francalanci et al (2008) and those by Maclean (1991), Ramakrishanan Rao and Sitaram (1999) and the present study.

5.4 EXPERIMENTAL RESULTS OF TESTS SUBJECTED TO INJECTION

The sediment transport rates with the presence of injection were measured only for Series 1-5 to 1-7, i.e., the median grain size, d_{50} = 0.9 mm. The range of injection rates applied is tabulated in Table 5.11. Due to physical constraints of the experimental apparatus, the maximum injection velocity applied is 0.435 cm/s and the quick condition is not reached yet for all the tests conducted.

Table 5.11 Range of Injection Rate for Each Series

d_{50} (mm)	Series	τ_{*o}	Range of Injection V_s (cm/s)
0.90	1-5	0.0317	0 – 0.435
	1-6	0.0436	0.019 – 0.319
	1-7	0.0525	0.014 – 0.251

The measured bedload transport rates are plotted against injection rate in Fig. 5.9. The detailed experimental results are tabulated in Appendix I. The experimental data show that the injection has an opposite effect on sediment transport rate when compared with that for suction. The sediment transport rate generally decreases with an increase in injection velocity. While the injection velocity increases from 0 to 0.25 cm/s, the bedload transport rate of Series 1-5 decreases by about 30% from 0.05×10^{-6} m^2/s to 0.035×10^{-6} m^2/s, that of Series 1-6 decreases by about 33% from 0.12×10^{-6} m^2/s to 0.08×10^{-6} m^2/s, and that of Series 1-7 decreases by about 40% from 0.25×10^{-6} m^2/s to 0.15×10^{-6} m^2/s. It may be inferred from this trend that the trend of reduction becomes more apparent for higher τ_{*o}-values.

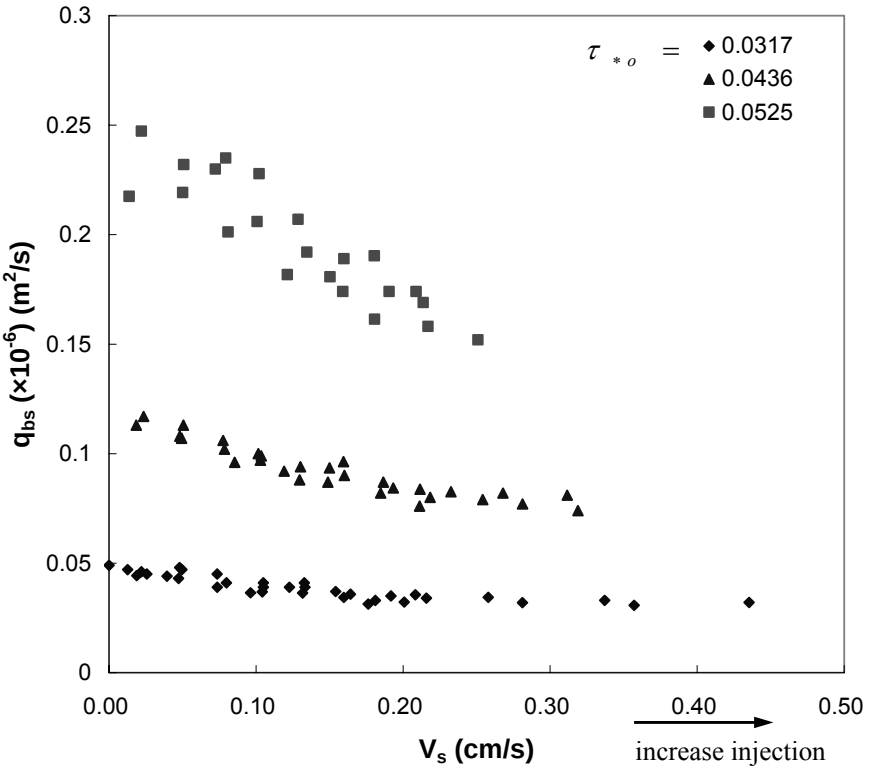

Figure 5.9 Relationship of q_{bs} and V_s for Different Undisturbed Flow Conditions with Injection

The experimental results for the case of injection, together with those with suction for the same series, are then plotted in terms of Φ against Ω as shown in Fig. 5.10. For the sake of completeness, the data for suction at the same τ_{*o} are also included in the figure for comparison. The solid symbols represent the series subjected to suction, whereas the open ones refer to that with injection. The points linking the suction and injection data are the results measured with no-seepage condition. The figure shows that with the same τ_{*o}, Φ decreases with a reduction in Ω, i.e., an increase in injection. It may be inferred from this trend that for the same undisturbed flow condition, the bedload transport rate, which also may be represented by Einstein's dimensionless parameter Φ, is decreasing with an increase in injection rate. However, the series with initial transporting bed, viz., Series 1-6 and 1-7 (the open triangle and open square, respectively), do not revert to the threshold condition within the range of injection applied during the tests. Figure

5.10 also shows that the magnitude of the reduction of sediment transport rate caused by the presence of injection is relatively small when compared with that of the increment in the same undisturbed condition but subjected to suction.

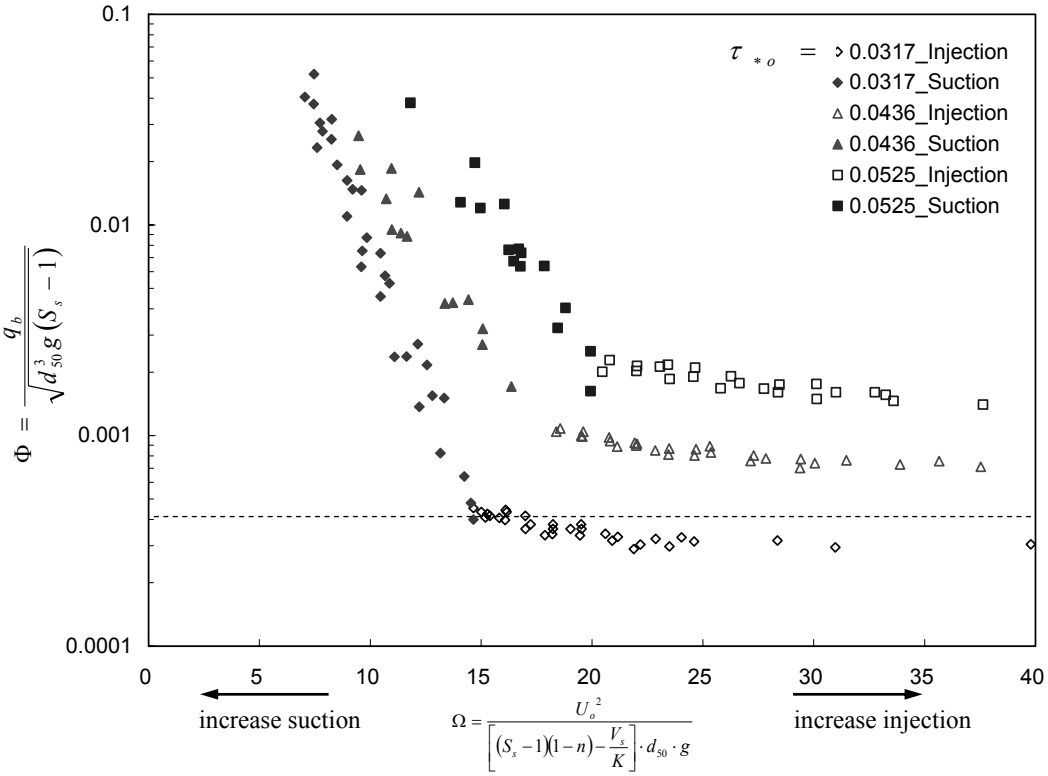

Figure 5.10 Relationship of Ω and Φ for Both Injection and Suction

5.5 EFFECT OF INJECTION ON SEDIMENT TRANSPORT

Cheng and Chiew (1998a) had shown that bed shear stresses decrease with injection rates. They derived a modified logarithmic law from turbulence kinetic energy equation to account for the effect of upward seepage on the velocity distribution in open-channel flow, in which the shear velocity is related to the depth-averaged velocity, water depth, boundary roughness, and seepage velocity as follows

$$U = \frac{u_{*s}}{\kappa}\left(\ln\frac{h}{y_*} - 1\right) + \frac{V_s}{4\kappa^2}\left[\ln^2\frac{h}{y_*} - 2\left(\ln\frac{h}{y_*} - 1\right)\right] \qquad (5.14)$$

where $y_* = k_s \exp\left(-\kappa \cdot R_f\right)$; and $R_f = \dfrac{8.5}{1+V_s/u_{*s}}$.

Additionally, Cheng and Chiew (1999) showed that the critical shear velocity is reduced in the presence of upward seepage or injection. The ratio of the critical shear velocity with seepage to that without seepage is expressed as a function of the ratio of injection velocity to its value at the quick condition as follow

$$\left(\frac{u_{*c}}{u_{*oc}}\right)^2 = 1 - \left(\frac{V_s}{V_{sc}}\right)^m \tag{5.15}$$

where $m = \dfrac{1+2\delta \cdot l_{\varepsilon*}^2}{1+\delta \cdot l_{\varepsilon*}^2}$; $l_{\varepsilon*} = \left(\dfrac{g}{\nu^2}\right)^{1/3} \dfrac{n \cdot d}{6(1-n)}$; and $\delta = 0.0027$.

5.5.1 Effect of Injection on Shear Velocity Excess

Based on the results of the work by Cheng and Chiew (1998a and1999), both shear velocity and critical shear velocity will decrease with an increase in injection. The concept that was used for suction is similarly applied here to investigate the effect of injection on shear velocity excess. If the shear velocity excess, $u_{*s} - u_{*cs}$ decreases, the difference between the driving force and resistance force becomes smaller and the sediment particles will move slower. When $u_{*s} - u_{*cs}$ reduces to a negative number, the sediment bed become immobile and the sediment particle will not move. The bed stability increases with a reduction in the shear velocity excess. Experimental observations showed that the sediment particles moved slower in the presence of injection. Hence, the reduction in shear velocity must be more than that of critical shear velocity, resulting in an overall decrease in shear velocity excess, $u_{*s} - u_{*cs}$. A simple inference from the measured data showing that bedload transport rate decreases with injection is that the shear velocity excess, $u_{*s} - u_{*cs}$, must have decreased.

An illustration is presented to understand this phenomenon. The shear velocities and critical shear velocities of two arbitrary injection velocities of V_s = 0.072 cm/s and 0.251 cm/s for Series 1-5 to 1-7 are computed using Eqs. 5.11 and 5.12. The results are tabulated in Table 5.12, which clearly shows that both the shear velocity and the critical shear velocity decrease with injection for all u_{*o}/u_{*co} tested. Moreover, the shear velocity excess also decreases with an increase in injection rate. For example, at the no-seepage condition, the shear velocity excess for Series 1-7 (u_{*o}/u_{*co} = 1.28) = 0.60 cm/s, i.e., that it is a transporting bed. The shear velocity decreases to 2.026 cm/s when the injection rate increases to 0.251 cm/s. At the same time the critical shear velocity also decreases to 1.715 cm/s. The resulting shear velocity excess now becomes 0.31 cm/s, showing that the bed is less mobile and the sand particles move slower. Referring to Series 1-5 (u_{*o}/u_{*co} = 0.99), the shear velocity excess = -0.01 ≈ 0 cm/s when V_s = 0, i.e., that it is at the threshold condition and therefore the bed particle is just about to move. When injection increases to 0.072 cm/s, the shear velocity and the critical shear velocity have decreased to 1.902 cm/s and 2.040 cm/s, respectively. The resulting shear velocity excess now becomes -0.14, showing that the bed has now become immobile. When injection increases further to 0.251 cm/s, the shear velocity excess further reduces to -0.36 cm/s, showing that the bed has become more stable and the sand particles become harder to move.

The same inference can be drawn for Series 1-6 (u_{*o}/u_{*co} = 1.17) as shown in Table 5.12. The illustrations in the previous paragraph and Table 5.12 confirm that injection reduces both the shear and critical shear velocity but the overall result is a reduction in the shear velocity excess, and hence a reduction in bedload transport rate. These results support the experimental observation that with the same undisturbed flow condition, the bedload transport rate reduces with injection.

Table 5.12 Shear Velocity Excess with Different Injection Rates

Series	u_{*o}/u_{*co}	$V_s = 0$ $u_{*co} = 2.156$ cm/s		$V_s = 0.072$ cm/s $u_{*cs} = 2.040$ cm/s		$V_s = 0.251$ cm/s $u_{*cs} = 1.715$ cm/s	
		u_{*o} (cm/s)	$u_{*o} - u_{*co}$ (cm/s)	u_{*s} (cm/s)	$u_{*s} - u_{*cs}$ (cm/s)	u_{*s} (cm/s)	$u_{*s} - u_{*cs}$ (cm/s)
1-5	0.99	2.145	-0.01	1.902	-0.14	1.357	-0.36
1-6	1.17	2.516	0.36	2.288	0.25	1.776	0.06
1-7	1.28	2.759	0.60	2.547	0.50	2.026	0.31

5.5.2 Determination of Empirical Function of Φ with Injection

Unlike that associated with suction, Fig. 5.10 shows that a linear relationship in the semi-logarithmic scale between Φ and Ω does not hold for the case of injection. The trend function of each test series associated with injection is different from each other. As a result, there is no general function likely to fit the experimental data with different undisturbed flow condition. Therefore, two new dimensionless terms are introduced to investigate the injection effect on sediment transport rate. The ratio of Einstein's parameter Φ with and without injection is plotted against the ratio of modified densimetric Froude number Ω with and without injection as shown in Fig. 5.11. Only with the use of these two dimensionless teams could we better collapse the experimental data.

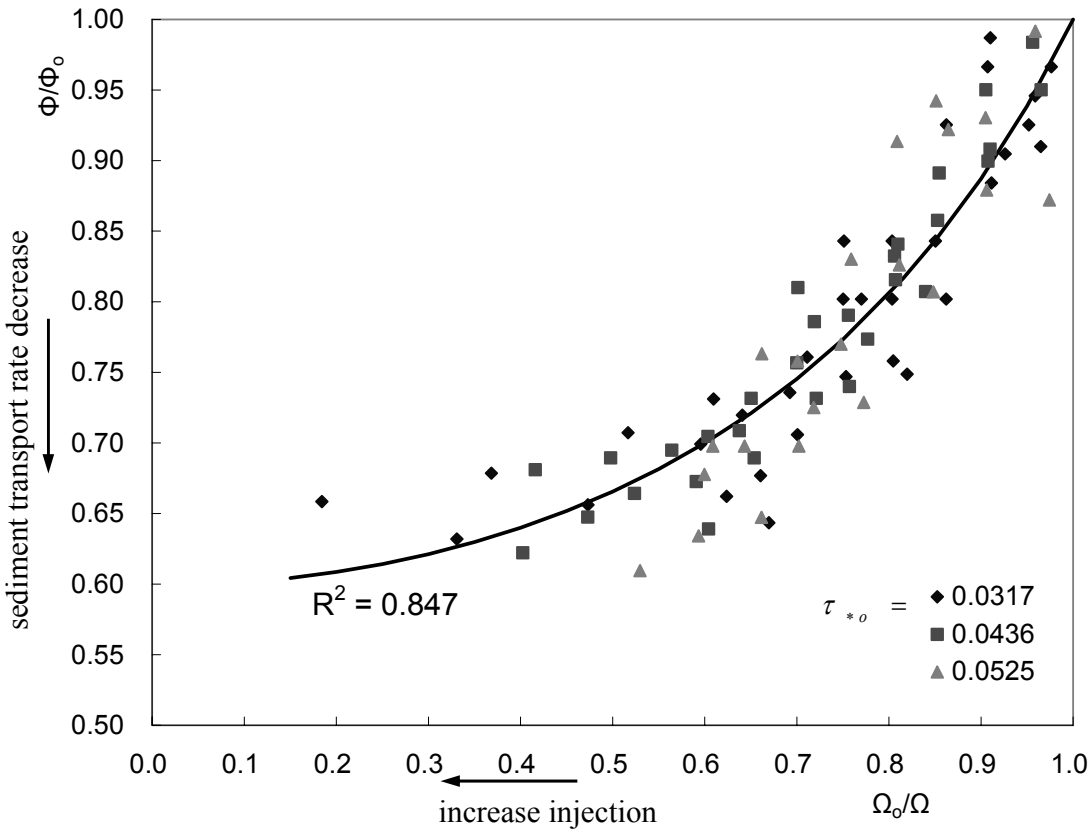

Figure 5.11 Relationship of Φ/Φ_o and Ω_o/Ω for Data Subjected to Injection

Figure 5.11 shows that regardless of the undisturbed flow conditions, Φ/Φ_o for all the series tested collapse to form a smooth curve when plotted against Ω_o/Ω, where Φ_o = Einstein's parameter without seepage; and Ω_o = modified densimetric Froude number without seepage. The coordinate with $\Omega_o/\Omega = \Phi/\Phi_o = 1$ refers to the case in the absence of injection or the no seepage condition. As shown in Fig. 5.11, a reduction in Ω_o/Ω, i.e., an increase in injection velocity, causes a reduction in Φ/Φ_o, resulting in a reduction in sediment transport rate. In addition, the magnitude of the reduction in sediment transport rate with the presence of injection is comparably smaller than that of the increment with suction.

By empirically fitting the experimental data, the relationship between Φ/Φ_o and Ω_o/Ω is giving as follow:

$$\frac{\Phi}{\Phi_o} = \frac{1}{-0.67\left(\frac{\Omega_o}{\Omega}\right)^2 + 1.67} \tag{5.16}$$

The above equation is valid for $0.18 \leq \Omega_o/\Omega \leq 1$, with R^2-value = 0.847. This relationship is valid only before the quick condition is reached. The effect of injection at the quick condition is not within the scope of this study. Even at the highest injection rate tested (Ω_o/Ω = 0.18), Φ/Φ_o = 0.66. This means that the sediment particles only move slower but have not reached the threshold condition even at the highest injection rate tested. As a result, we are unable to get data at the critical shear velocity under injection, and no comparison with the published results of Cheng and Chiew (1999) is possible.

5.6 SUMMARY

This chapter presented results collected in Experimental Series II. The study shows that both the bed shear velocity (the driving force component) and critical shear velocity (the resistant force component), decrease and increase with an increase in injection and suction rates, respectively. The results of the critical shear velocity with suction are consistent with the earlier work by Cheng and Chiew (1999), who showed that the critical shear velocity of the bed sediment decreases with injection. The data also show that the computed shear velocity excess, which is defined as the difference between the bed shear velocity and the critical shear velocity, decrease and increases with the increase of injection and suction rates, resulting in a reduction and increase in bedload transport rate, respectively.

The measured data show a significant increase in bedload transport rate with the increase of suction velocity for the same initial flow condition. The experimental results show that Φ has a linear relationship of Ω in semi-logarithmic scale (i.e., $\log \Phi = A \cdot \Omega + B$), where the coefficients A and B, which are uniquely related to τ_{*o}, may be calculated using Eqs. 5.5 and 5.6. Using the experimental results, the bedload transport rate can be predicted within a ±20% accuracy for a given τ_{*o} for $0.0217 \leq \tau_{*o} \leq 0.0525$.

The comparison with the published results of Ramakrishan Rao and Sitaram (1999) shows that the shear velocity excess increases with the increase of suction rate, leading to an increase in sediment transport rate. The proposed prediction method of sediment transport rate using Eqs. 5.4 to 5.6 is closed to Maclean's (1991) results with error ranging from 19.5% to 97.4%. Discussion of the fundamental difference between a sediment-recirculating system and sediment feed system was made when considering Francalanci et al's (2008) work. The use of two different

flume systems could be the reason for the discrepancy of the sediment transport behavior in the seepage zone.

The reduction in sediment transport rate in the presence of injection is relatively small comparing with that with suction. The ratio of Einstein's parameter with and without injection, Φ/Φ_o is found to be a function of the ratio of the modified densimetric Froude number without and with injection, Ω_o/Ω. The empirical expression is shown in Eq. 5.16 for $0.18 \leq \Omega_o/\Omega \leq 1$.

Chapter 6

Effect of Suction Zone Length on Sediment Transport Rate

6.1 INTRODUCTION

In Chapter 5, the effect of seepage on sediment transport rate was investigated. Since the sediment transport rate with suction is larger than that without, i.e., the sediment transport rate is higher in the suction zone, erosion will, therefore, occur. On the other hand, the empirical equations (Eqs. 5.4 to 5.6) proposed for predicting sediment transport rate with suction only consider the average sediment transport rate over the entire 2-m length seepage zone. It was observed during Experimental Series II that, with the presence of suction, the extent of erosion across the entire suction zone was not uniform. Figure 6.1 shows the erosion depths along the suction zone measured at 10-cm interval for Series 1-2 (τ_{*o} =0.0242) at V_s = -0.321 and -0.41 cm/s. The bed elevations for both cases were measured around 20 minutes after the tests started. The open square represents the data measured with V_s = -0.321 cm/s, whereas the black diamond refers to those measured with V_s = -0.41 cm/s. The positive and negative bed elevations refer to the extent of

deposition and erosion in the suction zone, respectively. This figure shows that erosion at the beginning of the suction zone is larger when compared with that at the downstream section. The erosion depth gradually reduces in the downstream direction along the seepage zone. It is interesting to notice that there is a hump around the middle length of suction zone. For instance, the erosion depth for the test run with V_s = -0.321 cm/s (open square in Fig. 6.1) is about 1 mm for the first 0.5 m of suction zone. The erosion depth gradually decreases to zero for next 0.5 m in the middle section; and then starts to increase again to 0.5 mm for next 0.6 m. At the last 0.4 m of the suction zone, the erosion depth is further reduced to zero. This phenomenon is more obvious with higher suction rates as shown in Fig. 6.1, in which the erosion depths along the suction zone with V_s = -0.41 cm/s (black diamond in Fig. 6.1) are larger than that with V_s = -0.321 cm/s.

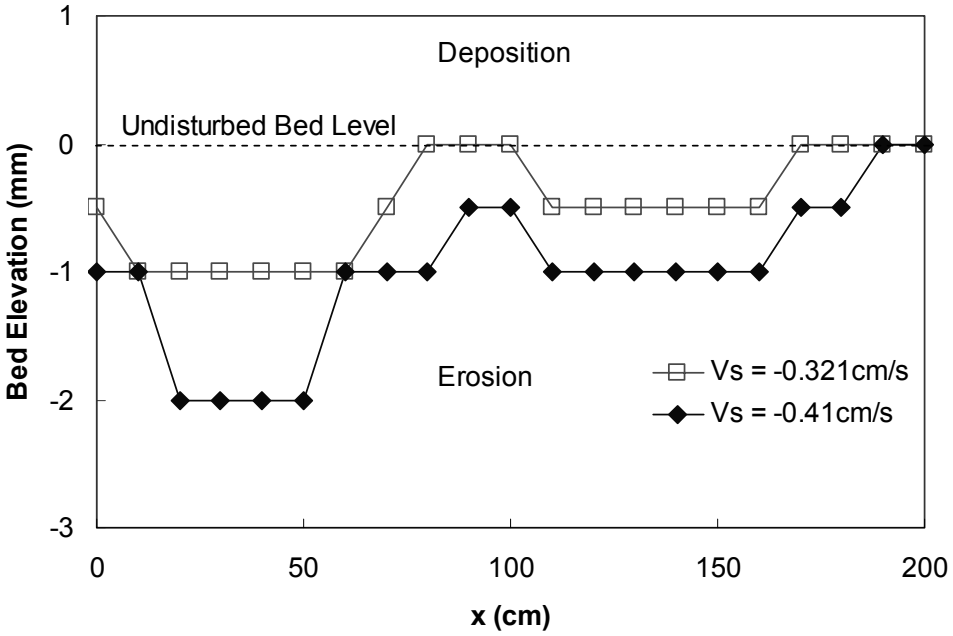

Figure 6.1 Longitudinal Distribution of Bed Elevation over the Suction Zone for Series 1-2 (τ_{*o} =0.0242)

The above phenomenon may be related to the shear stress distribution along the seepage zone when it is subjected to either suction or injection. As was discussed

in Chapter 2, Cheng & Chiew (1998a) investigated this distribution for the case of injection, while Chen & Chiew (2004) did that for suction. Both their measurements were obtained with 2-m length seepage zone. Figure 6.2 shows the longitudinal distribution of bed shear stress over the seepage zone for both upward and downward seepage reported in Cheng and Chiew (1998a) and Chen and Chiew (2004). Since Chen and Chiew (2004) reported only the streamwise variation of u_{*s}/u_{*o}, the values of τ_{bs}/τ_{bo} for the case of suction were computed as the square of their results. Each series of results represents different V_s/U_o ratio. The positive and negative V_s/U_o-values refer to the flow conditions subjected to injection and suction, respectively.

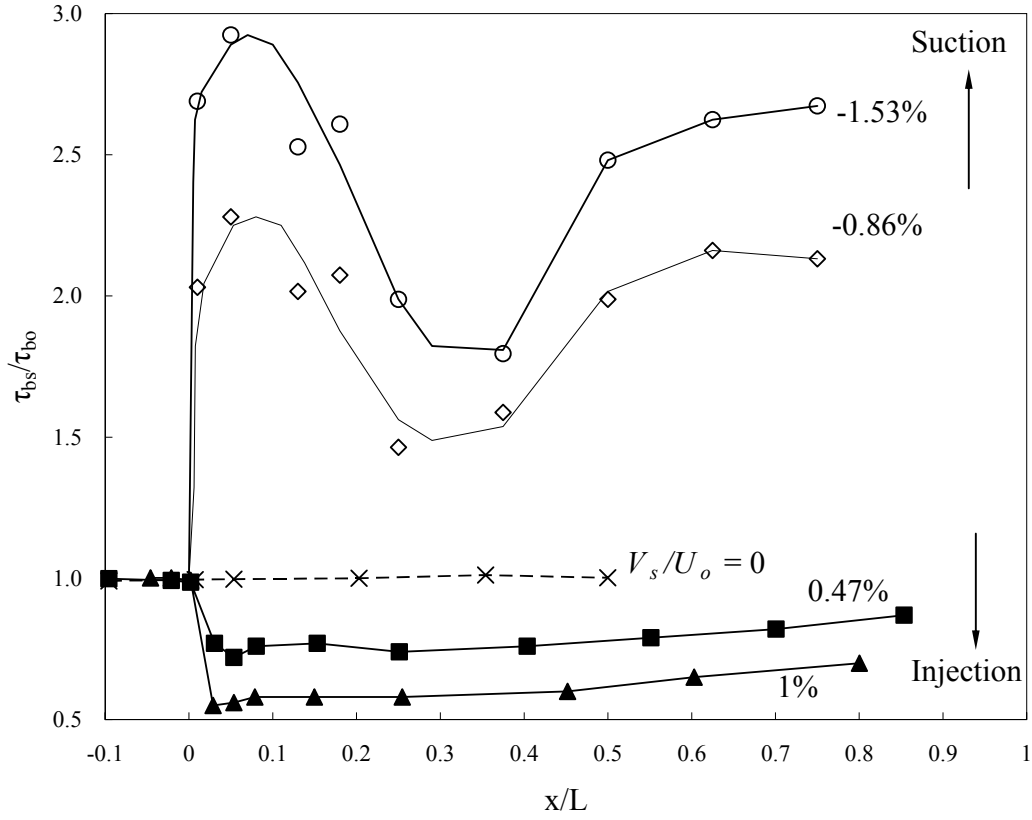

Figure 6.2 Longitudinal Distribution of Bed Shear Stress over the Seepage Zone

Taking the series with V_s/U_o = -0.86% for suction as an example, the data show that

the relative bed shear stress τ_{bs}/τ_{bo} increases to approximately 1.5 within the first 1/10 of the seepage zone length. The τ_{bs}/τ_{bo}-value then gradually decreases along the downstream and reaches about 1.21 at x/L = 0.3. Then the τ_{bs}/τ_{bo}-value gradually increases and eventually reaches 1.44 at x/L = 0.73. This abrupt change of bed shear stress at the upstream end of the seepage zone is apparent for both injection and suction. The data trend shows that there is a rapid increase and decrease in the bed shear stress with suction and injection, respectively, at this location. The increment or reduction is more apparent for higher seepage intensity. However, toward the downstream end of the seepage zone the bed shear stress exhibits a gradual increase and decrease for the case of injection and suction, respectively.

Based on these results and the experimental observation, the distributions of bed shear stress and sediment transport rate are not uniform across the entire seepage zone. One may infer from this that with the presence of seepage, the length of the seepage zone appears to affect the bed shear stress, and hence the sediment transport rate. Therefore, a question arises as to how the length of the seepage zone affects the sediment transport rate. An additional series of tests was conducted to examine this phenomenon.

Due to constrains of the experimental apparatus, it is more practical to reduce the length of suction zone. By placing an impermeable plastic plate underneath the sand within the seepage zone, the length of the suction area can be reduced. This method cannot be used for the case with injection, since the plastic plates may be "blown over" when they are subjected to upward seepage. Therefore, the effect of seepage zone length on sediment transport rate was investigated only for the case of suction with the length of suction zone to be less than 2 m. Experimental Series III was conducted to study the effect of suction zone length on sediment transport

rate. The details of the experimental apparatus and the experimental procedures are discussed in Section 3.5.3.

6.2 EXPERIMENTAL RESULTS

The sand particles with d_{50} = 0.9 mm were tested with 1-m and 2-m length suction zones, and that with d_{50} = 0.48 mm were tested with 0.5-m, 1-m and 2-m length suction zones. Each type of sand was tested with four different undisturbed flow conditions. The measured bedload transport rates are plotted in Fig 6.3 with q_b against V_s. The detail data of Experimental Series III are tabulated in Appendix II. Figure 6.3 shows that for the same undisturbed flow condition and suction rate, the sediment transport rate decreases with a reduction in the suction zone length.

To collapse the data with different undisturbed flow conditions tested in different length of the suction zone, the experimental results are plotted in terms of the dimensionless terms Φ and Ω in Fig. 6.4. The figure shows that the data for each series of test fit well to a straight line. In order to have a clearer perception on the effect of suction zone length on sediment transport rates, the trendline of each series of data is re-plotted in Fig. 6.5 without the data points. The slope of each straight line, A, and the corresponding R^2-value are tabulated in Table 6.1. The solid lines in Fig. 6.5 refer to the data measured with 2-m length suction zone; the long dash lines indicate the data measured with 1-m length suction zone; and the short dash lines represent those measured with 0.5-m length suction zone. The lines intersect at the same points for each undisturbed flow condition and d_{50}.

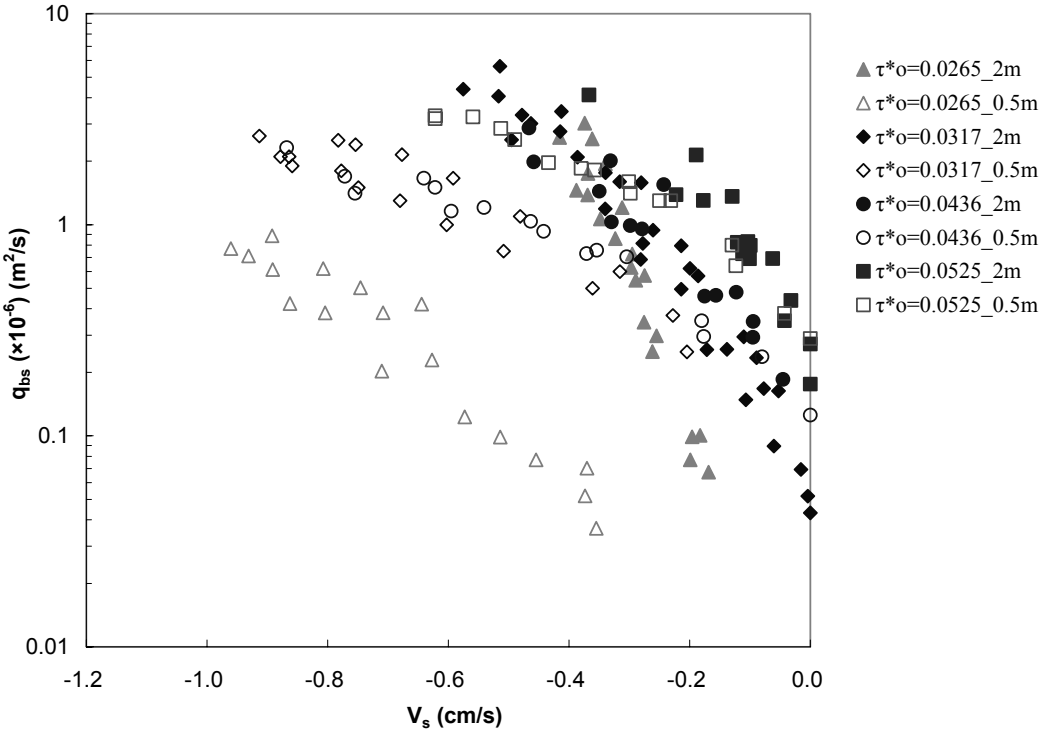

(a) q_{bs} against V_s under Different Suction Zone Length for d_{50} = 0.9 mm

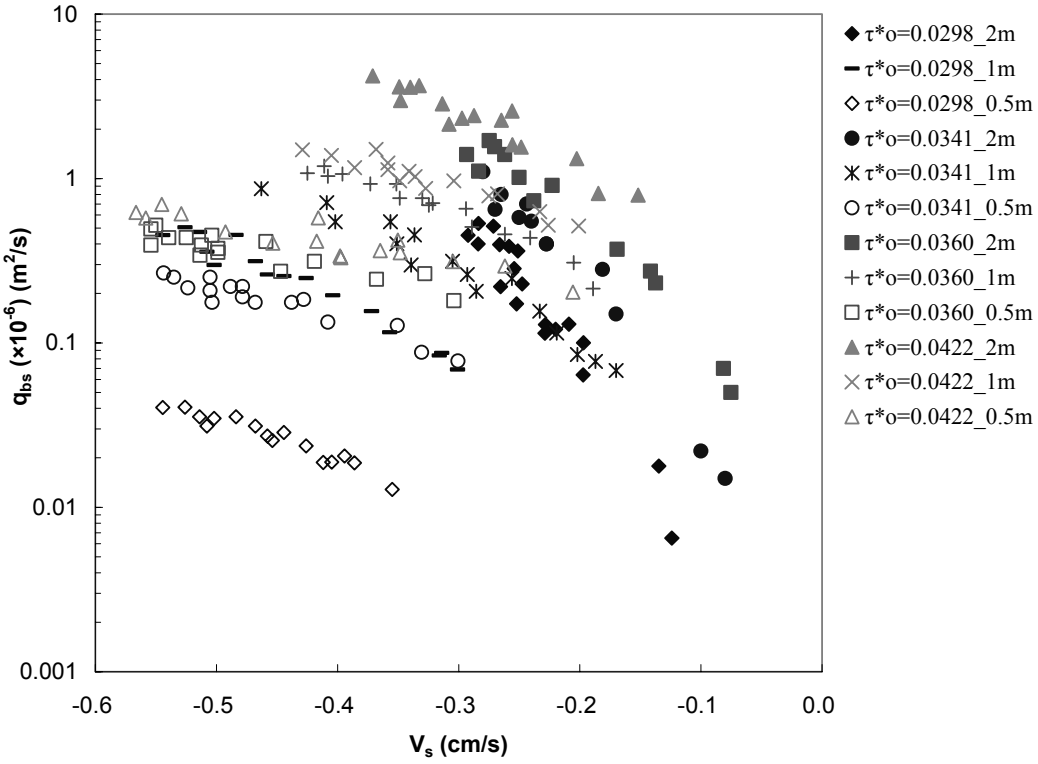

(b) q_{bs} against V_s under Different Suction Zone Length for d_{50} = 0.48 mm

Figure 6.3 Relationships of q_{bs} and V_s under Different Suction Zone Length

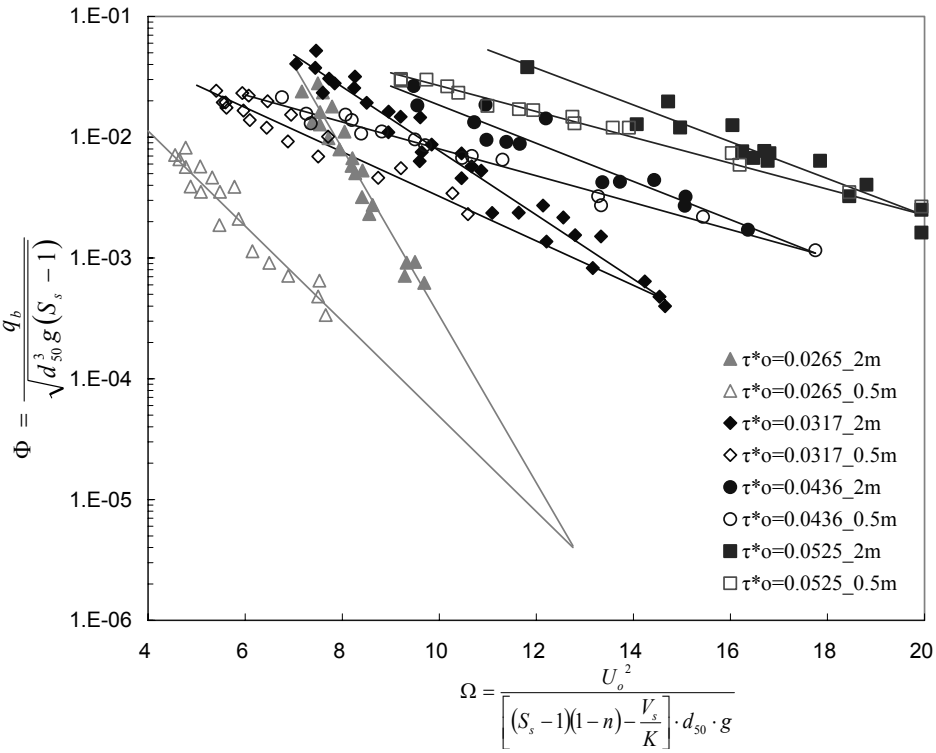

(a) Φ against Ω under Different Suction Zone Length for d_{50} = 0.9 mm

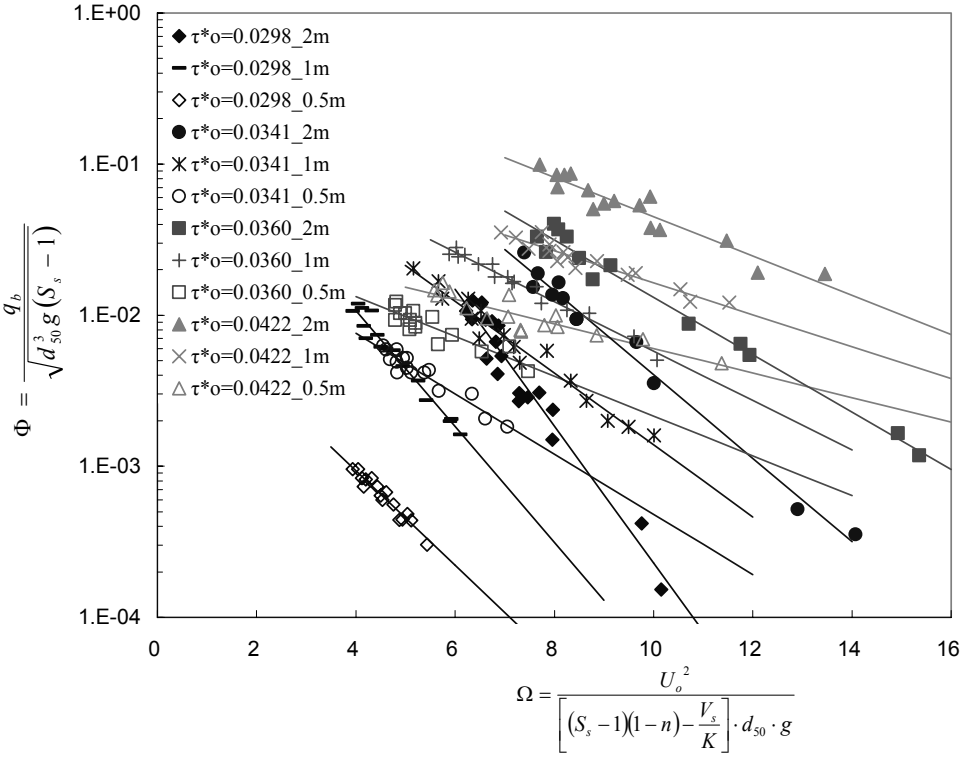

(b) Φ against Ω under Different Suction Zone Length for d_{50} = 0.48 mm

Figure 6.4 Relationships of *Ω* and *Φ* under Different Suction Zone Length (with Experimental Data)

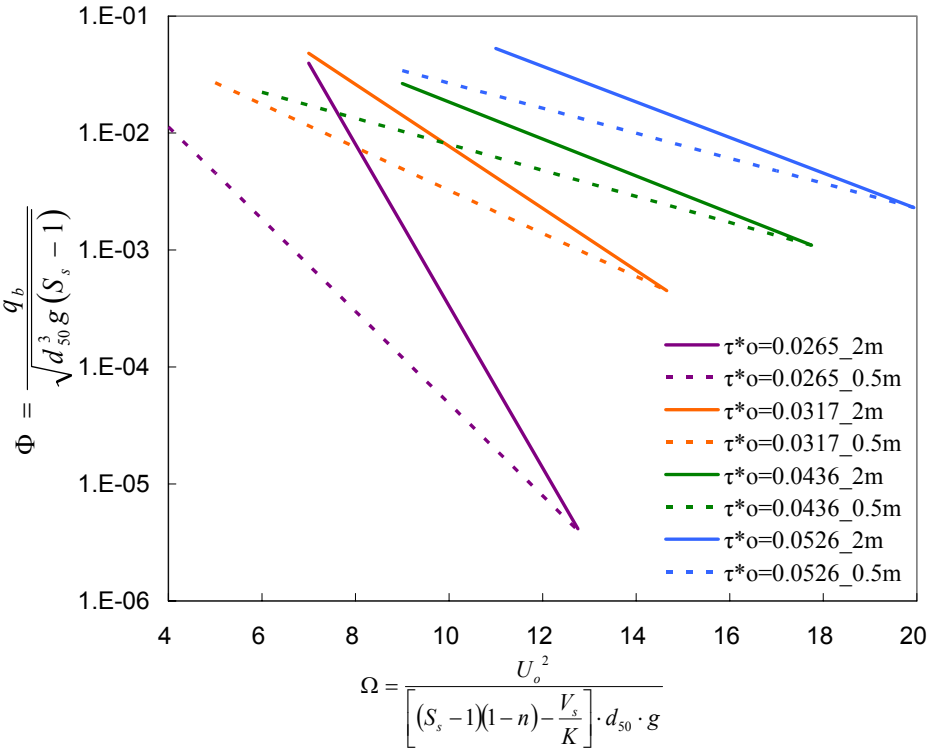

(a) Φ against Ω under Different Suction Zone Length for d_{50} = 0.9 mm

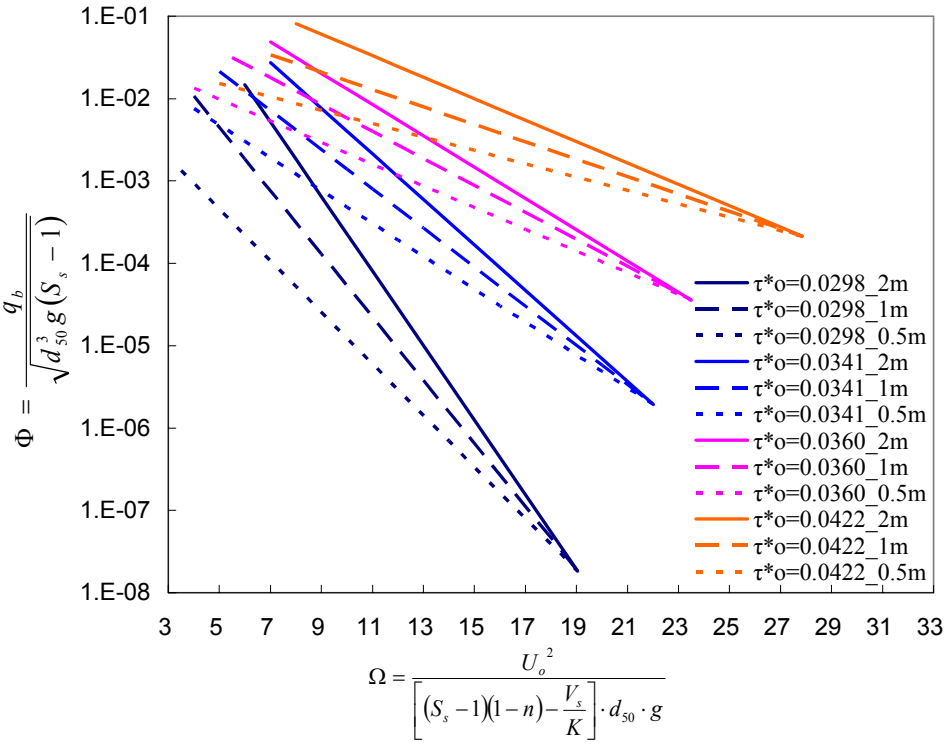

(b) Φ against Ω under Different Suction Zone Length for d_{50} = 0.48 mm

Figure 6.5 Relationships of *Ω* and *Φ* under Different Suction Zone Length (Trendline Only)

Table 6.1 Slopes and R^2-Values of Trendlines

d_{50} (mm)	Series	τ_{*o}	L = 2m		L = 1 m		L = 0.5 m	
			A	R^2	A	R^2	A	R^2
0.90	1-3	0.0265	-0.6919	0.9407	-	-	-0.3942	0.9251
	1-5	0.0317	-0.2651	0.9668	-	-	-0.1841	0.9086
	1-6	0.0436	-0.1580	0.9147	-	-	-0.1117	0.9789
	1-7	0.0525	-0.1522	0.9271	-	-	-0.1070	0.9815
0.48	2-1	0.0298	-0.4531	0.9468	-0.3834	0.9623	-0.3130	0.9397
	2-2	0.0341	-0.2765	0.9845	-0.2378	0.9617	-0.1995	0.9110
	2-3	0.0360	-0.1899	0.9817	-0.1636	0.9734	-0.1317	0.7954
	2-4	0.0422	-0.1302	0.9051	-0.1057	0.9153	-0.0814	0.8000

The intersection point of each test series represents the sediment transport rate in terms of Einstein's parameter Φ in the absence of suction for each undisturbed flow condition. The bedload transport rates without suction of all series tested are tabulated in Table 6.2, in which Ω_o and Φ_o = modified densimetric Froude number and Einstein's parameter without seepage, respectively. The values of Ω_o were calculated using Eq. 4.27, and the values of Φ_o were obtained using Eqs. 5.4 to 5.6. As shown in Fig. 6.4(a), the good agreement between the points of measured Φ_o for Series 1-5 to 1-7 and the intersection points support the accuracy of the results computed in Tables 6.2.

Table 6.2 Sediment Transport Rate without Suction for Each Series

d_{50} (mm)	*Series*	τ_{*o}	Ω_o	Φ_o
0.90	1-3	0.0265	12.75	4.00E-06
	1-5	0.0317	14.65	4.50E-04
	1-6	0.0436	17.75	1.10E-03
	1-7	0.0525	19.94	2.31E-03
0.48	2-1	0.0298	19.04	1.83E-08
	2-2	0.0341	22.01	1.93E-06
	2-3	0.0360	23.50	3.59E-05
	2-4	0.0422	27.86	2.12E-04

6.2.1 Effect of L on Φ with Constant τ_{*o}, d_{50} and V_s

Figures 6.4 or 6.5 clearly show that, for the same undisturbed flow condition and d_{50}, the slope of the trendline decreases with a reduction in suction zone length L. The data at V_s = -0.05 cm/s and τ_{*o} = 0.0298 (i.e., Ω = 14.1 for Series 2-1) is arbitrarily chosen as an illustration. The Φ-value reduces from 3.24×10^{-6} with the 2-m length suction zone to 1.46×10^{-6} with the 1-m length suction zone, and further reduces to 6.54×10^{-7} with 0.5-m length suction zone. This data trend shows that for the same sand, same undisturbed flow condition and suction rate, i.e. same Ω, the bed load transport rate, which is represented by Einstein's dimensionless parameter Φ, decreases with a reduction in suction zone length. One may infer from this trend that when the suction zone length reduces to zero, the slope of each series would reduce to zero, resulting in the bedload transport rate with suction reduced to the value without suction.

6.2.2 Effect of V_s on $\Phi|_{L=2m}/\Phi|_{L<2m}$ with Constant τ_{*o}, d_{50} and Change of L

For given undisturbed flow conditions, bed sediments and the reduction of suction zone length, the values of $\Phi|_{L=2m}/\Phi|_{L<2m}$ with different suction rate can be determined from Figs. 6.4 or 6.5. The computed values of $\Phi|_{L=2m}/\Phi|_{L<2m}$ are plotted in Fig. 6.6 against V_s for different d_{50} and change of L. Figure 6.6 shows that, for the same sand with the same undisturbed flow condition and reduction in suction zone length, the ratio of $\Phi|_{L=2m}/\Phi|_{L<2m}$ increases with an increase in suction rate. Table 6.3 tabulates the comparison of $\Phi|_{L=2m}/\Phi|_{L=0.5m}$ for V_s = -0.05 cm/s with that for V_s = -0.1 cm/s for Series 2-1 (τ_{*o} = 0.0298) when the length of suction zone changes from 2 m to 0.5 m. The ratio of $\Phi|_{L=2m}/\Phi|_{L=0.5m}$ increases from 4.96 to 12.67 when the suction rate increases from -0.05 to -0.1 cm/s. It may be inferred from this data that the bedload transport rate becomes more sensitive to suction zone length when it is subjected to a higher suction intensity.

Table 6.3 $\Phi|_{L=2m}/\Phi|_{L=0.5m}$ with Different V_s for Series 2-1 (τ_{*o} = 0.0298)

V_s (cm/s)	Ω	$\Phi\|_{L=2m}$	$\Phi\|_{L=0.5m}$	$\Phi\|_{L=2m}/\Phi\|_{L=0.5m}$
-0.05	14.08	3.24×10^{-6}	6.54×10^{-7}	4.96
-0.1	11.17	6.76×10^{-5}	5.33×10^{-6}	12.67

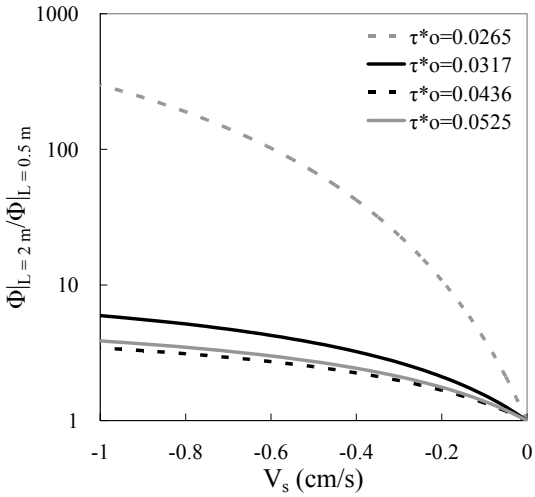

(a) $\Phi|_{L=2m}/\Phi|_{L=0.5m}$ against V_s with d_{50} = 0.9 mm sand

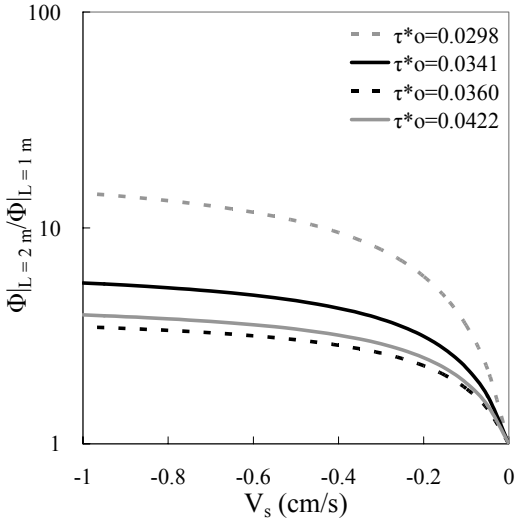

(b) $\Phi|_{L=2m}/\Phi|_{L=1m}$ against V_s with d_{50} = 0.48 mm sand

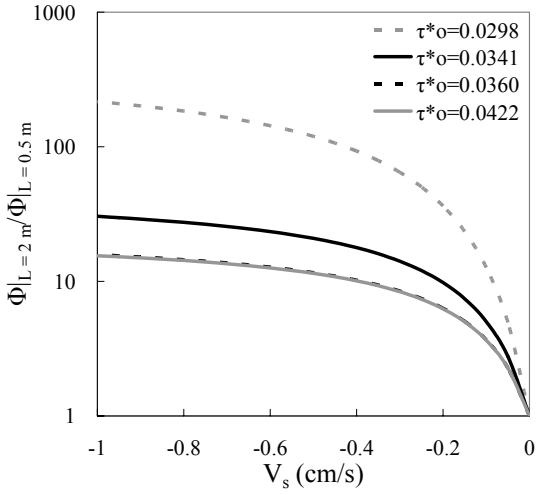

(c) $\Phi|_{L=2m}/\Phi|_{L=0.5m}$ against V_s with d_{50} = 0.48 mm sand

Figure 6.6 Relationship of $\Phi|_{L=2m}/\Phi|_{L<2m}$ against V_s with Different Change in L

6.2.3 Effect of τ_{*o} on $\Phi|_{L=2m}/\Phi|_{L<2m}$ with Constant V_s, d_{50} and Change of L

Figure 6.6 also shows that the ratio of $\Phi|_{L=2m}/\Phi|_{L<2m}$ reduces with an increase of τ_{*o} for the same suction rate. The data series tested with d_{50} = 0.48 mm sand at V_s = -0.1 cm/s is arbitrarily chosen as an illustration. When the length of suction zone is shortened from 2 m to 0.5 m, the ratio of $\Phi|_{L=2m}/\Phi|_{L=0.5m}$ for the different undisturbed flow conditions are tabulated in Table 6.4. This table clearly shows that with the same suction rate, the ratio of $\Phi|_{L=2m}/\Phi|_{L=0.5m}$ decreases with an increase in τ_{*o}. For example, $\Phi|_{L=2m}/\Phi|_{L=0.5m}$ reduces from 12.67 to 5.01 when τ_{*o} increase from 0.0298 to 0.0341.

Table 6.4 $\Phi|_{L=2m}/\Phi|_{L=0.5m}$ for Different τ_{*o} with V_s = -0.1 cm/s

Series	τ_{*o}	$\Phi\|_{L=2m}/\Phi\|_{L=0.5m}$
2-1	0.0298	12.67
2-2	0.0341	5.01
2-3	0.0360	3.68
2-4	0.0422	3.65

6.2.4 Effect of L on $\Phi|_{L=2m}/\Phi|_{L<2m}$ with Constant τ_{*o} V_s and d_{50}

The ratios of $\Phi|_{L=2m}/\Phi|_{L<2m}$ against suction rates for d_{50} =0.48 mm sand tested under different undisturbed flow conditions with the suction zone length changing from 2 m to 1m and those with the suction zone length changing from 2 m to 0.5 m are plotted on Fig. 6.7. The figure shows that $\Phi|_{L=2m}/\Phi|_{L=1m}$ is about half of $\Phi|_{L=2m}/\Phi|_{L=0.5m}$ in logarithmic scale for all τ_{*o}. An illustration is tabulated in Table 6.5 for Series 2-1 to 2-4 with V_s = -0.1 cm/s. Since the trendlines are plotted in logarithmic scale, the value of $\dfrac{\log\left(\Phi|_{L=2m}/\Phi|_{L=1m}\right)}{\log\left(\Phi|_{L=2m}/\Phi|_{L=0.5m}\right)} = \dfrac{A|_{L=2m} - A|_{L=1m}}{A|_{L=2m} - A|_{L=0.5m}}$, where A

= the slope of the trendline in semi-logarithmic scale. Thus, the change of the slope of the trendline when the suction zone length reduces from 2 m to 1 m should also be about the half of that when the suction zone length reduces from 2 m to 0.5 m. This phenomenon may not be valid for other change in the suction zone length. However, it serves as a constraint when deriving the prediction equations for the effect of suction zone length on sediment transport rate.

For a better understanding of the findings deduced from the experimental results, the physics within the seepage zone should be studied. The following section presents the force analysis for a flow passing through a seepage zone.

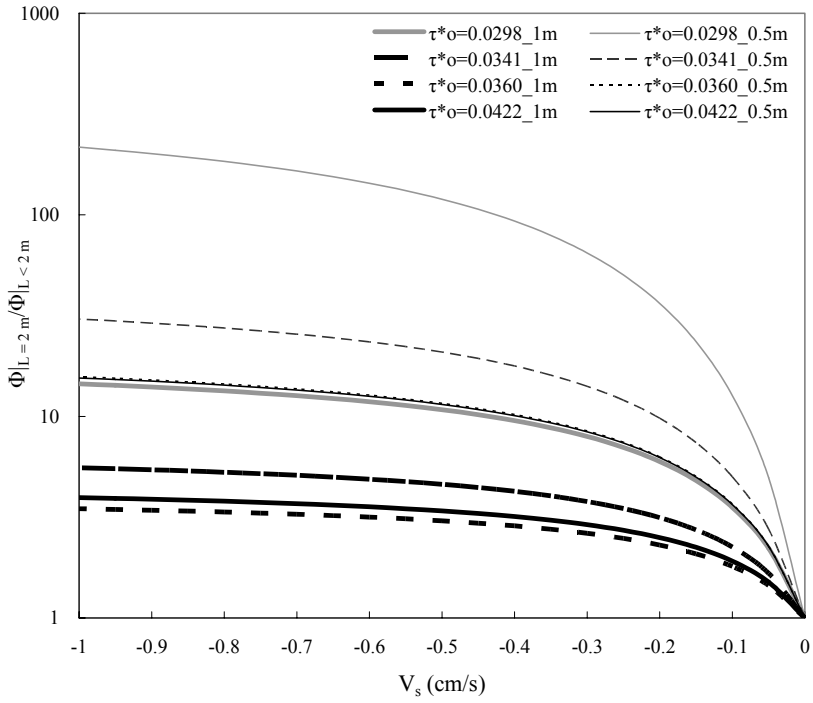

Figure 6.7 $\Phi|_{L=2m}/\Phi|_{L<2m}$ against V_s with d_{50} = 0.48 mm at Different Suction Zone Length

Table 6.5 Comparison of $\Phi|_{L=2m}/\Phi|_{L<2m}$ for Different Suction Zone Length for d_{50} = 0.48 mm Sand Tested with V_s = -0.1 cm/s

Series	τ_{*o}	Ω	$\frac{\Phi\|_{L=2m}}{\Phi\|_{L=1m}}$	$\frac{\Phi\|_{L=2m}}{\Phi\|_{L=0.5m}}$	$\frac{\log(\Phi\|_{L=2m}/\Phi\|_{L=1m})}{\log(\Phi\|_{L=2m}/\Phi\|_{L=0.5m})}$	$\frac{A\|_{L=2m}-A\|_{L=1m}}{A\|_{L=2m}-A\|_{L=0.5m}}$
2-1	0.0298	11.17	3.54	12.67	0.50	0.50
2-2	0.0341	12.91	2.25	5.01	0.50	0.50
2-3	0.0360	13.78	1.80	3.68	0.45	0.45
2-4	0.0422	16.34	1.91	3.65	0.50	0.50

6.3 FORCE ANALYSIS

The expression for bed shear stress with seepage could be derived based on the momentum equation similar to that shown in Chow (1959). Consider a flow in a horizontal open-channel with a rectangular cross sectional area passing through a seepage zone as shown in Fig. 6.8. The seepage discharge and mean seepage velocity are denoted as Q_s and V_s, respectively.

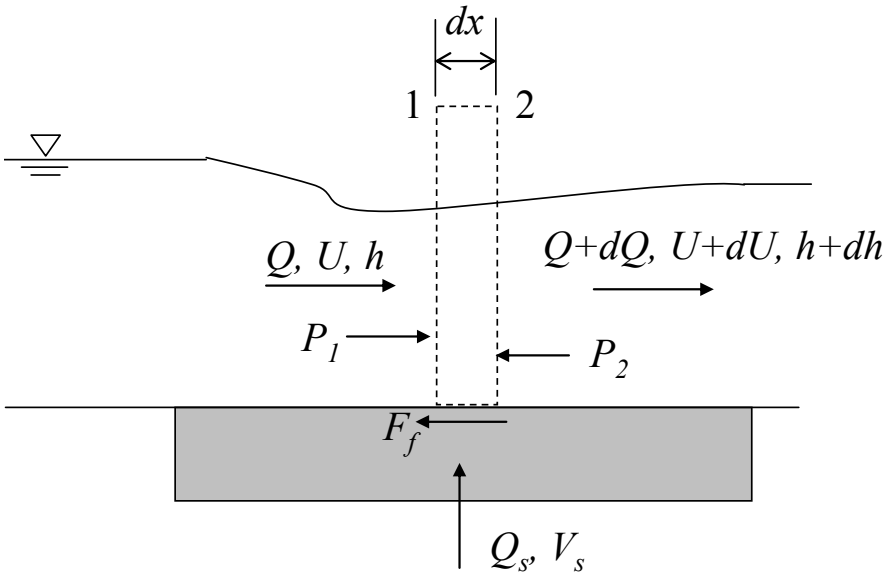

Figure 6.8 Schematic Diagram of an Open-Channel Flow Subjected to Seepage

With reference to Fig. 6.8, the flow within the suction zone with length = dx and width = w is considered as the control volume. Therefore the momentum passing section 1 per unit time in the horizontal direction, M_1 is

$$M_1 = \rho Q U \tag{6.1}$$

where Q and U = instantaneous discharge and mean velocity at section 1, respectively. Similarly, the momentum passing section 2 per unit time, M_2 is

$$M_2 = \rho(Q + dQ)(U + dU) \tag{6.2}$$

where dQ and dU = change of discharge and mean velocity between sections 1 and 2, respectively. Furthermore, one may define dQ as positive for the case of injection and negative for the case of suction. The momentum change of the body of water between section 1 and 2 in the horizontal direction is, therefore, equal to

$$M_2 - M_1 = \rho[QdU + (U + dU)dQ] \tag{6.3}$$

The frictional force generated between the flow and the sediment bed could be calculated in terms of bed shear stress τ_{bs} multiplied by the contact area as follows

$$F_f = \tau_{bs} w \cdot dx \tag{6.4}$$

The total pressure force on section 1 in the horizontal direction is equal to the unit hydrostatic pressure at the centroid of the water area multiplied by the area, which is equivalent to the moment of the water area about the free surface multiplied by ρg, or

$$P_1 = \rho g \frac{h^2 w}{2} \tag{6.5}$$

where h = water depth at section 1. Similarly, the total pressure force on section 2 is

$$P_2 = \rho g h w\left(\frac{h}{2} + dh\right) + \rho g w \frac{dh}{2} dh \tag{6.6}$$

where dh = change of water depth between sections 1 and 2. Neglecting the term containing differentials of higher order, Eq. 6.6 becomes

$$P_2 = \rho g h w \left(\frac{h}{2} + dh \right) \tag{6.7}$$

The resultant hydrostatic pressure acting on the body of water between section 1 and 2 is

$$P_1 - P_2 = -\rho g h w dh \tag{6.8}$$

Equating the momentum change of the water body to all the external forces acting on the body, i.e., the conservation of momentum, gives

$$M_2 - M_1 = P_1 - P_2 - F_f \tag{6.9}$$

Substituting Eqs. 6.3, 6.4 and 6.8 into Eq. 6.9 and neglecting $dUdQ$ gives

$$\tau_{bs} dx = -\rho g h dh - \frac{\rho}{w}\left(QdU + UdQ\right) \tag{6.10}$$

Since $U = Q/wh$ and $U + dU = \left(Q + dQ\right)/w\left(h + dh\right)$, the expression for dU is shown as follows

$$dU = \frac{hdQ - Qdh}{wh\left(h + dh\right)} \tag{6.11}$$

Substituting Eq. 6.11 into Eq. 6.10 gives

$$\tau_{bs} dx = -\rho g h dh - \frac{\rho}{w^2 h}\left(\frac{2QhdQ - Q^2 dh + QdhdQ}{h + dh} \right) \tag{6.12}$$

Neglecting dh in the denominator and $dhdQ$ in the numerator, Eq. 6.12 is simplified to

$$\tau_{bs} dx = -\rho g h dh - \frac{\rho}{w^2 h^2}\left(2QhdQ - Q^2 dh\right) \tag{6.13}$$

Differentiating both sides of Eq. 6.13 with respect to dx gives

$$\tau_{bs} = -\rho g h \frac{dh}{dx}\left(1 - \frac{U^2}{gh}\right) - \frac{2\rho U}{w}\frac{dQ}{dx} \tag{6.14}$$

where dh/dx = water surface slope. The term dQ/dx is the change of discharge per unit length of the channel and could be expressed in terms of seepage velocity V_s as follow

$$\frac{dQ}{dx} = V_s w \tag{6.15}$$

Substituting Eq. 6.15 into Eq. 6.14 gives

$$\tau_{bs} = -\rho g h \frac{dh}{dx}\left(1 - \frac{U^2}{gh}\right) - 2\rho U V_s \tag{6.16}$$

The above equation is the same as the bed shear stress equation derived by Cheng and Chiew (1998b) with the momentum correction factor equal to one.

When the flow is subjected to seepage, the continuity equation at the mid-section of the seepage zone is written as

$$U_o h_o + V_s L/2 = U_c h_c \tag{6.17}$$

where U_c and h_c = mean velocity and water depth at the middle section of the seepage zone, respectively. If the undisturbed flow conditions and the seepage velocity are constants, a change in the length of seepage zone would cause a change in U_c and h_c, leading to a change in bed shear stresses. In the present study, since the bedload transport rates collected with reduced seepage zone length are measured only for the case of suction, in the following discussion, the effects of seepage zone length are investigated with the presence of suction only.

6.4 EFFECT OF SUCTION ZONE LENGTH ON SEDIMENT TRANSPORT

Both Eqs. 6.16 and 5.3 derived by Chen and Chiew (2004) may be used to calculate the bed shear stress or shear velocity with suction. The comparison of the shear velocities with suction computed using both equations are tabulated in Table 6.6. The undisturbed flow condition and suction rate are chosen from the tests conducted, i.e., τ_{*o} = 0.0265 and V_s = -0.373 cm/s. The values of h_c were physically measured. U_c was then calculated using Eq. 6.17. The water surface slope within the suction zone is assumed to be a linear line for both 2-m and 0.5-m length. The values of *dh/dx* were then obtained from the difference of the water depths at the leading and end section of the suction zone divided by the suction zone length. The first and third rows show the u_{*s}-values for suction zone length = 2 m. The u_{*s}-value computed using both equations are almost the same. However, because it is difficult to measure the water surface slope *dh/dx* with high accuracy, the shear velocity equation derived by Chen and Chiew (2004), i.e., Eq. 5.3 was used to calculate the shear velocity with suction with 2-m suction zone length.

Table 6.6 Comparisons of Terms for Calculating τ_{bs} with τ_{*o} = 0.0265

	V_s (cm/s)	L (m)	h_c (m)	U_c (cm/s)	V_s/U_c (%)	dh/dx	τ_{bs} (N/m^2)	u_{*s} (cm/s)
Eq. 5.3	-0.373	2	0.119	32.65	1.14	-	0.940	3.066
		0.5	0.128	32.54	1.15	-	0.941	3.067
Eq. 6.16	-0.373	2	0.119	32.65	-	0.0014	0.950	3.082
		0.5	0.128	32.54	-	0.0014	0.817	2.858

On the other hand, the change in suction zone length would cause a change in U_c and h_c. Equation 5.3 shows that u_{*s} is only a function of U_c, ignoring the effect of h_c. In contrast, Eq. 6.16 includes both effects of U_c and h_c. Hence, when the

length of suction zone is shortened, u_{*s} is more accurately calculated using Eq. 6.16. Furthermore, Eq. 5.3 is an empirical equation derived using L = 2 m. There is no certainty that it will apply for $L \neq 2$ m. In contrast, Eq. 6.16 is an equation derived analytically. An illustration is also shown in Table 6.6. The reduction in L causes little effect on u_{*s}-value computed using Eq. 5.3, but a reduction when Eq. 6.16 is used. Therefore, in the following analysis, Eq. 6.16 is used to compute the shear velocity with suction, instead of the equation derived by Chen & Chiew (2004).

6.4.1 Φ Increases with an Increase in L with Constant τ_{*o}, d_{50} and V_s

The comparisons of each term in Eq. 6.16 for calculating bed shear stress when the length of seepage zone reduces from 2 m to 0.5 m are also tabulated in Table 6.6. The undisturbed flow condition (τ_{*o} = 0.0265) and suction rate (V_s = -0.373 cm/s) are the same in both cases.

The table shows that with the presence of suction, the bed shear stress reduces (from 0.950 to 0.817 N/m^2) with a reduction in seepage zone length from 2 m to 0.5 m for the same undisturbed flow condition and suction rate. When the length of suction zone is shortened, there is little effect on U_c and dh/dx. However, the increment in h_c affected by the reduction of suction zone length is very significant when compared with changes in the other terms. Therefore, one may infer from these results that for the same undisturbed flow condition and suction rate, the increase of local water depth h_c due to the reduction of suction zone length is the major factor in causing the reduction in bed shear stress.

As discussed in Chapter 5, the bedload transport rate, which is presented using Einstein's parameter Φ, is proportional to the shear velocity excess, $u_{*s} - u_{*cs}$. The

critical shear velocity with suction u_{*cs} is affected only by the suction velocity and the basic properties of sediment and fluid, regardless of the size of the suction zone. Hence, u_{*cs} is a constant as long as the suction rate and the sediment particle are fixed. However, when the length of suction zone is shortened, the bed shear stress or the bed shear velocity decreases. Thus, the shear velocity excess, $u_{*s} - u_{*cs}$, decreases, resulting in a reduction in bedload transport rate. This means that the bedload transport rate, or the Einstein's parameter Φ, decreases with the reduction in the length of suction zone, for the same undisturbed flow condition and suction rate, i.e. the same Ω.

6.4.2 $\Phi|_{L=2m}/\Phi|_{L<2m}$ Increases with an Increase in V_s with Constant τ_{*o}, d_{50} and Change of L

The bedload transport rate, represented by Einstein's parameter Φ, can be written in terms of shear velocity excess, $u_{*s} - u_{*cs}$, as follows

$$\Phi \sim \left(u_{*s} - u_{*cs}\right) \tag{6.18}$$

where the symbol "~" refers to "be related to". Since the Φ-value is normally plotted in logarithmic scale is the present study, Eq. 6.18 may be re-written as

$$\log\Phi \sim \left(u_{*s} - u_{*cs}\right) \tag{6.19}$$

When the length of suction zone is shortened from 2 m to 0.5 m, the reduction of $log\Phi$ can be expressed in a similar form as Eq. 6.19

$$\left(\log\Phi\big|_{L=2m} - \log\Phi\big|_{L=0.5m}\right) \sim \left[\left(u_{*s} - u_{*cs}\right)\big|_{L=2m} - \left(u_{*s} - u_{*cs}\right)\big|_{L=0.5m}\right] \tag{6.20}$$

Since u_{*cs} is a constant as long as the suction rate and sediment particle are fixed, Eq. 6.19 becomes

$$\log\left(\Phi\big|_{L=2m}/\Phi\big|_{L=0.5m}\right) \sim \left(u_{*s}\big|_{L=2m} - u_{*s}\big|_{L=0.5m}\right) \tag{6.21}$$

Since logarithmic function is an increasing function of its base, Eq. 6.21 can be re-written as follows

$$\log\left(\Phi\big|_{L=2m}/\Phi\big|_{L=0.5m}\right)\sim\left(\Phi\big|_{L=2m}/\Phi\big|_{L=0.5m}\right)\sim\left(u_{*s}\big|_{L=2m}-u_{*s}\big|_{L=0.5m}\right) \qquad (6.22)$$

As shown in Eq. 6.22, the ratio of $\Phi|_{L=2m}/\Phi|_{L=0.5m}$ is proportional to the reduction of u_{*s}. Hence, the effect of suction zone length on the ratio of $\Phi|_{L=2m}/\Phi|_{L=0.5m}$ can be achieved by examining the effect of suction zone length on the reduction of u_{*s}. When the undisturbed flow condition and the reduction of suction zone length remain the same, an increase in suction rate leads to a reduction in local water depth. The comparison of the measured local water depths subjected to two arbitrarily chosen suction rates with the same undisturbed flow condition (τ_{*o} = 0.0265) and reduction of suction zone length (from 2 m to 0.5 m) are tabulated in Table 6.7. The values of u_{*s} were calculated based on Eq. 6.16.

Table 6.7 Comparison of Reduction of u_{*s} for Different V_s at τ_{*o} = 0.0265

V_s (cm/s)	L (m)	h_c (m)	u_{*s} (cm/s)	$u_{*s}\|_{L=2m} - u_{*s}\|_{L=0.5m}$ (cm/s)	$\Phi\|_{L=2m}/\Phi\|_{L=0.5m}$
-0.373	2	0.119	3.082	0.224	36.47
	0.5	0.128	2.858		
-0.514	2	0.115	3.156	0.472	72.89
	0.5	0.127	2.684		

The reduction in h_c with the 2-m length suction zone is higher than that with 0.5-m suction zone, while the suction velocity increases (from -0.373 to -0.514 cm/s), leading to a higher reduction rate in u_{*s} with the higher suction rate. This means that the reduction of u_{*s}, i.e. ($u_{*s}|_{L=2m} - u_{*s}|_{L=0.5m}$), increases from 0.224 to 0.472 cm/s with the increase of the suction velocity (from -0.373 to -0.514 cm/s), resulting in an increase of $\Phi|_{L=2m}/\Phi|_{L=0.5m}$ from 36.47 to 72.89. Therefore, one may infer from this comparison that with the same undisturbed flow condition and reduction of suction zone length, the increase of suction rate causes an increase in the reduction of shear velocity excess, leading to a higher $\Phi|_{L=2m}/\Phi|_{L<2m}$ ratio.

6.4.3 $\Phi|_{L=2m}/\Phi|_{L<2m}$ Decreases with an Increase in τ_{*o} with Constant V_s, d_{50} and Change of L

The bed shear velocity with different suction zone length can be calculated using Eqs. 6.16 and 6.17. Table 6.8 tabulates the reductions of u_{*s} for different undisturbed flow conditions at V_s = -0.373 cm/s when the length of suction zone is shortened from 2 m to 0.5 m. The table clearly shows that the reduction of u_{*s} decreases with the increase of τ_{*o}, causing a reduction in $\Phi|_{L=2m}/\Phi|_{L=0.5m}$. Therefore, it may be inferred from this comparison that with the same suction rate, the ratio of $\Phi|_{L=2m}/\Phi|_{L<2m}$ with lower τ_{*o} is higher than that with higher τ_{*o}.

Table 6.8 Comparison of Reduction of u_{*s} for Different τ_{*o} at V_s = -0.373 cm/s

Series	τ_{*o}	$u_{*s}\|_{L=2m} - u_{*s}\|_{L=0.5m}$ *(cm/s)*	$\Phi\|_{L=2m}/\Phi\|_{L=0.5m}$
1-3	0.0265	0.224	36.47
1-5	0.0317	0.210	3.08
1-6	0.0436	0.148	2.18
1-7	0.0525	0.182	2.35

6.5 DIMENSIONAL ANALYSIS

The experimental data and analytical derivation discussed in this chapter have clearly shown that the bed shear stress with suction, τ_{bs}, is a function of the length of suction zone, L. This means that a change in the suction zone length L will cause a change in bed shear stress, resulting in a change in sediment transport rate. Hence, L is an additional variable affecting q_b.

If we were to add this variable into the dimensional analysis conducted in Chapter 4,

a new pi term is obtained as follow

$$\Pi_8 = \frac{L}{L_o} \tag{6.23}$$

where L_o = 2 m. The term L/L_o is used to account for the effect of suction zone length on sediment transport rate.

6.6 DETERMINATION OF EMPIRICAL PREDICTION FUNCTION

It is noticed that the slope of the trendline changes with the change of the length of suction zone (see Figs. 6.5 or 6.6). However, for the series with the same undisturbed flow condition, the trendlines start from the same point. This point corresponds to Einstein's parameter without suction, Φ_o, which is independent of the length of suction zone. In order to account for the length effect, a slope modifier ω, which is defined as $\omega = \left(A\big|_{L<2m} - A\big|_{L=2m}\right)$, is introduced. It is the difference of the slope between the slope of the trendline measured with any length of suction zone less than 2 m, and that with the 2-m length suction zone. This simply means that, for a given undisturbed flow condition, the coefficient A in the equation $\log\Phi = A\Omega + B$ for any length of suction zone < 2 m, is the sum of the coefficient A predicted using Eq. 5.2 and a slope modifier ω.

As discussed in section 6.2, the reduction of the slope of the trendline reduces not only with L but also τ_{*o}. In another words, the slope modifier, ω, is also a function of τ_{*o}, i.e.,

$$\omega = f\left(\tau_{*o}, L\right) \tag{6.24}$$

The symbols f denotes specified function. The values of ω for the τ_{*o} and L tested in this study are tabulated in Table 6.9, in which L_o = 2 m.

Table 6.9 Values of Slope Modifier ω at Different Suction Zone Length

L (m)	τ_{*o}	$\omega = A - A\|_{L=2m}$	$\omega/\log(L/L_o)$
0.5	0.0265	0.2977	-0.4945
	0.0317	0.0810	-0.1345
	0.0436	0.0463	-0.0769
	0.0525	0.0452	-0.0750
1	0.0298	0.0697	-0.2314
	0.0341	0.0387	-0.1285
	0.0360	0.0263	-0.0875
	0.0422	0.0245	-0.0813
0.5	0.0298	0.1401	-0.2326
	0.0341	0.0770	-0.1278
	0.0360	0.0582	-0.0966
	0.0422	0.0488	-0.0811

Before deriving the empirical prediction equation for ω, there are two constrains. First, when $L = L_o = 2$ m, the slope modifier ω is equal to zero. Second, the experimental data show that the value of ω at $L = 1$ m is about the half of that at $L = 0.5$ m. Hence, Eq. 6.24 can be empirically determined as follows

$$\omega = \log(L/L_o) f(\tau_{*o}) \tag{6.25}$$

The form of the Eq. 6.25 satisfies the two constraints stated early. Re-arrangement of Eq. 6.25 gives

$$\frac{\omega}{\log(L/L_o)} = f(\tau_{*o}) \tag{6.26}$$

The values of $\omega/\log(L/L_o)$ with different τ_{*o} are also tabulated in Table 6.9, and plotted as a function of τ_{*o} in Fig. 6.9. The black diamond represents the series tested using $d_{50} = 0.9$ mm sand with 0.5-m length suction zone. The open triangle and open circle are the series tested using $d_{50} = 0.48$ mm sand with 0.5-m and 1-m

length suction zone, respectively.

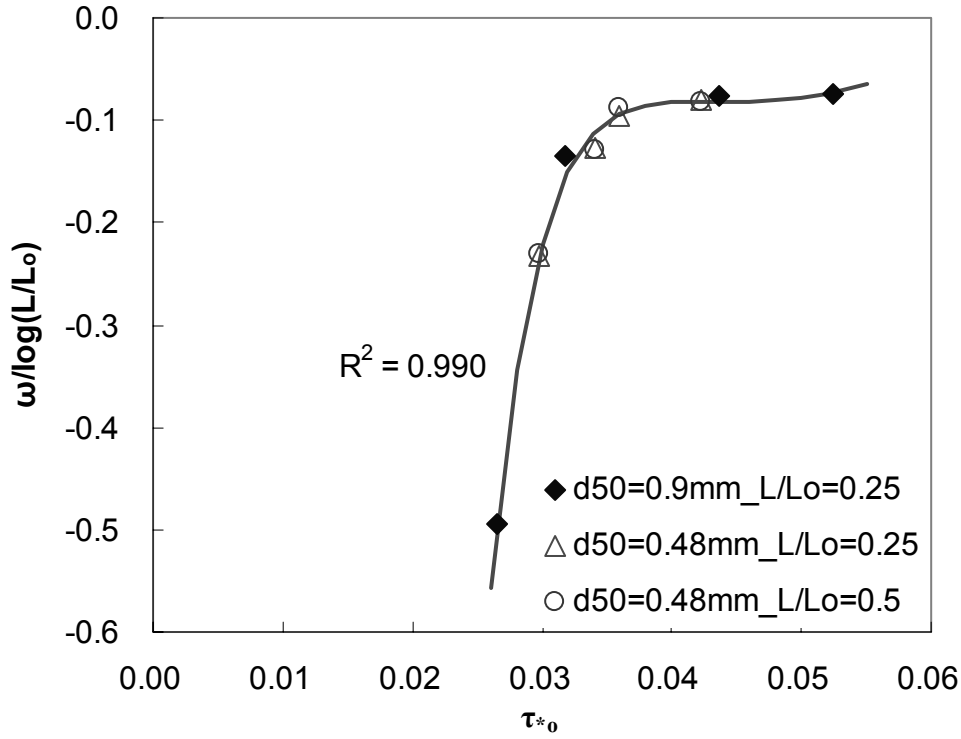

Figure 6.9 Relationship of $\omega/log(L/L_o)$ against τ_{*o}

The term $\omega/log(L/L_o)$ is empirically fitted with τ_{*o}, giving the following equation:

$$\frac{\omega}{\log(L/L_o)} = 1.602 - \frac{0.218}{\tau_{*o}} + \frac{9.37\times10^{-3}}{\tau_{*o}^2} - \frac{1.35\times10^{-4}}{\tau_{*o}^3} \tag{6.27}$$

By re-arranging Eq. 6.27, one gets

$$\omega = \log(L/L_o)\left(1.602 - \frac{0.218}{\tau_{*o}} + \frac{9.37\times10^{-3}}{\tau_{*o}^2} - \frac{1.35\times10^{-4}}{\tau_{*o}^3}\right) \tag{6.28}$$

The R^2-value for the above empirical fitting is 0.990, and the empirical equation above is valid for $0.0217 \le \tau_{*o} \le 0.0525$. The bedload sediment transport rate can then be calculated with the known bedload transport rate without suction based on the following equation

$$\log(\Phi) = (A+\omega)(\Omega - \Omega_o) + \log(\Phi_o) \tag{6.29}$$

The parameter A is the same as stated in Eq. 5.4 and can be calculated using Eq. 5.5.

The values of Ω_o were calculated using Eq. 4.27, and the values of Φ_o were obtained using Eqs. 5.4 to 5.6.

Figure 6.10 shows the comparison between the measured and computed Φ-values using Eqs. 6.28 and 6.29, and the data generally lie within an accuracy range of ±20%. The good agreement between the computed and measured data shows that the empirically determined equation (Eq. 6.28) may be used as the slope modifier to account for the effect of suction zone length. The semi-logarithmic function (Eq. 6.29) relating Φ with Ω may be used to calculate bedload transport rate under the influence of suction with suction zone length less than 2-m, once the coefficients A and the bedload transport rate without suction are known.

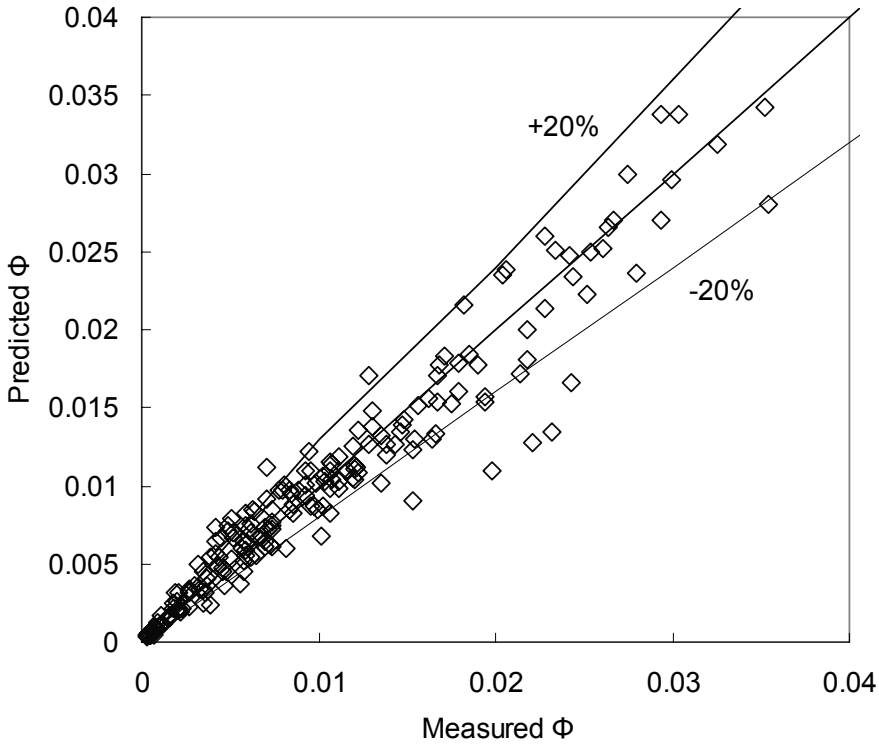

Figure 6.10 Predicted-Measured Comparison in Φ with Different Length of Suction Zone

6.7 COMPARISON WITH PREVIOUS INVESTIGATION

Section 5.3.4.1 compared the work of Maclean (1991) with the results obtained using Eqs. 5.4 to 5.6. This comparison, which is shown in Table 5.8, reveals that the Φ-values predicted using Eqs. 5.4 to 5.6 are generally greater than those from Maclean's results. This phenomenon is reasonable because the suction zone length used in Maclean (1991) (L = 0.13 m) is much shorter than that used in this study (L = 2 m). As discussed in Section 6.4, the suction discharge in short suction zone is smaller when compared with that in long suction zone with the same suction velocity. According to the continuity equation, the water depth in the suction zone then increases. Thus, there is a reduction in bed shear stress with short suction zone when compared with that in long suction zone, resulting in a reduction in shear stress excess, and hence a reduction in sediment transport rate.

As stated in Section 6.6, the slope modifier ω is introduced to the case of suction zone with length < 2 m. The predicted Φ can then be re-calculated using Eqs. 6.28 and 6.29. The results so-obtained were tabulated in Table 6.10.

Table 6.10 Comparison between Maclean's Results, Prediction Using Eqs. 5.4 to 5.6, and Prediction Using Eqs. 6.28 and 6.29

Test Number	U_o *(m/s)*	V_s *(cm/s)*	τ_{*o}	Φ *(Eqs. 5.4 to 5.6)*	Φ *(Eqs. 6.28 & 6.29)*	Φ *(Maclean)*
M1	0.294	-0.028	0.0307	0.0092	0.0073	0.0058
M2	0.339	-0.018	0.0425	0.0154	0.0141	0.0087
M3	0.339	-0.021	0.0425	0.0158	0.0142	0.0132
M4	0.392	-0.025	0.0567	0.0543	0.0481	0.0275
M5	0.392	-0.022	0.0567	0.0526	0.0474	0.0352
M6	0.392	-0.028	0.0567	0.0553	0.0485	0.0415

Table 6.10 clearly shows that the Φ-values predicted using Eqs. 6.28 and 6.29 are closer to the results obtain by Maclean (1991). It could be inferred from this calculation that Eqs. 6.28 and 6.29 yield a better accuracy in predicting the bedload transport rate under the influence of suction with suction zone length less than 2 m.

6.8 ENGINEERING PRACTICE

In the real engineering field, the undisturbed flow conditions, the properties of the bed sediment particles, the suction zone length and suction rate can be predetermined, which means that U_o, h_o, u_{*o}, S_s, n, K, d_{50}, L and V_s are known variables. The Shields' parameter τ_{*o} then can be obtained. The modified densimetric Froude number without seepage Ω_o is computed using Eq. 4.27. Equations 5.4 to 5.6 allow one to calculate the Einstein's parameter without seepage Φ_o in terms of τ_{*o} and Ω_o. The slope modifier ω can be obtained from Eq. 6.28. Hence, the bedload sediment transport rate, in terms of Einstein's parameter Φ, can be predicted using Eq. 6.29, for the case subjected to downward seepage (suction) with seepage zone length less than 2 m.

6.9 SUMMARY

This chapter presents the measured data collected in Experimental Series III. The results show that for the same undisturbed flow condition and suction rate, i.e. the same Ω, the bed load transport rate, which is represented by Einstein's dimensionless parameter Φ, decreases with a reduction in suction zone length. It also shows that for the same undisturbed flow condition and reduction in suction zone length, the ratio of Einstein's parameter Φ in the 2-m length suction zone to

that in the suction zone with length less than 2 m, i.e., $\Phi|_{L=2m}/\Phi|_{L<2m}$, increases with the increase of suction rate. Furthermore, with the same suction rate, $\Phi|_{L=2m}/\Phi|_{L<2m}$ decreases with an increase in τ_{*o}.

A new dimensionless term L/L_o is used to account for this length effect. The slope modifier ω, which is defined as the difference of the slope between the slope of the trendline measured with any length of suction zone less than 2 m, and that with the 2-m length suction zone, or $\omega = \left(A|_{L<2m} - A|_{L=2m}\right)$, is empirically found to be a function of τ_{*o} and $log(L/L_o)$. The empirical equation used to calculate the slope modifier ω is derived as shown in Eq. 6.28. The bedload transport rate subjected to the suction zone length less than 2 m, can be predicted within a ±20% accuracy for a given τ_{*o} for $0.0217 \le \tau_{*o} \le 0.0525$.

Chapter 7

Time Effects on Sediment Transport Rate

7.1 INTRODUCTION

As discussed in Chapter 5, the sediment transport rate in the suction zone is higher than that at the upstream section where suction is absent. Erosion, therefore, will occur in the suction zone. The erosion depth along the suction zone for the tests conducted using the d_{50} = 0.48 mm sand with τ_{*o} = 0.0360 and V_s = -0.246 cm/s are measured and plotted in Fig. 7.1. The data are measured at 10-cm interval. The positive and negative bed elevations refer to the extent of deposition and erosion in the suction zone, respectively. The open square represents the data measured at time = 35 minutes after the test started, whereas the black diamond refers to those measured at time = 170 minutes after the test started. Figure 7.1 clearly shows that the erosion depth increases with time. The degradation of the channel bed causes a change in the flow depth, resulting in a change in the friction between the sediment and water. Based on this analysis, the sediment transport rate likely will be affected by time.

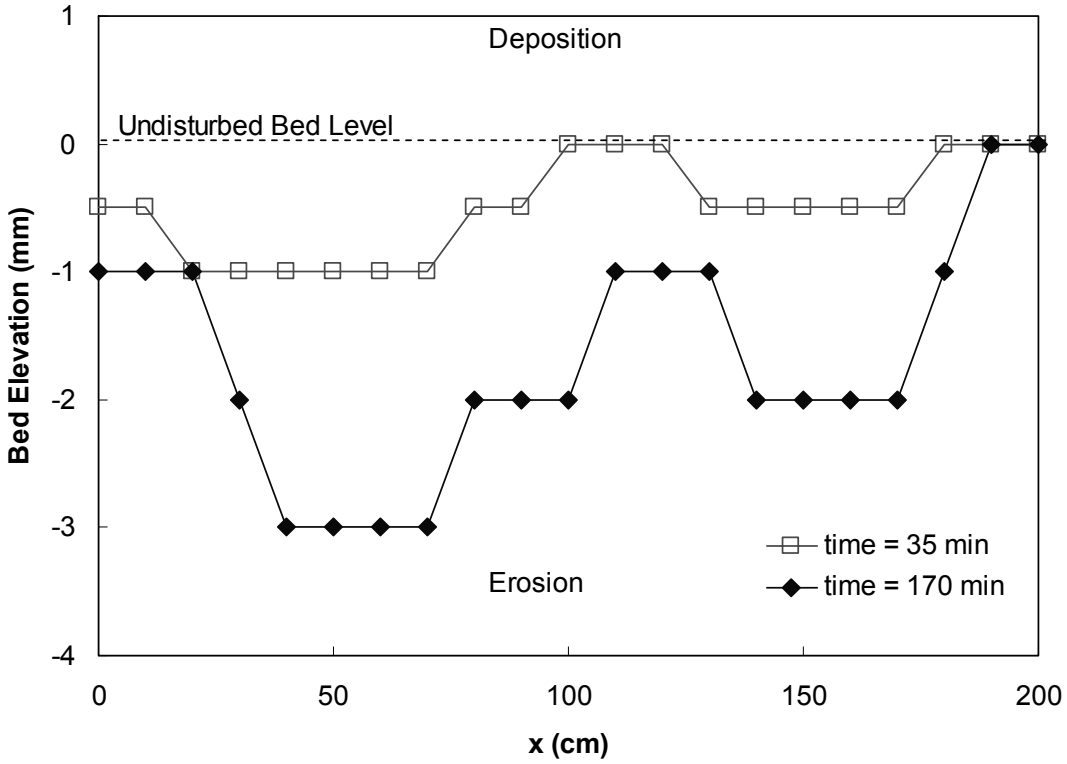

Figure 7.1 Longitudinal Distribution of Bed Elevation over the Suction Zone for τ_{*o} = 0.0360 and V_s = -0.246 cm/s

Chiew (2004) investigated bed degradation with an impermeable bed in a laboratory study. He reported that the general scour depth increases with an increase in time, reaching the equilibrium condition for time > 120 hours. This observation may also apply to the permeable sand bed with suction. Therefore, preliminary experimental results and discussions of the effect of time on sediment transport rate under the influence of suction are presented in this chapter. Three series of tests using the d_{50} = 0.48 mm sand with different undisturbed flow conditions and suction velocities are conducted to examine this effect in the 2-m length suction zone. The sediment transport rates at different time were measured for a maximum of 210 minutes. The details of the experimental apparatus and procedures are discussed in Section 3.5.4. The test data obtained from Experimental Series IV are presented in this chapter, and the conclusions drawn from the experimental results.

7.2 EXPERIMENTAL RESULTS

Experimental Series IV were conducted to study time effects on sediment transport rate subjected to downward seepage or suction. The measured bedload transport rates in terms of Einstein's dimensionless parameter Φ, are plotted against time as shown in Fig. 7.2. The detail data of Experimental Series IV are tabulated in Appendix III. In Fig. 7.2, the grey diamond, open square and black triangle represent the tests subjected to τ_{*o} = 0.0341 with V_s = -0.249 cm/s, τ_{*o} = 0.0360 with V_s = -0.215 cm/s, and τ_{*o} = 0.0360 with V_s = -0.246 cm/s, respectively. Table 7.1 shows the test conditions and some pertinent measured values from the tests. With the Ω-values used in the tests, the corresponding Φ_{comp}-values are calculated using Eqs 5.4 to 5.6. The t_{start} and Φ_{start} represent the time and Einstein's parameter for the first measured data point, respectively. Similarly, the t_{peak} refers to the time when the Einstein's parameter reaches its peak value, Φ_{peak}.

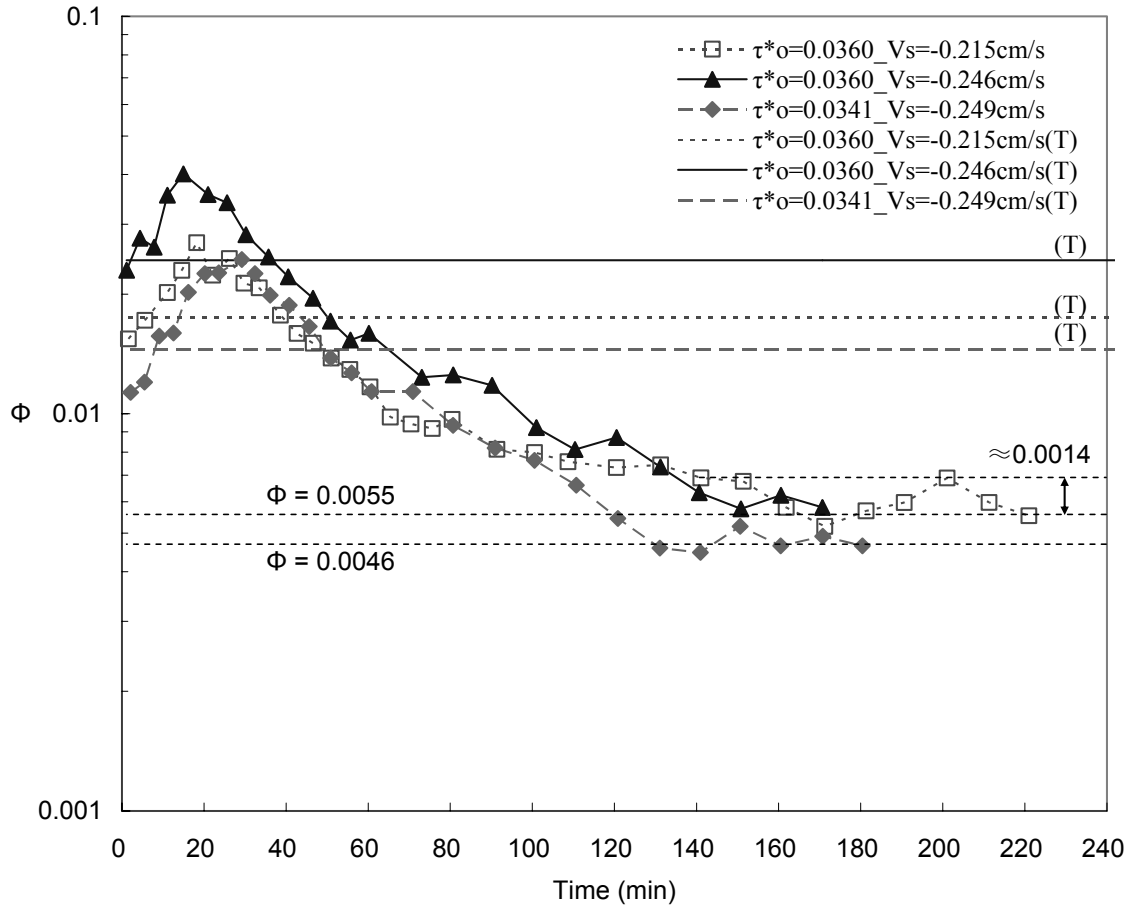

Figure 7.2 Time Effects on Bedload Transport Rate (Φ) with Suction

Table 7.1 Properties of Each Test Measured Using d_{50} = 0.48 mm

Test No.	τ_{*o}	*Vs (cm/s)*	Ω	Φ_{comp}	t_{start} *(min)*	Φ_{start}	t_{peak} *(min)*	Φ_{peak}	Φ_{peak}/Φ_{start}
1	0.0360	-0.215	9.34	0.018	1.6	0.015	18.2	0.027	1.75
2	0.0360	-0.246	8.58	0.024	1.1	0.023	14.9	0.040	1.75
3	0.0341	-0.249	7.99	0.016	2.1	0.011	29.2	0.024	2.16

Figure 7.2 shows that the bedload sediment transport rate rapidly increases with time for approximately the first 20 minutes. After it reaches the peak, it starts to decreases with time. When the time exceeds approximately 140 minutes, the trend of the reduction in sediment transport rate slows down, and has a very gentle horizontal slope. Taking Test 1 as an illustration, Fig. 7.2 shows that the Einstein's parameter Φ increases from 0.015 to the peak value at 0.027 when time increases from 1.6 to 18.2 minutes. The value of Φ then gradually decreases to 0.0069 at 141 minutes after the test starts. The reduction of Φ is considerably slower when time > 141 minutes; Φ reduces by approximately 0.0014 to 0.0055 in the next 80 minutes. For the duration tested in the study, the bedload transport rate in terms of Φ decrease to 0.0046 for Test 3 at 180 minutes, and to 0.0055 for Tests 1 and 2 at 221 and 170 minutes, respectively. This trend suggests that, with time the sediment transport rate will gradually reduce until an equilibrium state is reached, where the erosion depth keeps constant with time. In the present study, the tests were carried out for only three and a half hours, which may not be sufficiently long to reach the equilibrium or limiting condition. Notwithstanding this, the data do show a significant reduction in Φ coupled with a distinct reduction in $d\Phi/dt$.

The sediment transport rate for each test run computed using Eqs. 5.4 to 5.6 are superimposed in Fig. 7.2, labeled with "T". The intersection points indicate that the computed Φ using Eqs. 5.4 to 5.6 were consistently measured at 40 to 50 minutes after commencement of the tests. Since the measurements made for Experimental Series II and III were conducted with a similar time duration, the variation of Φ because of time effect could be neglected when the empirical Φ against Ω functions are determined in Chapters 5 and 6.

Table 7.1 shows that Φ_{peak} increases with Φ_{comp}, while t_{peak} decreases with Φ_{comp}. For example, Test 2, which has the largest Φ_{comp} (= 0.024), has the highest value of

Φ_{peak} (= 0.040) and the smallest t_{peak} (= 14.9 minutes). It may be inferred from these data that the duration for the sediment transport rate to reach its peak, is shorter for the flow with a higher sediment transport rate.

Since the time at which the first data points for all tests are measured is about the same and very close to zero (< 2 minutes), the first data points could be chosen as the reference point. A comparison of Tests 1 and 2 as shown in Table 7.1 reveals that the ratio of Φ at peak to the first Φ, i.e., Φ_{peak}/Φ_{start}, = 1.75 for τ_{*o} = 0.0360. One may infer that Φ_{peak}/Φ_{start} is the same for the flow subjected to the same τ_{*o}, even for different V_s. In order to compare the change of Φ with the same τ_{*o} but different V_s, the values of Φ/Φ_{peak} of Tests 1 to 3 are plotted against t/t_{peak} as shown in Fig. 7.3. The figure shows that when $t/t_{peak} < 6$, the data of Tests 1 and 2 collapse well with each other. When $t/t_{peak} > 6$, the data of two tests deviate from each other. However, referring to Fig. 7.2, as $t/t_{peak} > 6$ or time > 100 minutes, the data of Tests 1 and 2 start to merge together and decrease with time in the same trend. One may infer from this comparison that for the tests with the same undisturbed flow condition but different suction rates, the sediment transport rate collapse in terms of Φ/Φ_{peak} for $t/t_{peak} < 6$. When $t/t_{peak} > 6$, the sediment transport rates in terms of Φ with different suction rates start to merge together and the suction rate has little effect. Since the flows with different suction rates lose their identities, they will undergo the same reduction trend and their corresponding bedload transport rate decreases very slowly with time.

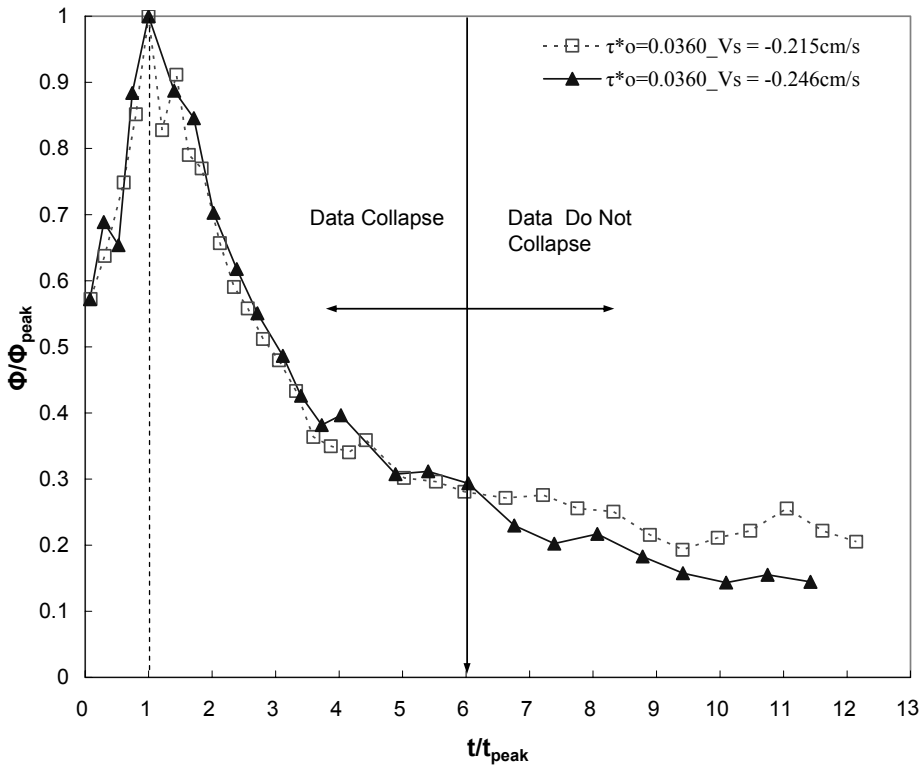

Figure 7.3 Comparison of Φ/Φ_{peak} against Time for Same τ_{*o} but Different V_s

It is pertinent to note that Tests 2 and 3 are measured with approximately the same suction rate but different undisturbed flow conditions. To examine the relationship between these two tests, Figure 7.4 is plotted with values of Φ/Φ_{peak} against time with peak value offset (t-t_{peak}) for both these tests. The term Φ/Φ_{peak} was used to normalize the different peak value of Φ for both series. The term (t-t_{peak}) was chosen for the intensive study on the falling limb of the graph of Φ against time. Figure 7.4 shows that the data for these two tests collapse with each other reasonably well. One may infer from this that, for the flows subjected to the same suction rate but different undisturbed flow condition, their falling limbs of the graph of Φ against time have a similar trend, and appear to be independent of τ_{*o}.

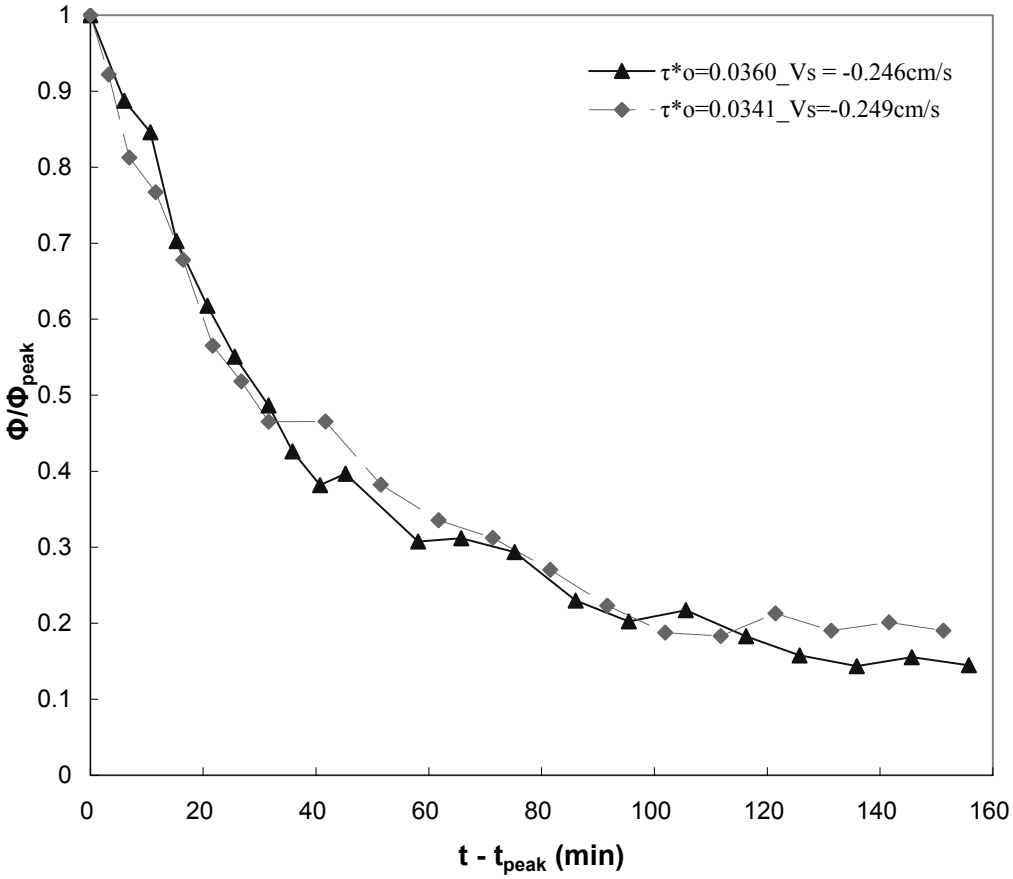

Figure 7.4 Comparison of Φ/Φ_{peak} against Time with Peak-Value Offset Correction for Same V_s but different τ_{*o}

7.3 DISCUSSION AND COMPARISON WITH PREVIOUS INVESTIGATIONS

After the commencement of a test, the sediment particles subjected to downward seepage or suction starts moving out of the seepage zone. The bedload transport rate across the entire suction zone is not uniform, and has a higher rate at the upstream section of the seepage zone, as discussed in Chapter 6. However, the sediment transport rate measured just after test commences is that measured at the downstream end of suction zone. With time the sediment particles at the upstream section of the suction zone, which have a higher rate, move out of the test section,

leading to an increase in bedload transport rate with time. The rising limb in the *Φ-time* distributions as shown in Fig. 7.2 is likely the results of this non-uniform distribution of bedload transport rate. As the sediment particles in the upstream end of the suction zone move to the downstream end, the bedload transport rate reaches the peak. Since the sediment transport rate subjected to suction is higher than that upstream of the suction zone, erosion occurs. As sediment transport continues, bed degradation takes place (see Fig. 7.1) leading to an increase in flow depth, and a corresponding reduction in flow velocity. This occurs because the downstream weir height is always kept constant throughout the experiment. As discussed in Chapter 6, the bed shear stress with suction can be calculated using Eq. 6.16 which is reproduced below

$$\tau_{bs} = -\rho g h \frac{dh}{dx}\left(1 - \frac{U^2}{gh}\right) - 2\rho U V_s \qquad (7.1)$$

The increase in flow depth and reduction in mean flow velocity cause a reduction in bed shear stress, and therefore bed shear velocity, leading to a reduction in shear velocity excess. Therefore, with an increase in time, the bedload transport rate reduces, and eventually reaches a balance between the incoming and outgoing sediment transport, called the equilibrium condition, i.e., the sediment transport with no seepage condition.

This phenomenon, i.e., that bedload transport rate decreases with time, is also observed by Maclean (1991), as he wrote: "as scour develops and the bed shear stress decreases, the effect of grain deposition again becomes significant, until eventually a balance between erosion and deposition is re-established and the bedform stabilizes." The observations from the previous investigation and the preliminary works in the present study confirm that the time effect is important in the analysis of sediment transport rate with suction. More detailed investigations on the time function of Φ and sediment transport behavior at equilibrium condition

are necessary to be carried out in the future.

7.4 SUMMARY

The effect of time on sediment transport rate is discussed in this chapter. The bedload transport rate in the presence of suction rapidly increases with time, eventually reaching a peak, beyond which it starts to decrease. The duration for the bedload transport rate to reach peak, t_{peak}, is shorter for flows with higher sediment transport rates. The trend of reduction is significantly reduced beyond 140 minutes after test starts. For flows with the same τ_{*o} but different V_s, the value of Φ/Φ_{peak} is approximately the same when t/t_{peak} <6. On the other hand, for the flow with different τ_{*o} but the same V_s, the value of Φ/Φ_{peak} is similar for the falling limb when time is corrected with the peak-value offset. It also confirms that the measurements of Experimental Series II and III were conducted with a similar time duration, and hence the variation of Φ because of time effect could be neglected when the empirical Φ against Ω function is determined in Chapters 5 and 6.

Due to the bed degradation in the suction zone, the flow depth and mean flow velocity in the suction zone increase and decreases, respectively, resulting in a reduction in shear velocity. Therefore, the increase of time leads a reduction in shear velocity excess, and hence, the sediment transport rate. This reduction reaches an equilibrium when the sediment transport rate at the downstream end of suction zone = that at the upstream, i.e., the sediment transport rate without suction.

Chapter 8

Summary, Conclusions and Recommendations

The experimental results and theoretical analyses are presented to study seepage effects on sediment transport rate. This study comprises three parts. First, both the injection and suction effects on sediment transport are examined. The prediction equations of bedload transport rate in the presence of seepage are derived empirically. In the second part, the effect of the seepage zone length on sediment transport subjected to downward seepage or suction is described. The prediction equation with the seepage zone length modification is presented. The last part of this study is to investigate time effects on bedload transport rate.

8.1 SEEPAGE EFFECT ON SEDIMENT TRANSPORT

The experimental results show that the computed shear velocity excess, which is defined as the difference between the bed shear velocity (the driving force component) and the critical shear velocity (the resistant force component), increases with an increase in suction rates, resulting in an increase in bedload transport rate.

In contrast, the shear velocity excess with the presence of upward seepage decreases as injection rate increases, leading to a reduction in sediment transport rate.

For the case of suction, the sediment transport rate in terms of Einstein's parameter is found to be a function of Shield's parameter without seepage and modified densimetric Froude number. The experimental results show that Φ is linearly related to of Ω in a semi-logarithmic scale, where the coefficients A and B, which are uniquely related to τ_{*o}, may be calculated using Eqs. 5.4 to 5.6. In order to maintain similar gravitational characteristics to those found in the model and prototype, the dimensionally scaling from laboratory model to the prototype is based on the dynamic similarity through the Froude law.

The reduction in sediment transport rate with the presence of injection is relatively small when compared to that with suction. The ratio of Einstein's parameter with and without injection, Φ/Φ_o is found to be a function of the ratio of the modified densimetric Froude number without and with injection, Ω_o/Ω, shown in Eq. 5.16.

8.2 EFFECT OF SUCTION ZONE SIZE ON SEDIMENT TRANSPORT

The experimental results show that the bedload sediment transport rate in the presence of suction decreases with a reduction in the length of suction zone for the same undisturbed flow condition and suction rate. It also shows that for the same undisturbed flow condition and reduction in suction zone length, $\Phi|_{L=2m}/\Phi|_{L<2m}$, increases with the increase of suction rate. Furthermore, with the same suction rate, $\Phi|_{L=2m}/\Phi|_{L<2m}$ decreases with an increase in τ_{*o}. A new dimensionless term L/L_o is used to account for this length effect. The slope modifier $\omega = \left(A\big|_{L<2m} - A\big|_{L=2m}\right)$ is empirically determined in terms of τ_{*o} and $log(L/L_o)$ as

given in Eq. 6.28.

8.3 TIME EFFECT ON SEDIMENT TRANSPORT

The bedload transport rate in the presence of suction rapidly increases with time, eventually reaching a peak, beyond which it starts to decrease. The duration for the bedload transport rate to reach peak, t_{peak}, is shorter for flows with higher sediment transport rates. The trend of reduction is significantly reduced beyond 140 minutes after the commencement of the test. The measurements of Experimental Series II and III were conducted with a similar time duration, and hence the variation of Φ because of time effect could be neglected when the empirical Φ against Ω function is determined in Chapters 5 and 6.

8.4 RECOMMENDATIONS

The measured data in the present study for analyzing the effect of injection on sediment transport rate were comparably less than those for the case of suction. Moreover, the injection velocities tested were less than half of V_{sc}. The quick condition was not observed during the experiments. For further research, it is recommended that the injection effects on sediment transport rate, especially with high injection rates and quick conditions, should be studied more intensively.

Due to the limitation of the experimental apparatus, the experiments in the present research were conducted only with $L \leq 2$ m, to study the effect of suction zone length on sediment transport in this research. Further investigation should examine the sediment transport rate with a suction zone length > 2 m.

The preliminary works of time effects on sediment transport rate are presented in this study. In the present study, the tests were carried out for only three and a half hours, which may not be long enough to reach the equilibrium condition. It is suggested that the time effects, such as the time function of Φ and sediment transport behavior at equilibrium condition, should be studied more intensively in further study.

REFERENCES

1. Ackers, P., and White, W. R., (1974) “Sediment transport: new approach and analysis.” J. Hydraul. Div., ASCE, 99(11), 2041-2060.
2. Aguirre-Pe, J., Olivero, M., L., and Moncade, A., T., (2003). “Particle densimetric Froude number for estimating sediment transport.” J. Hydraul. Engrg., ASCE, 129(6), 428-437.
3. Ali, K. H. M., Achterberg, J., Li, M., and Zhu, Y., (2003). “Effect of seepage on sediment transport in channels.” Proc., Int. Conf. on Estuaries and Coasts, IAHR, Hangzhou, China, 461-466.
4. Bagnold, R. A., (1996). “An approach to the sediment transport problem from general physics.” U.S. Geological Survey Professional Paper, 422-I, 37.
5. Bear, J., (1988). “Dynamics of fluids in porous media.” Dover Publication, Inc., New York.
6. Chen, X., and Chiew, Y. M., (2004). “Velocity distribution of turbulent open-channel flow with bed suction.” J. Hydraul. Engrg., ASCE, 130(2), 140-148.
7. Cheng, N. S., (2002). “Exponential formula for bedload transport.” J. Hydraul. Engrg., ASCE, 128(10), 942-946.
8. Cheng, N. S., and Chiew, Y. M., (1998a). “Modified logarithmic law for velocity distribution subjected to upward seepage.” J. Hydraul. Engrg., ASCE, 124(12), 1235-1241.
9. Cheng, N. S., and Chiew, Y. M., (1998b). “Turbulent open-channel flow with upward seepage.” J. Hydraul. Res., 36(3), 415-431.
10. Cheng, N. S., and Chiew, Y. M., (1999). “Incipient sediment motion with upward seepage.” J. Hydraul. Res., 37(5), 665-681.
11. Chiew, Y. M., (2004). “Local scour and riprap stability at bridge piers in a

degrading channel." J. Hydraul. Engrg., ASCE, 130(3), 218-226.

12. Chiew, Y. M., and Parker, G., (1994). "Incipient sediment motion on non-horizontal slopes." J. Hydraul. Res., 32(5), 649-660.
13. Chow, V. T., (1959). "Open-channel hydraulics." McGraw-Hill Book Co., New York.
14. Dey, S., and Zanke, U. C. E., (2004). "Sediment threshold with upward seepage." J. Engrg. Mech., ASCE, 130(9), 1118-1123.
15. Einstein, H. A., (1950). "The bed-load function for sediment transportation in open channel flows." Tech. Bull. No. 1026, U.S. Department of Agriculture, Washington, D.C.
16. Engelund, F. and Hansen, E. (1967). "A monograph on sediment transport in alluvial streams." Teknisk Forlag, Copenhagen, Denmark.
17. Fernandez Luque, R., (1974). "Erosion and transport of bed load sediment." Thesis presented to the Technische Hogeschool, at Delft, The Netherlands, in partial fulfillment of the requirements for the degree of Doctor in de Technische Wetenschappen.
18. Fox, G. A., Wilson, G. V., R. Periketi, Gordji, L., and Cullum, R. F., (2005). "The role of subsurface water in contributing to streambank erosion." Proceedings of the US-China Workshop on Advanced Computational Modeling in Hydroscience and Engineering, August 2-5, Oxford, Mississippi, USA, 10 pages (CD-ROM).
19. Francalanci, S., (2006). "Sediment transport processes and local scale effects on river morphodynamics." Ph.D. thesis, Univ. of Padova, Padova Italy.
20. Francalanci, S., Parker, G., and Solari, L., (2008). "Effect of seepage-induced nonhydrostatic pressure distribution on bed-load transport and bed morphodynamics." J. Hydraul. Engrg., ASCE, 134(4), 378-389.
21. Harrison, S. S., and Clayton, L., (1970). "Effects of groundwater seepage on fluvial processes." Bulletin of the Geological Society of America, No. 811,

1217-1225.

22. Keulegan, G.H., (1938). “Laws of turbulent flow in open channels.” Journal of Research of the National Bureau of Standards 21, Research Paper RP1151, 707-741.
23. Lu, Y., and Chiew, Y. M., (2007). “Seepage effects on dune dimensions.” J. Hydraul. Engrg., ASCE, 133(5), 560-563.
24. Lu, Y., and Chiew, Y. M., and Cheng, N. S., (2008). “Review of seepage effects on turbulent open-channel flow and sediment entrainment.” Journal of Hydraulic Research, IAHR, 46(4), 476-488.
25. Maclean, A. G., (1991). “Bed shear stress and scour over bed-type river intake.” J. Hydraul. Engrg., ASCE, 117(4), 436-451.
26. Maclean, A. G., and Willetts, B. B., (1984). “River bed water intakes: a laboratory investigation with mobile bed.” Proc. of the First Int. Conf. on Hydraulic Design in Water Resources Engineering: Channels and Channel Control Structure, University of Southampton, Southampton, England, Apr, 2.53-2.67.
27. Maclean, A. G., and Willetts, B. B., (1986). “Measurement of boundary shear stress in non-uniform open channel flow.” J. Hydraul. Res., 24(1), 39-51.
28. Meyer-Peter, E., and Muller, R., (1948). “Formulas for bedload transport.” Proc., 2nd Meeting, IAHR, Stockholm, Sweden, 39-64.
29. Nezu, I., (1977). “Turbulent structure in open channel flow.” Ph.D. thesis, Kyoto Univ., Kyoto, Japan.
30. Nielsen, P., Robert, S., Christiansen, B., M., Oliva, P., (2001). “Infiltration effects on sediment mobility under waves.” Proc. 42th. Int. Conf. Coastal Engineering, Orlando, ASCE, pp. 2677-2690.
31. O’Donnell, C., O’Connor, B.A., and Ali, K.H.M., (2002). “Effect of seepage flows on sediment transport rates.” Environmental Study, Vol 8, 445-453.
32. Oldenziel, D. M., and Brink, W. E., (1974). “Influence of suction and blowing

on entrainment of sand particles." J. Hydraul. Div., ASCE, 100(7), 935-949.

33. Owoputi, L. O., and Stolte, W. J., (2001). "The role of seepage in erodibility." Hydrological Processes, 15(1), 13-22.
34. Parker, G., and Wilcock, P., R., (1993). "Sediment feed and recirculating flume fundamental difference." J. Hydraul. Engrg., ASCE, 119(11), 1192-1204.
35. Ramakrishna Rao, A., Subrahmanyam, V., Thayumanavan, S., and Damodaran, N., (1994). "Seepage effects on sand-bed channels." J. Irrig. and Drain. Engrg., ASCE, 120(1), 60-79.
36. Ramakrishna Rao, A., and Sitaram, N., (1999). "Stability and mobility of sand-bed channels affected by seepage." J Irrig. and Drain. Engrg., ASCE, 125(16), 370-379.
37. Richardson, J. R., Abt, S. R., and Richardson, E. V., (1985). "Inflow seepage influence on straight alluvial channels." J. Hydraul. Engrg., ASCE, 111(8), 1133-1147.
38. Shen, H. W., (1971). "River mechanics." Vol. 1, Colorado State University Press, Fort Collins, Colo.
39. Shields, A., (1936). "Application of similitude mechanics and research on turbulence to bed load movement." Mitteilungender Preussischer Versuchsanstalt fur Wasserbau und Schiffbau 26 (in German).
40. Turcotte, D. L., (1960). "A sublayer theory for fluid injection into incompressible turbulent boundary layer." Journal of the Aerospace Science, 27(9), 675-678.
41. Van Rijn, L. C., (1984). "Sediment transport, part I: bed load transport." J. Hydraul. Engrg., ASCE, 110(10), 1431-1456.
42. Willetts, B. B., and Drossos, M. E., (1975). "Local erosion caused by rapid forced infiltration." J. Hydraul. Div., ASCE, 101(12), 1477-1488.
43. Wong, M., and Parker, G., (2006). "Reanalysis and correction of bed-load relation of Meyer-Peter and Muller using their own database." J. Hydraul.

Engrg., ASCE, 132(11), 1159-1168.

44. Yalin, M. S., (1977). “Mechanics of sediment transport.” Pergamon, Oxford.
45. Yang, S. Q., and Lim, S. Y., (2003) “Total load transport formula for flow in alluvial channels.” J. Hydraul. Engrg., ASCE, 129(1), 68-72.

Appendix I

Data of Sediment Transport Rate with Seepage

The detail data of sediment transport rate with presence of injection and suction mentioned in Chapter 5 are shown in AI.1 and AI.2, respectively.

AI.1 SEDIMENT TRANSPORT RATE UNDER INJECTION

The sediment transport rates of the Experimental Series II subjected with upward seepage (injection) were measured only for Series 1-5 to 1-7. The details are shown below in Table AI.1.

Table AI.1 Sediment Transport Rate under Injection

(a) Series 1-5, τ_{*o} = 0.0317

No	V_s *(cm/s)*	q_b *(10^-6)* (m^2/s)	Ω	Φ
1-5-I-1	0.000	0.049	14.65	0.000452
1-5-I-2	0.013	0.047	15.01	0.000434
1-5-I-3	0.019	0.044	15.19	0.000409
1-5-I-4	0.022	0.046	15.28	0.000425
1-5-I-5	0.026	0.045	15.40	0.000416
1-5-I-6	0.039	0.044	15.82	0.000406
1-5-I-7	0.047	0.043	16.08	0.000397
1-5-I-8	0.048	0.048	16.10	0.000443
1-5-I-9	0.050	0.047	16.15	0.000434
1-5-I-10	0.073	0.045	16.99	0.000416
1-5-I-11	0.074	0.039	17.00	0.000360
1-5-I-12	0.080	0.041	17.23	0.000379
1-5-I-13	0.096	0.036	17.88	0.000336
1-5-I-14	0.104	0.037	18.21	0.000340
1-5-I-15	0.105	0.039	18.24	0.000360
1-5-I-16	0.105	0.041	18.24	0.000379
1-5-I-17	0.123	0.039	19.03	0.000360
1-5-I-18	0.132	0.036	19.45	0.000335
1-5-I-19	0.133	0.041	19.51	0.000379
1-5-I-20	0.133	0.039	19.53	0.000360
1-5-I-21	0.154	0.037	20.61	0.000342
1-5-I-22	0.160	0.034	20.91	0.000317
1-5-I-23	0.164	0.036	21.17	0.000330
1-5-I-24	0.176	0.031	21.88	0.000289
1-5-I-25	0.181	0.033	22.18	0.000304
1-5-I-26	0.192	0.035	22.87	0.000323
1-5-I-27	0.201	0.032	23.49	0.000297
1-5-I-28	0.208	0.036	24.04	0.000328
1-5-I-29	0.216	0.034	24.61	0.000314
1-5-I-30	0.258	0.034	28.36	0.000318
1-5-I-31	0.281	0.032	30.97	0.000295
1-5-I-32	0.337	0.033	39.79	0.000305
1-5-I-33	0.357	0.031	44.29	0.000284
1-5-I-34	0.435	0.032	79.54	0.000296

(b) Series 1-6, τ_{*o} = 0.0436

No	V_s *(cm/s)*	q_b *(10^-6)* (m^2/s)	*Ω*	*Φ*
1-6-I-1	0.019	0.113	18.39	0.001043
1-6-I-2	0.023	0.117	18.57	0.001080
1-6-I-3	0.048	0.108	19.51	0.000997
1-6-I-4	0.049	0.107	19.56	0.000988
1-6-I-5	0.051	0.113	19.61	0.001043
1-6-I-6	0.078	0.106	20.77	0.000979
1-6-I-7	0.079	0.102	20.81	0.000942
1-6-I-8	0.085	0.096	21.14	0.000886
1-6-I-9	0.102	0.100	21.92	0.000923
1-6-I-10	0.103	0.097	22.00	0.000896
1-6-I-11	0.104	0.099	22.02	0.000914
1-6-I-12	0.119	0.092	22.85	0.000850
1-6-I-13	0.130	0.088	23.45	0.000813
1-6-I-14	0.130	0.094	23.48	0.000868
1-6-I-15	0.149	0.087	24.62	0.000803
1-6-I-16	0.150	0.093	24.69	0.000863
1-6-I-17	0.159	0.096	25.32	0.000890
1-6-I-18	0.160	0.090	25.36	0.000831
1-6-I-19	0.185	0.082	27.15	0.000757
1-6-I-20	0.187	0.087	27.29	0.000803
1-6-I-21	0.193	0.084	27.84	0.000778
1-6-I-22	0.211	0.076	29.38	0.000702
1-6-I-23	0.212	0.084	29.41	0.000774
1-6-I-24	0.218	0.080	30.05	0.000739
1-6-I-25	0.233	0.083	31.47	0.000763
1-6-I-26	0.254	0.079	33.89	0.000729
1-6-I-27	0.268	0.082	35.65	0.000757
1-6-I-28	0.281	0.077	37.53	0.000711
1-6-I-29	0.312	0.081	42.67	0.000748
1-6-I-30	0.319	0.074	44.11	0.000683

(c) Series 1-7, τ_{*o} = 0.0525

No	V_s *(cm/s)*	q_b *(10^-6)* (m^2/s)	*Ω*	*Φ*
1-7-I-1	0.014	0.217	20.46	0.002008
1-7-I-2	0.022	0.247	20.79	0.002283
1-7-I-3	0.050	0.219	22.00	0.002024
1-7-I-4	0.051	0.232	22.03	0.002142
1-7-I-5	0.072	0.230	23.06	0.002123
1-7-I-6	0.079	0.235	23.42	0.002170
1-7-I-7	0.081	0.201	23.50	0.001858
1-7-I-8	0.101	0.206	24.57	0.001902
1-7-I-9	0.102	0.228	24.65	0.002103
1-7-I-10	0.121	0.182	25.80	0.001678
1-7-I-11	0.129	0.207	26.26	0.001911
1-7-I-12	0.134	0.192	26.65	0.001773
1-7-I-13	0.150	0.181	27.75	0.001670
1-7-I-14	0.159	0.174	28.39	0.001607
1-7-I-15	0.160	0.189	28.45	0.001745
1-7-I-16	0.180	0.190	30.12	0.001757
1-7-I-17	0.181	0.161	30.14	0.001490
1-7-I-18	0.190	0.174	31.00	0.001607
1-7-I-19	0.209	0.174	32.75	0.001607
1-7-I-20	0.214	0.169	33.25	0.001561
1-7-I-21	0.217	0.158	33.60	0.001460
1-7-I-22	0.251	0.152	37.63	0.001404

AI.2 SEDIMENT TRANSPORT RATE UNDER SUCTION

The sediment transport rates of the Experimental Series II subjected with downward seepage (suction) were measured for all series tabulated in Table 5.1. The details are shown below in Table AI.2 and AI.3 for sand particle sizes of d_{50} = 0.9 mm and 0.48 mm, respectively.

Table AI.2 Sediment Transport Rate under Suction (d_{50} = 0.9 mm)

(a) Series 1-1, τ_{*o} = 0.0217

No	V_s *(cm/s)*	q_b *(10^-6)* (m^2/s)	Ω	Φ
1-1-S-1	-0.290	0.022	6.23	0.000202
1-1-S-2	-0.309	0.102	6.08	0.000945
1-1-S-3	-0.316	0.081	6.03	0.000745
1-1-S-4	-0.318	0.039	6.02	0.000365
1-1-S-5	-0.336	0.086	5.90	0.000792
1-1-S-6	-0.356	0.219	5.76	0.002018
1-1-S-7	-0.363	0.172	5.72	0.001589
1-1-S-8	-0.365	0.207	5.71	0.001915
1-1-S-9	-0.384	0.328	5.59	0.003031
1-1-S-10	-0.385	0.307	5.58	0.002831
1-1-S-11	-0.390	0.375	5.55	0.003459
1-1-S-12	-0.393	0.850	5.53	0.007848
1-1-S-13	-0.393	0.412	5.53	0.003807
1-1-S-14	-0.394	0.505	5.53	0.004664
1-1-S-15	-0.396	0.629	5.52	0.005804
1-1-S-16	-0.414	0.468	5.41	0.004319
1-1-S-17	-0.418	0.408	5.39	0.003770
1-1-S-18	-0.421	0.642	5.37	0.005931
1-1-S-19	-0.439	0.667	5.27	0.006156
1-1-S-20	-0.440	0.911	5.27	0.008416

(b) Series 1-2, τ_{*o} = 0.0242

No	V_s *(cm/s)*	q_b *(10^-6)* (m^2/s)	Ω	Φ
1-2-S-1	-0.231	0.022	8.04	0.000199
1-2-S-2	-0.246	0.017	7.88	0.000153
1-2-S-3	-0.273	0.034	7.62	0.000312
1-2-S-4	-0.281	0.051	7.55	0.000471
1-2-S-5	-0.281	0.055	7.54	0.000508
1-2-S-6	-0.329	0.109	7.13	0.001008
1-2-S-7	-0.330	0.077	7.12	0.000715
1-2-S-8	-0.330	0.137	7.11	0.001266
1-2-S-9	-0.345	0.149	7.00	0.001379
1-2-S-10	-0.358	0.142	6.89	0.001315
1-2-S-11	-0.370	0.318	6.80	0.002937
1-2-S-12	-0.389	0.313	6.66	0.002887
1-2-S-13	-0.396	0.174	6.61	0.001605
1-2-S-14	-0.410	0.281	6.52	0.002592
1-2-S-15	-0.410	0.423	6.51	0.003909
1-2-S-16	-0.428	0.455	6.39	0.004197
1-2-S-17	-0.442	0.897	6.30	0.008281
1-2-S-18	-0.467	0.906	6.14	0.008368
1-2-S-19	-0.479	0.645	6.07	0.005953
1-2-S-20	-0.505	0.531	5.92	0.004901

(c) Series 1-3, τ_{*o} = 0.0265

No	V_s *(cm/s)*	q_b *(10^-6)* (m^2/s)	*Ω*	*Φ*
1-3-S-1	-0.169	0.067	9.69	0.000622
1-3-S-2	-0.183	0.101	9.50	0.000929
1-3-S-3	-0.196	0.099	9.33	0.000914
1-3-S-4	-0.199	0.077	9.29	0.000711
1-3-S-5	-0.255	0.298	8.63	0.002748
1-3-S-6	-0.262	0.251	8.56	0.002316
1-3-S-7	-0.275	0.575	8.42	0.005306
1-3-S-8	-0.276	0.346	8.41	0.003191
1-3-S-9	-0.289	0.546	8.27	0.005042
1-3-S-10	-0.295	0.726	8.21	0.006705
1-3-S-11	-0.297	0.628	8.19	0.005795
1-3-S-12	-0.312	1.205	8.05	0.011129
1-3-S-13	-0.323	0.860	7.94	0.007941
1-3-S-14	-0.340	1.946	7.79	0.017970
1-3-S-15	-0.348	1.065	7.72	0.009834
1-3-S-16	-0.361	2.552	7.60	0.023563
1-3-S-17	-0.369	1.748	7.54	0.016138
1-3-S-18	-0.369	1.384	7.54	0.012776
1-3-S-19	-0.374	3.029	7.50	0.027966
1-3-S-20	-0.388	1.457	7.39	0.013450
1-3-S-21	-0.416	2.593	7.17	0.023946

(d) Series 1-4, τ_{*o} = 0.0294

No	V_s *(cm/s)*	q_b *(10^-6)* (m^2/s)	*Ω*	*Φ*
1-4-S-1	-0.063	0.016	12.64	0.000152
1-4-S-2	-0.078	0.028	12.33	0.000256
1-4-S-3	-0.092	0.027	12.05	0.000251
1-4-S-4	-0.118	0.029	11.58	0.000266
1-4-S-5	-0.121	0.052	11.53	0.000483
1-4-S-6	-0.157	0.066	10.92	0.000606
1-4-S-7	-0.180	0.133	10.57	0.001226
1-4-S-8	-0.215	0.151	10.08	0.001395
1-4-S-9	-0.259	0.365	9.52	0.003367
1-4-S-10	-0.277	0.386	9.31	0.003564
1-4-S-11	-0.292	0.469	9.13	0.004331
1-4-S-12	-0.342	0.827	8.62	0.007637
1-4-S-13	-0.342	0.636	8.61	0.005875
1-4-S-14	-0.358	0.975	8.45	0.009002
1-4-S-15	-0.365	1.064	8.39	0.009827
1-4-S-16	-0.384	1.193	8.22	0.011019
1-4-S-17	-0.406	1.541	8.03	0.014227
1-4-S-18	-0.408	1.793	8.01	0.016553
1-4-S-19	-0.415	1.757	7.95	0.016222

(e) Series 1-5, τ_{*o} = 0.0317

No	V_s *(cm/s)*	q_b *(10^-6)* (m^2/s)	Ω	Φ
1-5-S-1	0.000	0.043	14.65	0.000399
1-5-S-2	-0.004	0.052	14.54	0.000479
1-5-S-3	-0.016	0.069	14.24	0.000640
1-5-S-4	-0.053	0.163	13.33	0.001507
1-5-S-5	-0.060	0.089	13.16	0.000825
1-5-S-6	-0.077	0.167	12.80	0.001547
1-5-S-7	-0.089	0.234	12.55	0.002165
1-5-S-8	-0.107	0.148	12.21	0.001369
1-5-S-9	-0.110	0.294	12.14	0.002719
1-5-S-10	-0.138	0.257	11.64	0.002373
1-5-S-11	-0.171	0.256	11.09	0.002364
1-5-S-12	-0.186	0.572	10.87	0.005284
1-5-S-13	-0.199	0.621	10.67	0.005736
1-5-S-14	-0.214	0.495	10.46	0.004575
1-5-S-15	-0.214	0.795	10.46	0.007343
1-5-S-16	-0.261	0.942	9.84	0.008701
1-5-S-17	-0.278	0.816	9.64	0.007532
1-5-S-18	-0.280	1.581	9.61	0.014601
1-5-S-19	-0.281	0.685	9.60	0.006327
1-5-S-20	-0.316	1.599	9.20	0.014764
1-5-S-21	-0.340	1.763	8.95	0.016276
1-5-S-22	-0.340	1.190	8.95	0.010985
1-5-S-23	-0.386	2.090	8.50	0.019295
1-5-S-24	-0.413	3.441	8.26	0.031772
1-5-S-25	-0.415	2.765	8.25	0.025533
1-5-S-26	-0.463	3.018	7.85	0.027872
1-5-S-27	-0.478	3.310	7.73	0.030561
1-5-S-28	-0.495	2.524	7.60	0.023303
1-5-S-29	-0.514	5.635	7.46	0.052037
1-5-S-30	-0.517	4.065	7.44	0.037536
1-5-S-31	-0.575	4.390	7.05	0.040540

(f) Series 1-6, τ_{*o} = 0.0436

No	V_s *(cm/s)*	q_b *(10^-6)* (m^2/s)	*Ω*	*Φ*
1-6-S-1	-0.045	0.185	16.36	0.001710
1-6-S-2	-0.095	0.348	15.08	0.003216
1-6-S-3	-0.095	0.293	15.06	0.002704
1-6-S-4	-0.123	0.479	14.43	0.004425
1-6-S-5	-0.157	0.463	13.72	0.004277
1-6-S-6	-0.175	0.459	13.36	0.004236
1-6-S-7	-0.243	1.550	12.20	0.014308
1-6-S-8	-0.279	0.956	11.66	0.008827
1-6-S-9	-0.298	0.991	11.38	0.009151
1-6-S-10	-0.330	1.030	10.97	0.009511
1-6-S-11	-0.331	2.011	10.95	0.018565
1-6-S-12	-0.350	1.442	10.72	0.013312
1-6-S-13	-0.458	1.986	9.55	0.018335
1-6-S-14	-0.466	2.876	9.47	0.026552

(g) Series 1-7, τ_{*o} = 0.0525

No	V_s *(cm/s)*	q_b *(10^-6)* (m^2/s)	*Ω*	*Φ*
1-7-S-1	0.000	0.272	19.94	0.002512
1-7-S-2	0.000	0.176	19.94	0.001625
1-7-S-3	-0.032	0.438	18.80	0.004040
1-7-S-4	-0.043	0.351	18.45	0.003243
1-7-S-5	-0.062	0.692	17.85	0.006386
1-7-S-6	-0.099	0.798	16.80	0.007371
1-7-S-7	-0.101	0.690	16.77	0.006369
1-7-S-8	-0.103	0.833	16.70	0.007696
1-7-S-9	-0.112	0.729	16.47	0.006734
1-7-S-10	-0.121	0.826	16.24	0.007626
1-7-S-11	-0.129	1.362	16.04	0.012576
1-7-S-12	-0.177	1.303	14.96	0.012035
1-7-S-13	-0.189	2.140	14.72	0.019762
1-7-S-14	-0.223	1.388	14.07	0.012815
1-7-S-15	-0.367	4.118	11.81	0.038022

Table AI.3 Sediment Transport Rate under Suction (d_{50} = 0.48 mm)

(a) Series 2-1, τ_{*o} = 0.0298

No	V_s *(cm/s)*	q_b *(10^-6)* (m^2/s)	Ω	Φ
2-1-S-1	-0.124	0.006	10.16	0.000153
2-1-S-2	-0.135	0.018	9.76	0.000420
2-1-S-3	-0.197	0.100	7.97	0.002359
2-1-S-4	-0.197	0.064	7.97	0.001503
2-1-S-5	-0.209	0.130	7.70	0.003061
2-1-S-6	-0.220	0.121	7.46	0.002851
2-1-S-7	-0.228	0.129	7.29	0.003041
2-1-S-8	-0.229	0.115	7.29	0.002699
2-1-S-9	-0.248	0.229	6.94	0.005384
2-1-S-10	-0.251	0.362	6.87	0.008526
2-1-S-11	-0.252	0.173	6.85	0.004073
2-1-S-12	-0.254	0.283	6.82	0.006669
2-1-S-13	-0.258	0.386	6.75	0.009100
2-1-S-14	-0.265	0.220	6.63	0.005181
2-1-S-15	-0.266	0.397	6.62	0.009338
2-1-S-16	-0.271	0.513	6.54	0.012082
2-1-S-17	-0.284	0.533	6.35	0.012558
2-1-S-18	-0.284	0.400	6.34	0.009427
2-1-S-19	-0.292	0.452	6.22	0.010648

(b) Series 2-2, τ_{*o} = 0.0341

No	V_s *(cm/s)*	q_b *(10^-6)* (m^2/s)	Ω	Φ
2-2-S-1	-0.075	0.050	15.35	0.001177
2-2-S-2	-0.081	0.070	14.93	0.001648
2-2-S-3	-0.137	0.232	11.94	0.005456
2-2-S-4	-0.142	0.274	11.76	0.006442
2-2-S-5	-0.169	0.371	10.71	0.008748
2-2-S-6	-0.223	0.909	9.14	0.021397
2-2-S-7	-0.238	0.733	8.77	0.017261
2-2-S-8	-0.250	1.015	8.50	0.023911
2-2-S-9	-0.262	1.400	8.25	0.032970
2-2-S-10	-0.270	1.562	8.09	0.036791
2-2-S-11	-0.275	1.700	8.00	0.040035
2-2-S-12	-0.284	1.109	7.83	0.026127
2-2-S-13	-0.293	1.400	7.66	0.032970

(c) Series 2-3, τ_{*o} = 0.0360

No	V_s *(cm/s)*	q_b *(10^-6)* (m^2/s)	*Ω*	*Φ*
2-3-S-1	-0.080	0.015	14.07	0.000353
2-3-S-2	-0.100	0.022	12.91	0.000518
2-3-S-3	-0.170	0.150	10.01	0.003532
2-3-S-4	-0.181	0.280	9.66	0.006594
2-3-S-5	-0.228	0.400	8.45	0.009420
2-3-S-6	-0.228	0.400	8.45	0.009420
2-3-S-7	-0.240	0.550	8.17	0.012952
2-3-S-8	-0.244	0.700	8.09	0.016485
2-3-S-9	-0.250	0.580	7.96	0.013659
2-3-S-10	-0.265	0.800	7.67	0.018840
2-3-S-11	-0.270	0.650	7.58	0.015307
2-3-S-12	-0.280	1.100	7.40	0.025905

(d) Series 2-4, τ_{*o} = 0.0422

No	V_s *(cm/s)*	q_b *(10^-6)* (m^2/s)	*Ω*	*Φ*
2-4-S-1	-0.152	0.794	13.45	0.018690
2-4-S-2	-0.185	0.812	12.10	0.019129
2-4-S-3	-0.202	1.322	11.48	0.031133
2-4-S-4	-0.248	1.554	10.13	0.036603
2-4-S-5	-0.256	1.604	9.94	0.037765
2-4-S-6	-0.256	2.577	9.93	0.060679
2-4-S-7	-0.265	2.264	9.72	0.053326
2-4-S-8	-0.287	2.416	9.21	0.056903
2-4-S-9	-0.297	2.330	9.00	0.054877
2-4-S-10	-0.308	2.138	8.78	0.050358
2-4-S-11	-0.313	2.850	8.68	0.067112
2-4-S-12	-0.333	3.674	8.33	0.086518
2-4-S-13	-0.340	3.596	8.20	0.084691
2-4-S-14	-0.348	2.982	8.07	0.070226
2-4-S-15	-0.349	3.610	8.05	0.085025
2-4-S-16	-0.371	4.209	7.70	0.099121

Appendix II

Data of Sediment Transport Rate with Different Suction Zone Length

The detail data of sediment transport rate under different suction zone length with presence of suction mentioned in Chapter 6 are shown in AII.1 and AII.2 for particle size d_{50} = 0.9 mm and 0.48 mm, respectively.

AII.1 SEDIMENT TRANSPORT RATE UNDER SHORTENED SUCTION ZONE FOR d_{50} = 0.9 mm

The sediment transport rates of the Experimental Series III subjected with downward seepage (suction) were measured for Series 1-3, and 1-5 to 1-7 with particles size d_{50} = 0.9 mm. The details shown in Table AII.1 are the data tested with the 0.5-m suction zone.

Table AII.1 Sediment Transport Rate with 0.5-m Length Suction Zone (d_{50} = 0.9 mm)

(a) Series 1-3, τ_{*o} = 0.0265

No	V_s *(cm/s)*	q_b *(10^-6) (m²/s)*	*Ω*	*Φ*
1-3-L'-1	-0.355	0.036	7.66	0.000337
1-3-L'-2	-0.370	0.070	7.53	0.000649
1-3-L'-3	-0.373	0.052	7.50	0.000480
1-3-L'-4	-0.455	0.077	6.89	0.000711
1-3-L'-5	-0.514	0.099	6.50	0.000911
1-3-L'-6	-0.573	0.123	6.15	0.001136
1-3-L'-7	-0.627	0.229	5.86	0.002111
1-3-L'-8	-0.644	0.421	5.78	0.003886
1-3-L'-9	-0.708	0.383	5.48	0.003534
1-3-L'-10	-0.710	0.203	5.47	0.001871
1-3-L'-11	-0.746	0.503	5.32	0.004644
1-3-L'-12	-0.804	0.382	5.09	0.003531
1-3-L'-13	-0.807	0.620	5.07	0.005728
1-3-L'-14	-0.863	0.423	4.87	0.003908
1-3-L'-15	-0.891	0.614	4.78	0.005666
1-3-L'-16	-0.892	0.887	4.77	0.008191
1-3-L'-17	-0.931	0.711	4.65	0.006566
1-3-L'-18	-0.960	0.771	4.55	0.007123

(b) Series 1-5, τ_{*o} = 0.0317

No	V_s *(cm/s)*	q_b *(10^-6)* (m^2/s)	*Ω*	*Φ*
1-5-L'-1	-0.205	0.250	10.59	0.002308
1-5-L'-2	-0.228	0.372	10.27	0.003436
1-5-L'-3	-0.316	0.600	9.21	0.005540
1-5-L'-4	-0.361	0.500	8.74	0.004617
1-5-L'-5	-0.481	1.096	7.71	0.010120
1-5-L'-6	-0.508	0.750	7.50	0.006925
1-5-L'-7	-0.592	1.662	6.95	0.015344
1-5-L'-8	-0.603	1.000	6.88	0.009234
1-5-L'-9	-0.677	2.147	6.46	0.019827
1-5-L'-10	-0.680	1.300	6.44	0.012004
1-5-L'-11	-0.749	1.500	6.10	0.013851
1-5-L'-12	-0.754	2.394	6.07	0.022108
1-5-L'-13	-0.777	1.800	5.96	0.016621
1-5-L'-14	-0.783	2.512	5.94	0.023196
1-5-L'-15	-0.859	1.900	5.62	0.017544
1-5-L'-16	-0.864	2.100	5.60	0.019391
1-5-L'-17	-0.878	2.100	5.54	0.019391
1-5-L'-18	-0.913	2.631	5.40	0.024290

(c) Series 1-6, τ_{*o} = 0.0436

No	V_s *(cm/s)*	q_b *(10^-6)* (m^2/s)	*Ω*	*Φ*
1-6-L'-1	0.000	0.125	17.75	0.001158
1-6-L'-2	-0.080	0.237	15.44	0.002188
1-6-L'-3	-0.177	0.295	13.33	0.002727
1-6-L'-4	-0.180	0.351	13.27	0.003242
1-6-L'-5	-0.304	0.705	11.30	0.006513
1-6-L'-6	-0.354	0.757	10.67	0.006990
1-6-L'-7	-0.371	0.730	10.47	0.006741
1-6-L'-8	-0.442	0.931	9.71	0.008597
1-6-L'-9	-0.464	1.038	9.50	0.009585
1-6-L'-10	-0.541	1.207	8.82	0.011145
1-6-L'-11	-0.595	1.160	8.39	0.010711
1-6-L'-12	-0.622	1.503	8.20	0.013878
1-6-L'-13	-0.640	1.662	8.07	0.015347
1-6-L'-14	-0.755	1.409	7.35	0.013010
1-6-L'-15	-0.771	1.696	7.26	0.015661
1-6-L'-16	-0.868	2.321	6.76	0.021432

(d) Series 1-7, τ_{*o} = 0.0525

No	V_s *(cm/s)*	q_b *(10^-6)* (m^2/s)	*Ω*	*Φ*
1-7-L'-1	0.000	0.289	19.94	0.002668
1-7-L'-2	-0.043	0.380	18.45	0.003509
1-7-L'-3	-0.123	0.640	16.19	0.005907
1-7-L'-4	-0.130	0.800	16.03	0.007387
1-7-L'-5	-0.231	1.300	13.91	0.012000
1-7-L'-6	-0.250	1.300	13.58	0.012004
1-7-L'-7	-0.298	1.410	12.79	0.013023
1-7-L'-8	-0.301	1.600	12.75	0.014774
1-7-L'-9	-0.358	1.816	11.94	0.016765
1-7-L'-10	-0.380	1.850	11.64	0.017083
1-7-L'-11	-0.434	1.968	10.99	0.018176
1-7-L'-12	-0.490	2.530	10.39	0.023361
1-7-L'-13	-0.513	2.860	10.16	0.026409
1-7-L'-14	-0.559	3.243	9.74	0.029944
1-7-L'-15	-0.622	3.182	9.21	0.029383
1-7-L'-16	-0.622	3.282	9.21	0.030305

AII.2 SEDIMENT TRANSPORT RATE UNDER SHORTENED SUCTION ZONE FOR d_{50} = 0.48 mm

The sediment transport rates of the Experimental Series III subjected with downward seepage (suction) were measured for Series 2-1 to 2-4 with particles size d_{50} = 0.48. The details shown in Table AII.2 and AII.3 are the data tested with the 0.5-m and 1-m suction zone, respectively.

Table AII.2 Sediment Transport Rate with 0.5-m Length Suction Zone (d_{50} = 0.48 mm)

(a) Series 2-1, τ_{*o} = 0.0298

No	V_s *(cm/s)*	q_b *(10^-6)* (m^2/s)	Ω	Φ
2-1-L'-1	-0.355	0.013	5.437	0.000302
2-1-L'-2	-0.386	0.019	5.116	0.000439
2-1-L'-3	-0.394	0.021	5.037	0.000484
2-1-L'-4	-0.405	0.019	4.940	0.000444
2-1-L'-5	-0.412	0.019	4.877	0.000442
2-1-L'-6	-0.426	0.024	4.755	0.000557
2-1-L'-7	-0.444	0.029	4.607	0.000672
2-1-L'-8	-0.454	0.026	4.533	0.000601
2-1-L'-9	-0.458	0.027	4.503	0.000640
2-1-L'-10	-0.468	0.031	4.429	0.000734
2-1-L'-11	-0.484	0.036	4.316	0.000836
2-1-L'-12	-0.502	0.035	4.195	0.000819
2-1-L'-13	-0.508	0.031	4.156	0.000734
2-1-L'-14	-0.514	0.036	4.118	0.000836
2-1-L'-15	-0.526	0.041	4.043	0.000958
2-1-L'-16	-0.544	0.041	3.936	0.000955

(b) Series 2-2, τ_{*o} = 0.0341

No	V_s *(cm/s)*	q_b *(10^-6)* (m^2/s)	*Ω*	*Φ*
2-2-L'-1	-0.301	0.078	7.055	0.001829
2-2-L'-2	-0.331	0.088	6.607	0.002064
2-2-L'-3	-0.351	0.128	6.339	0.003006
2-2-L'-4	-0.408	0.134	5.677	0.003151
2-2-L'-5	-0.428	0.184	5.478	0.004328
2-2-L'-6	-0.438	0.177	5.383	0.004160
2-2-L'-7	-0.468	0.177	5.118	0.004160
2-2-L'-8	-0.478	0.221	5.032	0.005194
2-2-L'-9	-0.478	0.191	5.032	0.004488
2-2-L'-10	-0.488	0.221	4.952	0.005194
2-2-L'-11	-0.504	0.176	4.836	0.004156
2-2-L'-12	-0.505	0.251	4.823	0.005918
2-2-L'-13	-0.505	0.208	4.823	0.004906
2-2-L'-14	-0.524	0.216	4.690	0.005098
2-2-L'-15	-0.535	0.251	4.610	0.005918
2-2-L'-16	-0.544	0.266	4.553	0.006276

(c) Series 2-3, τ_{*o} = 0.0360

No	V_s *(cm/s)*	q_b *(10^-6)* (m^2/s)	*Ω*	*Φ*
2-3-L'-1	-0.304	0.181	7.474	0.004262
2-3-L'-2	-0.328	0.264	7.094	0.006214
2-3-L'-3	-0.368	0.244	6.537	0.005743
2-3-L'-4	-0.419	0.314	5.941	0.007388
2-3-L'-5	-0.447	0.272	5.659	0.006414
2-3-L'-6	-0.459	0.414	5.545	0.009743
2-3-L'-7	-0.499	0.356	5.201	0.008379
2-3-L'-8	-0.499	0.376	5.201	0.008850
2-3-L'-9	-0.504	0.452	5.161	0.010650
2-3-L'-10	-0.512	0.394	5.093	0.009290
2-3-L'-11	-0.514	0.342	5.084	0.008052
2-3-L'-12	-0.525	0.438	4.998	0.010312
2-3-L'-13	-0.539	0.437	4.891	0.010286
2-3-L'-14	-0.550	0.520	4.816	0.012238
2-3-L'-15	-0.554	0.394	4.788	0.009269
2-3-L'-16	-0.554	0.494	4.788	0.011624

(d) Series 2-4, τ_{*o} = 0.0422

No	V_s *(cm/s)*	q_b *(10^-6)* (m^2/s)	Ω	Φ
2-4-L'-1	-0.206	0.204	11.371	0.004795
2-4-L'-2	-0.262	0.294	9.788	0.006915
2-4-L'-3	-0.305	0.312	8.849	0.007354
2-4-L'-4	-0.348	0.354	8.061	0.008344
2-4-L'-5	-0.350	0.422	8.030	0.009938
2-4-L'-6	-0.365	0.364	7.799	0.008582
2-4-L'-7	-0.397	0.330	7.330	0.007777
2-4-L'-8	-0.398	0.338	7.319	0.007969
2-4-L'-9	-0.416	0.577	7.084	0.013580
2-4-L'-10	-0.417	0.416	7.067	0.009803
2-4-L'-11	-0.453	0.405	6.638	0.009537
2-4-L'-12	-0.493	0.474	6.228	0.011158
2-4-L'-13	-0.529	0.610	5.889	0.014376
2-4-L'-14	-0.545	0.696	5.751	0.016397
2-4-L'-15	-0.558	0.575	5.643	0.013537
2-4-L'-16	-0.566	0.623	5.579	0.014675

Table AII.3 Sediment Transport Rate with 1-m Length Suction Zone (d_{50} = 0.48 mm)

(a) Series 2-1, τ_{*o} = 0.0298

No	V_s *(cm/s)*	q_b *(10^-6)* (m^2/s)	*Ω*	*Φ*
2-1-L"-1	-0.301	0.069	6.098	0.001625
2-1-L"-2	-0.314	0.087	5.924	0.002049
2-1-L"-3	-0.316	0.084	5.899	0.001978
2-1-L"-4	-0.357	0.116	5.414	0.002732
2-1-L"-5	-0.372	0.156	5.256	0.003673
2-1-L"-6	-0.404	0.195	4.948	0.004592
2-1-L"-7	-0.426	0.248	4.755	0.005840
2-1-L"-8	-0.444	0.255	4.607	0.006005
2-1-L"-9	-0.458	0.261	4.503	0.006147
2-1-L"-10	-0.468	0.314	4.429	0.007395
2-1-L"-11	-0.484	0.454	4.316	0.010689
2-1-L"-12	-0.502	0.298	4.195	0.007025
2-1-L"-13	-0.508	0.359	4.156	0.008454
2-1-L"-14	-0.514	0.473	4.118	0.011139
2-1-L"-15	-0.526	0.506	4.043	0.011916
2-1-L"-16	-0.544	0.453	3.936	0.010668

(b) Series 2-2, τ_{*o} = 0.0341

No	V_s *(cm/s)*	q_b *(10^-6)* (m^2/s)	*Ω*	*Φ*
2-2-L"-1	-0.170	0.068	10.010	0.001601
2-2-L"-2	-0.187	0.077	9.492	0.001820
2-2-L"-3	-0.202	0.085	9.078	0.002002
2-2-L"-4	-0.219	0.115	8.650	0.002708
2-2-L"-5	-0.233	0.156	8.327	0.003673
2-2-L"-6	-0.256	0.247	7.846	0.005817
2-2-L"-7	-0.285	0.206	7.305	0.004851
2-2-L"-8	-0.293	0.261	7.178	0.006147
2-2-L"-9	-0.305	0.314	6.985	0.007395
2-2-L"-10	-0.337	0.454	6.525	0.010689
2-2-L"-11	-0.339	0.298	6.489	0.007025
2-2-L"-12	-0.351	0.401	6.333	0.009443
2-2-L"-13	-0.356	0.546	6.266	0.012852
2-2-L"-14	-0.402	0.546	5.739	0.012852
2-2-L"-15	-0.409	0.714	5.667	0.016815
2-2-L"-16	-0.463	0.867	5.161	0.020418

(c) Series 2-3, τ_{*o} = 0.0360

No	V_s *(cm/s)*	q_b *(10^-6)* (m^2/s)	*Ω*	*Φ*
2-3-L"-1	-0.189	0.214	10.073	0.005040
2-3-L"-2	-0.205	0.308	9.608	0.007254
2-3-L"-3	-0.241	0.436	8.705	0.010268
2-3-L"-4	-0.262	0.458	8.253	0.010786
2-3-L"-5	-0.289	0.507	7.735	0.011940
2-3-L"-6	-0.294	0.655	7.646	0.015425
2-3-L"-7	-0.322	0.708	7.192	0.016673
2-3-L"-8	-0.325	0.689	7.143	0.016226
2-3-L"-9	-0.330	0.760	7.063	0.017891
2-3-L"-10	-0.349	0.760	6.793	0.017891
2-3-L"-11	-0.351	0.927	6.757	0.021838
2-3-L"-12	-0.373	0.927	6.473	0.021838
2-3-L"-13	-0.396	1.067	6.196	0.025128
2-3-L"-14	-0.408	1.034	6.061	0.024351
2-3-L"-15	-0.411	1.189	6.028	0.028001
2-3-L"-16	-0.425	1.077	5.879	0.025363

(d) Series 2-4, τ_{*o} = 0.0422

No	V_s *(cm/s)*	q_b *(10^-6)* (m^2/s)	*Ω*	*Φ*
2-4-L"-1	-0.201	0.514	11.525	0.012105
2-4-L"-2	-0.226	0.521	10.742	0.012269
2-4-L"-3	-0.233	0.629	10.541	0.014813
2-4-L"-4	-0.268	0.808	9.641	0.019028
2-4-L"-5	-0.275	0.784	9.479	0.018463
2-4-L"-6	-0.304	0.968	8.862	0.022791
2-4-L"-7	-0.327	0.873	8.422	0.020548
2-4-L"-8	-0.336	1.028	8.269	0.024209
2-4-L"-9	-0.341	1.107	8.183	0.026070
2-4-L"-10	-0.349	0.968	8.057	0.022791
2-4-L"-11	-0.358	1.246	7.898	0.029331
2-4-L"-12	-0.358	1.133	7.898	0.026682
2-4-L"-13	-0.368	1.506	7.745	0.035460
2-4-L"-14	-0.386	1.165	7.486	0.027436
2-4-L"-15	-0.405	1.382	7.226	0.032546
2-4-L"-16	-0.429	1.497	6.922	0.035254

Appendix III

Data of Sediment Transport Rate against Time

The detail data of sediment transport rate against time with presence of suction mentioned in Chapter 7 are shown in AII.1.

AI.1 SEDIMENT TRANSPORT RATE AGAINST TIME FOR d_{50} = 0.48 mm

The sediment transport rates of the Experimental Series IV subjected with downward seepage (suction) were measured for Series 2-2 and 2-3 with particles size d_{50} = 0.48 mm. The details shown in Table AIII.1 and AIII.2 are the data tested for Series 2-2 and 2-3, respectively.

Table AIII.1 Sediment Transport Rate against Time for Series 2-3 (τ_{*o} = 0.0360)

(a) V_s = -0.215 cm/s

No	*Time (min)*	q_b (10^{-6}) (m^2/s)	Φ
T1-1	1.58	0.627	0.015423
T1-2	5.59	0.729	0.017178
T1-3	11.07	0.857	0.020172
T1-4	14.57	0.974	0.022947
T1-5	18.20	1.144	0.026945
T1-6	22.10	0.947	0.022310
T1-7	26.17	1.043	0.024564
T1-8	29.74	0.904	0.021298
T1-9	33.43	0.881	0.020743
T1-10	38.62	0.752	0.017698
T1-11	42.66	0.676	0.015914
T1-12	46.62	0.639	0.015037
T1-13	51.00	0.586	0.013793
T1-14	55.55	0.549	0.012922
T1-15	60.45	0.496	0.011674
T1-16	65.38	0.416	0.009803
T1-17	70.42	0.400	0.009422
T1-18	75.64	0.390	0.009177
T1-19	80.47	0.411	0.009672
T1-20	91.38	0.345	0.008132
T1-21	100.56	0.339	0.007982
T1-22	108.71	0.321	0.007567
T1-23	120.49	0.311	0.007316
T1-24	131.26	0.316	0.007433
T1-25	141.09	0.293	0.006892
T1-26	151.40	0.287	0.006755
T1-27	161.87	0.247	0.005808
T1-28	171.26	0.221	0.005204
T1-29	181.31	0.242	0.005692
T1-30	190.64	0.254	0.005976
T1-31	201.08	0.292	0.006886
T1-32	211.29	0.254	0.005979
T1-33	221.00	0.235	0.005533

(b) V_s = -0.246 cm/s

No	*Time (min)*	*q_b (10^{-6}) (m^2/s)*	*Φ*
T2-1	1.12	0.975	0.022961
T2-2	4.39	1.174	0.027649
T2-3	7.84	1.114	0.026244
T2-4	11.08	1.507	0.035489
T2-5	14.94	1.705	0.040141
T2-6	20.96	1.513	0.035622
T2-7	25.60	1.442	0.033956
T2-8	30.22	1.198	0.028206
T2-9	35.69	1.053	0.024796
T2-10	40.54	0.939	0.022107
T2-11	46.54	0.829	0.019528
T2-12	50.80	0.726	0.017103
T2-13	55.68	0.651	0.015321
T2-14	60.18	0.676	0.015925
T2-15	73.05	0.524	0.012344
T2-16	80.71	0.531	0.012515
T2-17	90.17	0.500	0.011783
T2-18	100.98	0.392	0.009227
T2-19	110.39	0.345	0.008126
T2-20	120.53	0.370	0.008714
T2-21	131.20	0.312	0.007342
T2-22	140.69	0.269	0.006329
T2-23	150.83	0.245	0.005762
T2-24	160.57	0.265	0.006234
T2-25	170.69	0.239	0.005808

Table AIII.2 Sediment Transport Rate against Time for Series 2-2 (τ_{*o} = 0.0341)

(a) V_s = -0.249 cm/s

No	*Time (min)*	*q_b (10^{-6}) (m^2/s)*	*Φ*
T3-1	2.09	0.480	0.011314
T3-2	5.50	0.510	0.012001
T3-3	9.05	0.666	0.015681
T3-4	12.52	0.678	0.015956
T3-5	16.19	0.858	0.020205
T3-6	20.20	0.957	0.022529
T3-7	23.57	0.960	0.022617
T3-8	29.17	1.038	0.024435
T3-9	32.41	0.957	0.022527
T3-10	36.09	0.843	0.019857
T3-11	40.75	0.796	0.018744
T3-12	45.63	0.704	0.016570
T3-13	50.87	0.586	0.013808
T3-14	55.96	0.538	0.012663
T3-15	60.79	0.483	0.011369
T3-16	70.85	0.483	0.011370
T3-17	80.69	0.397	0.009343
T3-18	90.93	0.348	0.008198
T3-19	100.52	0.324	0.007630
T3-20	110.72	0.281	0.006606
T3-21	120.82	0.231	0.005449
T3-22	131.08	0.195	0.004587
T3-23	140.95	0.190	0.004475
T3-24	150.65	0.221	0.005203
T3-25	160.52	0.197	0.004649
T3-26	170.77	0.209	0.004914
T3-27	180.41	0.215	0.004649